

Revista ALCONPAT

Latin American Journal of Quality Control, Pathology and Construction Recovery

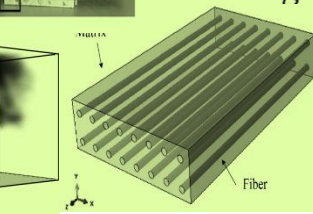
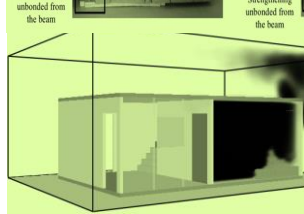
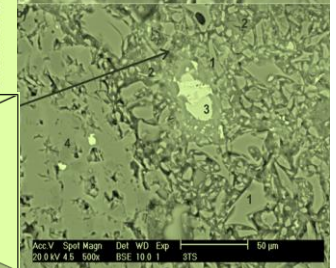
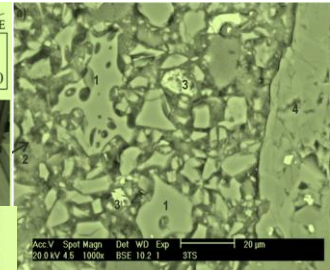
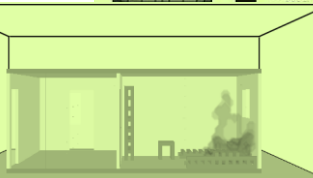
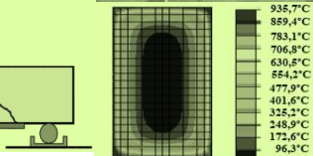
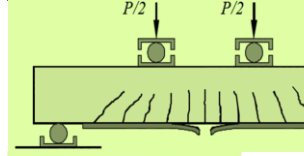
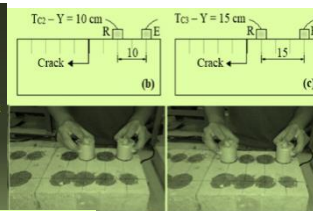
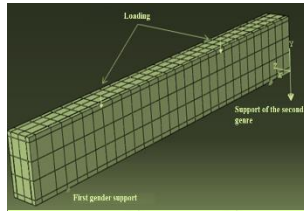
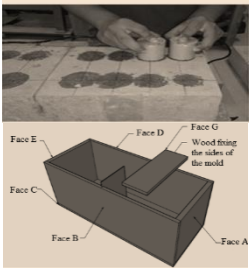
DOI: <http://dx.doi.org/10.21041/ra.v9i1>
editorial.revista.alconpat@gmail.com

eISSN: 2007-6835

Volume 9

January – April 2019

Issue 1



Latin American Journal of Quality Control, Pathology and Construction Recovery

<http://www.revistaalconpat.org>



ALCONPAT International

Founders members:

Liana Arrieta de Bustillos – **Venezuela**
Antonio Carmona Filho - **Brazil**
Dante Domene – **Argentina**
Manuel Fernández Cánovas – **Spain**
José Calavera Ruiz – **Spain**
Paulo Helene, **Brazil**

Board of Directors International:

President of Honor

Angélica Ayala Piola, **Paraguay**

President

Carmen Andrade Perdriz, **Spain**

General Director

Pedro Castro Borges, **Mexico**

Executive Secretary

José Iván Escalante García, **Mexico**

Technical Vice President

Enio Pazini Figueiredo, **Brazil**

Administrative Vice President

Luis Álvarez Valencia, **Guatemala**

Manager

Paulo Helene, **Brazil**

Revista ALCONPAT

Editor in Chief:

Dr. Pedro Castro Borges
Centro de Investigación y de Estudios Avanzados del Instituto
Politécnico Nacional, Unidad Mérida (CINVESTAV IPN –
Mérida)
Merida, Yucatan, **Mexico**

Co-Editor in Chief:

Arch. Margita Kliewer
Universidad Católica “Nuestra Señora de la Asunción”
Asuncion, **Paraguay**

Executive Editor:

Dr. José Manuel Mendoza Rangel
Universidad Autónoma de Nuevo León, Facultad de Ingeniería
Civil
Monterrey, Nuevo Leon, **Mexico**

Associate Editors:

Dr. Manuel Fernandez Canovas Universidad
Politécnica de Madrid. Madrid, **Spain**

Ing. Raúl Husni

Facultad de Ingeniería Universidad de Buenos Aires. Buenos
Aires, **Argentina**

Dr. Paulo Roberto do Lago Helene

Universidade de São Paulo.

São Paulo, **Brazil**

Dr. José Iván Escalante García

Centro de Investigación y de Estudios Avanzados del
Instituto Politécnico Nacional (Unidad Saltillo) Saltillo,
Coahuila, **Mexico**.

Dr. Mauricio López.

Departamento de Ingeniería y Gestión de la Construcción,
Escuela de Ingeniería,
Pontificia Universidad Católica de Chile
Santiago de Chile, **Chile**

Dra. Oladis Troconis de Rincón Centro de Estudios de

Corrosión Universidad de Zulia

Maracaibo, **Venezuela**

Dr. Fernando Branco Universidad

Técnica de Lisboa

Lisboa, **Portugal**

Dr. Pedro Garcés Terradillos

Universidad de Alicante

San Vicente, **Spain**

Dr. Andrés Antonio Torres Acosta

Instituto Mexicano del Transporte / Universidad Marista de
Querétaro

Querétaro, **Mexico**

Dr. Luiz Fernández Luco

Universidad de Buenos Aires – Facultad de Ingeniería –
INTECIN

Buenos Aires, **Argentina**

RA V9 N1, January - April 2019

Message from the Editor in Chief

**JOURNAL OF THE LATIN-AMERICAN ASSOCIATION
OF QUALITY CONTROL, PATHOLOGY AND RECOVERY
OF CONSTRUCTION**

<http://www.revistaalconpat.org>

With great satisfaction, we present the first issue of the ninth year of the ALCONPAT journal.

The aim of the journal is to publish case studies within the scope of the Association, namely quality control, pathology and recovery of constructions, including basic and applied research, reviews and documentary research.

The V9 N1 issue begins with a work where Nicolle Christine Sotsek and colleagues provide, through a systematic review of the literature and focused on the quality control of buildings, a consistent database to present the most used criteria by the Building Performance Evaluation (BPE). It was possible to define 9 dimensions of analysis that are presented and discussed in this document.

In the second work, Cristiano Corrêa et. al. present the computational simulation of a fire previously carried out as an experiment in a room that reproduced a single-family residence room, typically burnt down in the city of Recife (Pernambuco, Brazil). The objective of the article is to compare the results of the development of the temperatures of the gases obtained through computer simulation with the Fire Dynamics Simulator software (FDS) through the measurements obtained in the experiment. It was verified that the results obtained through the model developed in the FDS were coherent with those obtained experimentally.

In the third article, Mauricio de Pina Ferreira et. al. evaluate the influence of anchoring on the flexural strength of beams reinforced with Carbon Fiber Reinforced Polymer (PRFC) blankets. The parameters affecting the performance and strength of the beams are evaluated, and the sizing criteria of FIB Bulletin 14 (2001) and ACI 440-2R (2008) are discussed. It was observed that, even with auxiliary devices in the anchoring of the PRFC, there is the possibility of premature failures, and that both recommendations lead to safe, but overly conservative estimates in cases where the anchoring of the PRFC blanket is carried out properly.

In the fourth article, by Yagho de Souza Simões and Carol Ferreira Rezende Santos, we compare two techniques of structural reinforcement, carbon fiber and metal foil, used for the recovery of reinforced concrete structures degraded by fire. A deterioration of a beam in a fire situation is simulated from a thermal numerical modeling and, next, the reinforcements are calculated. It is concluded that carbon fiber has greater advantages regarding the reinforcement of beams.

The fifth work in this issue is written by Ricardo José Carvalho Silva and colleagues, who analyze the efficiency of reinforcement in reinforced concrete

beams by adding steel bars and epoxy adhesive. The tests showed that the clamps reduced the strength of the beams, compared to those that did not. The reinforced beams without clamps obtained better results, but the most important limiting factor was the adhesion between the epoxy and the beam. The use of clamps to try to solve the problem of adherence gave originality to this investigation.

In the sixth work, Marcela Tavares de Araujo Silva and colleagues evaluate an ultrasound test to estimate the depth of cracks in the concrete, using a mathematical model of the literature, in addition to checking the depth with better results. The results show that the test is sensitive to detect the presence of cracks in the concrete. The mathematical model used allowed to estimate the most depths of fissures; but the results are scattered and with a high margin of error for the depths of 5 cm and 15 cm, since for 10 cm better results were observed.

The seventh work in this issue is written by Renato Guilherme Pereira and colleagues, who present an experimental program to determine the residual strength of bi-supported reinforced concrete beams subjected to pure bending after fires. The beams presented, up to 120 minutes of exposure to fire, a good performance after the fire, not showing a significant reduction in their residual strength, and the numerical model was accurate in forecasting the temperatures and the residual rupture load when the experimental results were compared.

The article that closes this edition is by Erick Maldonado et. al. they present the results of concrete manufactured with supersulfated cements (SSC) volcanic material bases. After 180 days, the concrete with a cementitious compound of 5% An-10% CP-10% CaO-75% PM exposed to the CaSO₄ solution reached a compressive strength of 46 MPa and 44 MPa in dry conditions. laboratory. The microstructure was analyzed by scanning electron microscopy, energy dispersion spectroscopy and XRD, showed that the main hydration products are C-S-H and ettringite.

We are confident that the articles in this issue will be an important reference for those readers involved with issues of modeling applications and service life, as well as inspections with modern and / or improved methodologies. We thank the authors participating in this issue for their willingness and effort to present quality articles and meet the established times.

On behalf of the Editorial Board



Pedro Castro Borges
Editor in Chief



CONTENT

REVIEW

N. Christine Sotsek, D. Sanchez Leitner, A. P. Lacerda Santos: A systematic review of Building Performance Evaluation criterias (BPE).

Página

1 - 14

APPLIED RESEARCH

R. Tabaczenski, C. Corrêa, T. Ancelmo Pires, J. J. Rêgo Silva: Numerical simulation and fire experiment in residential dormitory.

15 - 29

M. P. Ferreira, M. H. Oliveira, A. F. Lima Neto, L. S. Tapajós, A. Nascimento, M. C. Freire: Influence of anchorage on flexural strength of beams strengthened with CFRP sheets.

30 - 47

Y. S. Simões, C. F. R. Santo: Contribution to reinforced concrete beams degraded in fire situations: Comparative analysis between structural reinforcement with carbon fibers and sheet metal.

48 - 64

R. J. C. Silva, M. B. S. Muniz, F. E. S. da Silva Júnior, É. M. F. Lima, C. V. dos S. Araújo: Experimental analysis of reinforced concrete beams strengthened with steel bars and epoxy structural adhesive.

64 - 78

M. T. A. Silva, J. H. A. Rocha, E. C. B. Monteiro, Y. V. Póvoas, E. R. Kohlman Rabbani: Evaluation of the ultrasound test for estimating the depth of cracks in concrete.

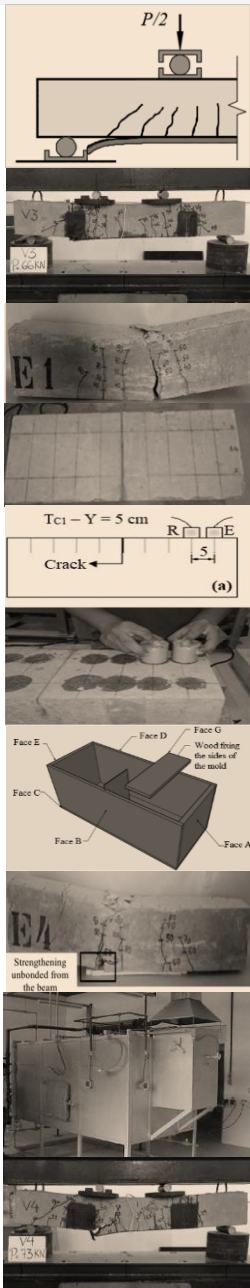
79 - 92

R. G. S. Pereira, T. A. Carvalho Pires, D. Duarte, J. J. Rêgo Silva: Assess of residual mechanical resistance of reinforced concrete beams after fire.

93 - 105

K. Cabrera Luna, J. I. Escalante García, D. Nieves Mendoza, E. E. Maldonado Bandala: Resistance to compression and microstructure of concrete manufactured with supersulfated cements-based materials of volcanic origin exposed to a sulphate environment

106 - 116



A systematic review of Building Performance Evaluation criterias (BPE)

N. Christine Sotsek^{1*} , D. Sanchez Leitner¹ , A. P. Lacerda Santos¹ 

*Contact author: nicollesotsek@yahoo.com.br

DOI: <http://dx.doi.org/10.21041/ra.v9i1.260>

Reception: 25/09/2017 | Acceptance: 01/08/2018 | Publication: 30/12/2018

ABSTRACT

The objective of this article is to provide, through a systematic review of the literature, focused on the quality control of buildings, a database to present the Building Performance Evaluation (BPE) most used criteria. Through this review, 782 articles were identified, of which 15 were selected considering the subject's adherence to the research and publication period. It was discussed the main information about the articles, their authors and journals. The performance criteria compiled by the analyzed articles used as basis: literature, questionnaires and interviews with users and professionals of the area, consultation with specialists in the segment and technical visits to buildings. With these identified criteria, it was possible to define 9 dimensions of analysis that are presented and discussed in this document.

Keywords: performance; evaluation; criteria; construction; systematic review.

Cite as: N. Christine Sotsek, D. Sanchez Leitner, A. P. Lacerda Santos (2019), "A systematic review of Building Performance Evaluation criterias (BPE)", Revista ALCONPAT, 9 (1), pp. 1 – 14, DOI: <http://dx.doi.org/10.21041/ra.v9i1.260>

¹ Universidade Federal do Paraná, Brasil.

Legal Information

Revista ALCONPAT is a quarterly publication by the Asociación Latinoamericana de Control de Calidad, Patología y Recuperación de la Construcción, Internacional, A.C., Km. 6 antigua carretera a Progreso, Mérida, Yucatán, 97310, Tel.5219997385893, alconpat.int@gmail.com, Website: www.alconpat.org

Responsible editor: Pedro Castro Borges, Ph.D. Reservation of rights for exclusive use No.04-2013-011717330300-203, and ISSN 2007-6835, both granted by the Instituto Nacional de Derecho de Autor. Responsible for the last update of this issue, Informatics Unit ALCONPAT, Elizabeth Sabido Maldonado, Km. 6, antigua carretera a Progreso, Mérida, Yucatán, C.P. 97310.

The views of the authors do not necessarily reflect the position of the editor.

The total or partial reproduction of the contents and images of the publication is strictly prohibited without the previous authorization of ALCONPAT Internacional A.C.

Any dispute, including the replies of the authors, will be published in the third issue of 2019 provided that the information is received before the closing of the second issue of 2019.

Uma revisão sistemática dos critérios do Building Performance Evaluation (BPE)

RESUMO

O objetivo deste artigo é fornecer, por meio de uma revisão sistemática da literatura focada no controle de qualidade das edificações, um banco de dados para apresentar os critérios mais utilizados pelo Building Performance Evaluation (BPE). Mediante a esta revisão, 782 artigos foram identificados, dos quais 15 foram selecionados considerando aderência do tema a pesquisa e período de publicação. As principais informações sobre os artigos, seus autores e revistas foram debatidas. Os critérios de desempenho compilados pelos artigos analisados utilizaram como base: a literatura, questionários e entrevistas com usuários e profissionais da área, consulta a especialistas do segmento e visitas técnicas as edificações. Com tais critérios identificados foi possível definir 9 dimensões de análise que são apresentadas e discutidas neste documento.

Palavras chave: desempenho; avaliação; critérios; construção; revisão sistemática.

Una revisión sistemática de los criterios del Building Performance Evaluation (BPE)

RESUMEN

El objetivo de este artículo es proporcionar, a través de una revisión sistemática de la literatura enfocada en el control de calidad de las edificaciones, una base de datos consistente para presentar los criterios más utilizados por el Building Performance Evaluation (BPE). Mediante esta revisión, 782 artículos fueron identificados, de los cuales 15 fueron seleccionados considerando adherencia del tema a la investigación y período de publicación. Las principales informaciones sobre los artículos, sus autores y revistas fueron debatidas. Los criterios de desempeño compilados por los artículos analizados utilizaron como base: la literatura, cuestionarios y entrevistas con usuarios y profesionales del área, consulta a especialistas del segmento y visitas técnicas a las edificaciones. Con estos criterios identificados fue posible definir 9 dimensiones de análisis que son presentadas y discutidas en este documento.

Palabras clave: desempeño; evaluación; criterios; construcción; revisión sistemática.

1. INTRODUCTION

A building is built with the aim of providing the human being with a pleasant and comfortable working environment, and protected against climatic inclement weather (Khalil et al., 2008). However, a building is the result of a project and planning built and managed based on specific standards established by governments, professionals and specialists who must meet not only the current technical requirements of each country, but also the expectations and aspirations established by the users (Ibem et al., 2013).

Based on this discussion, it is important to realize the importance of this research by considering that high population indexes is essential for more buildings to be built, but at the same time continue to meet the requirements established by the standards and by the final owners.

The performance of a building can be defined as its capacity to operate at maximum efficiency, fulfilling its function throughout its life cycle (Khalil et al 2016). To provide this maximum operation and to improve its efficiency, regular and continuous evaluation of building performance, called building performance evaluation (BPE), is essential. The BPE is a process of systematic comparison of the real performance of a building, that is, it relates the objectives of the client with the criteria of performance established by the specialists in order to measure the degree of satisfaction and performance of a building for those users (Preiser, 1994). This process aims to

improve the quality of management, design and construction by providing a more sustainable construction (Ibem et al., 2013); provide basic information on users' needs, preferences and satisfaction (Vischer, 2008) and provide feedback on the causes and effects of environmental issues related to buildings, thus informing the long-term planning and management of the life cycle of buildings (Meir et al., 2009). To do so, the BPE serves as a tool that adds value, assisting managers in decision making at strategic and operational levels during construction of a building (Khalil et al., 2008). However, for the application of the BPE it is necessary to define the evaluation criteria that can help in the process of measuring the performance of a building. According to Teicholz (2003), one can not improve what can not be measured. Measuring the performance of a building, according to Koleoso et al. (2013), is the safest way to improve the economic, physical and functional development of a building, ensuring that its objectives are met. Based on this assumption, this article aims to present a brief overview, through a systematic review of the literature, of the main academic studies that have studied and established performance criteria for the evaluation of buildings in order to assist in the expansion of this area of research focused on the control of quality of buildings.

2. MATERIALS AND METHODS:

This research adopted a systematic review approach proposed by Kitchenham et al. (2009) and followed three main steps (Figure 1): (1) Review planning; (2) Conduct of review; (3) Dissemination and reporting.

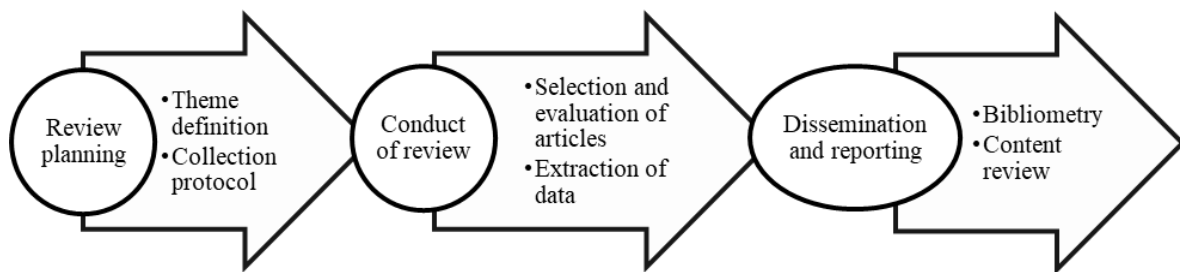


Figure 1. Process of applying the systematic review.
Adapted from Kitchenham et al., (2009)

The first phase of the research proposes to align the research theme and elaborate the collection protocol. The central theme established for research was to identify the criteria established in the literature for evaluating the performance of buildings. Based in this thematic, the collection protocol was elaborated, selecting 3 international databases: Web of Science, Scopus and Science Direct, and a Brazilian database, the CAPES. In each database, terms related with performance evaluation in construction had been tested. In the search *string* it had used the logical boolean operators AND, OR and the quotations marks for bigger precision of the research, until two terms were defined: “*building performance evaluation*” and “*building performance criteria*”.

In the second phase of the research, the articles were selected based on the scope of the theme, that is, if the article had as its essence the definition of criteria for performance evaluation of buildings; the period of publication (2010-2017) and the search for articles of *Journals*, discarding articles of congresses. After this selection, a dynamic reading of the articles was performed and in this step, it was possible to obtain more articles by referential means cited by the authors. This process created a *looping* and stopped only when no articles were applied to the topic. The identified articles were organized in an Excel spreadsheet.

This technique of searching for new articles from those already selected is known as Snowball Sampling (ABN) and was reported by (Biernacki and Waldorf, 1981). Finally, in the third phase of the research it was possible to elaborate the articles bibliometry and content revision. In the first

one, we tried to measure the main aspects related to the articles, the authors and the magazines. The mechanism used to identify the citations of articles and the scores of journals was the platforms “Scopus- Search for an author profile”, “Scopus- Journal Metrics” and “Scimago Journal & Country Rank”. Based on all the keywords identified in the articles, the word cloud was created using the online software “Word it out”. The objective of this stage was to understand the panorama of research in the world, identifying the main authors and journals. In the second stage, the proposal was to compile the information present in the articles, organizing them into four groups: (1) methods used to elaborate the performance criteria; (2) conducting the questionnaires used; (3) organization of the criteria identified in 9 dimensions and (4) preparation of a table compiling all the criteria identified in the established dimensions.

3. RESULTS AND DISCUSSION

Through the systematic review of the literature, the two selected keywords «*building performance evaluation*» and «*building performance criteria*» were inserted into the four selected databases: Web of Science, Scopus, Science Direct and CAPES. In the first round, 782 articles were identified. With this sample we selected articles from 2010-2017, peer-reviewed *Journal* and *Journal* articles, reducing the sample to 424. With these, a dynamic reading was performed, which is a reading of the main topics such as abstract, method and result, and it were chosen the articles that presented in their conception the elaboration of a BPE method and selection of criteria. Then, the technique of Snowball Sampling was applied until the end of the identification of articles adhering to the theme. Table 1 presents in detail the procedure performed up to the selected number of 15 articles.

Table 1. Conduct of research: selection of articles.

Key Words	Data Base	Web of Science	Science Direct	Scopus	Capes	Total
	“building performance evaluation”		67	195	4	370
“building performance criteria”		27	19	2	98	146
Total search without filter and with duplicity						782
Filters	1° Selection of the year (2010-2017) 2° <i>Journal</i> and <i>Journal</i>	47	134	0	243	424
	3° Dynamic reading: article has elaboration of the BPE method and selection of evaluation criteria	0	4*	0	9*	9
	4° Snowball (2010-2017)		19			
	5° Dynamic reading		4			3
	6° Snowball (2010-2017)		4			
	7° Dynamic reading		4			2
	8° Snowball (2010-2017)		1			
	9° Dynamic reading		1			1
	Total adherent research					

*With the 15 articles selected, it was possible to perform bibliometric and content revision.

3.1 Bibliometric

In Table 2 it is possible to identify the authors name, the database where the article was identified, the name of the journals, their "DOI" registry and the country of origin. The journals that published the most works (from 2010 to July 2017) identifying criteria for performance evaluation in buildings were: United Kingdom (60%), followed by the Netherlands (13.33%), China, USA, Egypt and Lithuania (6.66%). It is noticed that more than 85% of the publishing magazines are from Nordic countries.

Table 2. Summary of information related to the 15 reviewed sources.

Nº	Authors	Data Base					Journal	DOI	Journal origin (country)
		Science direct	Scopus	Web of Science	Capes	Snow ball			
1	Gopikrishnan e Topkar (2017)	x			x		<i>Housing and Building National Research Center</i>	dx.doi.org/10.1016/j.hbrej.2015.08.004	Egypt
2	Ibem et al (2013)	x			x		<i>Frontiers of architectural research</i>	dx.doi.org/10.1016/j.foar.2013.02.001	China
3	Khalil et al (2016)				x		<i>Ecological Indicators</i>	doi.org/10.1016/j.ecolind.2016.07.032	Netherlands
4	Khan e Kotharkar (2012)	x					<i>Procedia - Social and Behavioral Sciences</i>	doi: 10.1016/j.sbspro.2012.08.052	England
5	Steinke et al (2010)				x		<i>Health environments research & design journal</i>		EUA
6	Nazeer e Silva 2016				x		<i>Built Environment Project and Asset Management</i>	doi 10.1108/BEPAM-09-2014-0049	England
7	Talib et al 2013	x					<i>Facilities</i>	doi.org/10.1108/f-06-2012-0042	England
8	Støre-Valen e Lohne 2016	x					<i>Facilities</i>	doi 10.1108/F-12-2014-0103	England
9	Mohit e Azim (2012)					x	<i>Procedia- Social and Behavioral Sciences</i>	doi: 10.1016/j.sbspro.2012.08.078	England
10	Nik-Mat et al (2011)					x	<i>Procedia Engineering</i>	doi:10.1016/j.proeng.2011.11.174	England
11	Hashim et al (2012)					x	<i>Procedia - Social and Behavioral Sciences</i>	doi: 10.1016/j.sbspro.2012.12.231	England
12	Lavy et al (2010)					x	<i>Facilities</i>	doi.org/10.1108/02632771011057189	England
13	Mohit e Nazyddah (2011)					x	<i>Journal of Housing and the Built Environment,</i>	doi 10.1007/s10901-011-9216-y	Netherlands
14	Lai e Man (2017)					x	<i>International Journal of Strategic Property Manag.</i>	doi:10.3846/1648715X.2016.1247304	Lithuania
15	Elyna Myeda et al (2011)					x	<i>Journal of Facilities Management</i>	doi.org/10.1108/14725961111148090	England

However, it can be seen from Figure 2 that most research and research authors are concentrated in Western countries. Malaysia is the country with the largest number of researchers.



Figure 2. Information about the country of origin of the research and the authors.

Through the "Scopus- Search for an author profile" platform, it was possible to verify the most cited articles and the co-quotations made between them (Table 3). The article by (Steinke et al., 2016) was the most cited in the literature, followed by the article by (Mohit and Naydaah, 2011). Table 3 shows how many times the articles were cited in the literature in general, and where there were cases of citations between them.

Table 3. Citations and co-citations identified in the 15 revised articles.

Articles that have been cited	Gopikrishnan e Topkar (2017)	Ibem et al (2013)	Khalil et al (2016)	Khan e Kotharkar (2012)	Steinke et al (2010)	Nazeer e Silva (2016)	Talib et al (2013)	Støre-Valen e Lohne (2016)	Mohit e Azim (2012)	Nik-Mat et al (2011)	Hashim et al (2012)	Mohit e Nazyddah (2011)	Lavy et al (2010)	Lai e Man (2017)	Elyna Myeda et al (2011)
Number of citations in the literature	0	6	2	0	15	0	0	1	1	1	0	8	0	1	0
Steinke et al (2010)						1		1							
Lavy et al (2010)					1	1		1		1				1	
Myeda et al (2011)					1			1						1	
Nik-Mat et al (2011)	1														

Mohit e Azim (2012)	1													
Ibem et al (2013)	1													

The “*Scopus- Journal Metrics*” and “*Scimago Journal & Country Rank*” platforms made possible to know more about the magazines identified. The information presented in Table 4 refers to the number of publications for the years 2015-2016, the score of each journal according to its area of registration, its rank and its impact on the platform *Scopus* and *Scimago*.

Table 4. Journals Metrics

Journals	JCR (2017)	SJR 2015	SJR 2016	Cite Score	SRJ	H index	Total cites (2015)	Total cites (2016)	Documentos 2013/2015	Cite Score Rank	Nº artigos
Frontiers of architectural research	-	0,432	0,392	0,88	0,392	10	151	112	128	37/223	1
Ecological Indicators	3,983	1,481	1,308	4,07	1308	78	5039	5218	1286	20/291	1
Built Environment Project and Asset Management	-	0,243	0,317	1,07	0,317	8	53	75	71	93/245	1
Facilities	-	0,369	0,421	1,06	0,421	25	118	148	141	14/87	3
Procedia Engineering	-	0,238	0,282	0,74	0,282	31	6130	6732	9257	108/265	1
Journal of Housing and the Built Environment	1,329	0,649	0,866	1,16	0,866	31	132	142	120	30/134	1
International Journal of Strategic Property Management	-	0,561	0,293	0,92	0,293	19	117	82	90	161/347	1
Procedia - Social and Behavioral Sciences	-	0,159	-	-	0,159	29	185	-	-	-	3
Journal of Facilities Management	-	-	-	-	-	-	-	-	-	-	1
Housing and Building National Research Center	-	-	-	-	-	-	-	-	-	-	1
Health environments research & design journal*	1,387	-	-	-	-	-	-	-	-	-	1

6	x	x	x	x			
7	x		x				
8	x						
9	x		x	x			
10	x		x		x	x	
11	x		x		x	x	
12	x	x	x				
13	x		x	x			
14	x						
15	x				x	x	

The questionnaire was the second method most used by the authors to identify the criteria needed to evaluate a construction. Of these, 80% were applied, and 20% were not applied, that is, in the case of the 20%, the authors present the questionnaire as a reference and as an instrument to test the criteria but did not actually use it. In the questionnaires applied, in short, about 3,196 questionnaires were sent. Only the work of (Nik-Mat et al., 2011) sent 1,230 questionnaires. The response rate varied from 20.4% to 100% in the applied works. To select the respondents to the questionnaires, the most used criteria was the working time in the area, in the case of the specialists, and for the users, the dwelling time of the dwellings. The works organized the criteria into dimensions that were validated. In some cases, the criteria were reorganized and then validated by the authors (Table 6).

Table 6. Summary of applied questionnaires.

Nº	Dimensions and Performance Criteria	Sample size	Replies per article	Response rate (%)	Result	Applicability
1	13 dimensions with n criteria (not detailed)				13 dimensions	No applied
2	5 dimensions with 27 criteria	670	452	67,5%	5 dimensions	Applied
4	5 dimensions with 22 criteria				5 dimensions	No applied
6	7 dimensions with 57 criteria	37 specialists	31 specialists	83,80%	7 dimensions	Applied
7	3 dimensions with 58 criteria	225	166 e 192	74%/85%	3 dimensions with 11 criteria validated	Applied
9	4 dimensions with 46 criteria	100	100	100%	4 dimensions	Applied
10	3 dimensions with 17 criteria	2 categories: users and construction team: 1230	252	20,40%	3 dimensions	Applied / Not detailed
11	7 dimensions with 34 criteria	3 categories: users; external public and			7 dimensions	Applied / Not detailed

		construction team				
12	4 dimensions with 35 criteria	11 industry representatives	7	63,60%	4 dimensions	Applied
13	5 dimensions with 45 criteria	3 categories: residents groups; individuals and residents in transit: 960	250	27,60%	5 dimensions	Applied

In full, each article provides a range of criteria that should be analyzed to evaluate the performance of a building. In some cases, the articles created dimensions to organize their criteria, in others, the articles presented the criteria without presenting a specific group. In this way, the authors of this paper organized the criteria identified in the articles in 9 dimensions established from the reading of the works (Table 7).

Table 7. Dimensions established to organize the performance evaluation criteria of a construction.

Authors	Dimensions to measure performance									
	Functional	Technical / Maintenance	Environment (spaces / location)	Financial / Economic	Environmental	Image / Appearance	Neighborhood relation	Process	Leadership	Types of construction
Gopikrishnan e Topkar (2017)	x	x	x							n/s
Ibem et al (2013)	x	x	x	x		x				habitation
Khalil et al (2016)	x	x	x							Education
Khan e Kotharkar (2012)	x	x	x				x			Education
Steinke et al (2010)	x	x	x	x						health
Nazeer e Silva 2016	x	x	x	x	x			x	x	Education
Talib et al (2013)	x	x	x							health
Støre-Valen e Lohne (2016)	x	x	x		x					n/s
Mohit e Azim (2012)		x	x			x	x			Habitation
Nik-Mat et al (2011)	x	x				x				Habitation
Hashim et al (2012)	x	x	x	x		x				habitation
Lavy et al (2010)	x	x	x	x						n/s
Mohit e Nazyddah (2011)	x		x		x		x			habitation
Lai e Man (2017)	x	x		x	x					commercial
Elyna Myeda et al (2011)	x	x	x			x				commercial

It can be seen from Table 7 that 20% of the articles are concerned with creating criteria that evaluate constructions in general. However, the other 80% show that it is important to establish specific criteria for each type of construction, in the case of housing, education, health and commerce.

The nine dimensions elaborated involve the analysis of aspects related to the functional condition of a building, such as: air condition, ambient (acoustic and thermal comfort), noise, fire protection, lighting, among others; the technical condition involves the structure of the building, plumbing and electrical services, for example. The environment dimension refers to the spaces (of the rooms) and location of the enterprise; the financial dimension involves expenses related to building (maintenance, light, water). The environmental dimension refers to the spending index on light, water and garbage collection; the image dimension involves the aesthetics and appearance of the buildings.

The dimension "relationship between neighborhood" presents the contact of the residents with the surroundings. The "processes" dimension involves the control and management of the services provided within an enterprise and finally the leadership dimension refers to the instructions established to the owners and employees in the construction occupation. The most used dimensions during the constructive evaluation refer to Functional (93%) and Technical (93%), followed by Environment (88%).

The evaluation criteria identified in the 15 articles studied and organized in 9 dimensions are presented below:

- Gopikrishnan and Topkar (2017): Thermal comfort; ventilation; visual comfort (natural lighting); fire safety, lightning, accidents in general; acoustic comfort; water control; control of air quality; control of drinking water and electricity services; building maintenance (fissures, leaks, infiltration, humidity, sewage); control of basic sanitation; control of internal and external finishes to the building; evaluation of spaces such as size of internal and external areas, accessibility to the connectivity of the building (networks), the surrounding roads, stairs and elevators internal to the building. Control of garbage collection and maintenance of building aesthetics.
- Ibem et al (2013): Visual control; thermal and acoustic; control of air quality; fire safety, insects, dangerous animals, moisture; building maintenance; control of electrical and sanitary services; evaluation of the internal spaces, the design of the building and its location (accessibility for residents); control of the costs with the building; control of the aesthetic appearance of the construction and materials used in construction.
- Khalil et al (2016): fire safety; thermal comfort; visual comfort (artificial and natural lighting); waste control; ventilation; acoustic comfort; assessment of structural stability; electrical and sanitary services; control of finishing materials; building cleaning control; evaluation of the size of the spaces and the circulation and evaluation of the signage of the environments in the building.
- Khan and Kotharkar (2012): fire safety; visual comfort; assessment of structural stability; control of sanitation services; evaluation of internal space sizes; evaluation of the flexibility of the internal environments and control of the aesthetics of the building.
- Steinke et al (2010): evaluation of how the building contributes to the quality of life of residents / employees; level of innovation and practicality of the building; level of expenditure (energy and water) and level of satisfaction of the residents / employees.
- Nazeer e Silva (2016): visual control (natural lighting); thermal comfort; control of safety equipment, internal hygiene of buildings; olfactory control of environments; evaluation of internal and external signaling of environments; acoustic control; ventilation; internal maintenance of the building; structural control; durability of materials; assessment of accessibility and flexibility of spaces by residents; accessibility that the building possesses to those with physical disabilities; evaluation of signage of the environments in the building; evaluation of costs related to building (financing and maintenance of the

building); waste control; assessment of existing resources to assist in waste management; control of building aesthetics; existing processes check the residents' knowledge regarding maintenance, use of resources; waste management; fire safety, among others and level of training that the users obtained to do proper maintenance of the building.

- Talib et al (2013): evaluation of how the construction contributes to the quality of life of residents / employees; control of the structural and electrical quality of the building; accessibility of spaces and evaluation of the quality of building design.
- Støre-Valen and Lohne (2016): Evaluation of the functionality, usability, flexibility of the building and the sustainable resources existing in the building.
- Mohit and Azim (2012): environment ventilation; accessibility of electricity services, such as quantity of power plugs; control of electrical and sanitation services; evaluation of the size of spaces; location of the building (accessibility to residents); parking leisure areas; control of waste collection and neighbor relationship (level of security, involvement with the neighborhood).
- Nik-Mat et al (2011): air quality control; visual control; security level of the building; control of cleaning, maintenance of internal and external building and accessibility of internal and external spaces (parking).
- Hashim et al (2012): thermal comfort, acoustic, visual, ventilation; comfort of the environment; control of building maintenance, materials used in construction; cleaning; evaluation of the size of the internal spaces of the building and its adaptability to the residents; costs related to building (maintenance, energy, waste, among others) and evaluation of the aesthetics of construction.
- Lavy et al (2010): evaluation of how the building brings a sense of comfort to the residents, considering level of safety and hygiene; thermal comfort, acoustic, visual (natural lighting), air quality; building maintenance; control of sanitary and electrical services; evaluation of the accessibility of the building for residents in terms of location, room space, parking and accessibility for the physically handicapped; evaluation of the costs of maintenance of buildings, energy, water); control of waste collection; control of the aesthetics of the building (finishing) and relation of involvement of the neighborhood with the building.
- Mohit and Nazyddah (2011): acoustic comfort; ventilation; accessibility of electricity services, such as quantity of power plug; fire safety; evaluation of the rooms (physical structure); assessment of accessibility of the building, such as presence of suitable corridors, stairs, elevators, parking; building access to community conveniences and control of waste collection.
- Lai and Man (2017): thermal comfort; visual; acoustic; air quality; satisfaction of users and / or professionals; security percentage of the building; building efficiency in relation to maintenance time; evaluation of preventive and corrective maintenance; building costs (maintenance, staffing, site insurance, among others) and control of energy consumption by building users.
- Elyna Myeda et al (2011): Visual comfort (lighting); air quality; building safety; control of the finishes (internal and external) of the building; general maintenance of the building; control of cleaning and electrical and sanitary services; evaluation of the accessibility of the building to the residents, such as stairs, elevators, spaces signaling, parking and control / maintenance of the landscaping and design of the building.

4. CONCLUSIONS

In this paper, a set of criteria established by authors for *building performance evaluation* (BPE) is presented in detail. The systematic review approach, together with the Snowball Sampling technique resulted in the identification of 15 articles. Both bibliometric and the content of these

articles were investigated. The United Kingdom is the country responsible for publishing the largest number of papers in this area, although most of the research conducted and the authors are from the eastern countries like Malaysia and India. The citations of the articles and the punctuation of the respective journals were also verified, realizing that there is a reasonable number of co-citations among the studied subjects.

In addition to the literature search by the BPE criteria, the articles also used practical methods, such as questionnaires, expert consultation, interviews and technical visits to buildings. The articles show a concern in the elaboration of specific criteria for each type of construction instead of establishing criteria for buildings in general. The criteria identified were grouped into 9 dimensions: functional, technical, environment, financial, environmental, physical image / appearance, neighborhood relation, process and leadership. The criteria most used to evaluate a building were the criteria listed in the functional and technical dimensions, such as: thermal comfort, visual (lighting), acoustic, fire safety, air quality, maintenance and cleaning of facilities (sanitary and electrical) of the building.

The authors hope that this research will help those who study the performance evaluation of constructions in order to facilitate the identification and more adequate selection of the studied criteria.

5. ACKNOWLEDGEMENTS

This research was supported by the Post-Graduate Program in Engineering and Civil Construction (PPGECC) at the Federal University of Paraná (UFPR).

6. REFERENCES

- Biernacki, P., Waldorf, D. (1981), “*Snowball Sampling: problems and technique of chain referral sampling*”. Sociological Methods & Research, v.10, n.2, p.141-163. <https://doi.org/10.1177/004912418101000205>
- Elyna Myeda, N., Nizam Kamaruzzaman, S., Pitt, M. (2011), “*Measuring the performance of office buildings maintenance management in Malaysia*”. Journal of Facilities Management, 9(3), 181-199. <https://doi.org/10.1108/14725961111148090>
- Gopikrishnan, S., Topkar, V. M. (2017), “*Attributes and descriptors for building performance evaluation*”. HBRC Journal, Volume 13, Issue 3, December 2017, Pages 291-296. <https://doi.org/10.1016/j.hbrej.2015.08.004>
- Hashim, A. E., Aksah, H., Said, S. Y. (2012). “*Functional assessment through post occupancy review on refurbished historical public building in Kuala Lumpur*”. Procedia-Social and Behavioral Sciences, 68, 330-340. <https://doi.org/10.1016/j.sbspro.2012.12.231>.
- Ibem, E. O., Opoko, A. P., Adeboye, A. B., Amole, D. (2013), “*Performance evaluation of residential buildings in public housing estates in Ogun State, Nigeria: Users' satisfaction perspective*”. Frontiers of Architectural Research, 2(2), 178-190. <http://dx.doi.org/10.1016/j.foar.2013.02.001>.
- Khan, S., Kotharkar, R. (2012), “*Performance evaluation of school environs: Evolving an appropriate methodology building*”. Procedia-Social and Behavioral Sciences, 50, 479-491. <http://dx.doi.org/10.1016/j.sbspro.2012.08.052>
- Khalil, N., Nawawi, A. H. (2008), “*Performance assessment of government and public buildings via post occupancy evaluation*”. Journal Asian Social Science, 4 (9), pp: 103–112. <http://dx.doi.org/10.5539/ass.v4n9p103>
- Khalil, N., Kamaruzzaman, S. N., Baharum, M. R. (2016), “*Ranking the indicators of building performance and the users' risk via Analytical Hierarchy Process (AHP): case of Malaysia*”. Ecological Indicators, 71, 567-576. <http://dx.doi.org/10.1016/j.ecolind.2016.07.032>.

- Kim, S., Yang, I., Yeo, M., Kim, K. (2005), “*Development of a housing performance evaluation model for multifamily residential building in Korea*”. Building and Environment, Volume 40, Issue 8, pp: 1103-1116. <https://doi.org/10.1016/j.buildenv.2004.09.014>
- Kitchenham, B., Brereton, O. P., Budgen, D., Turner, M., Bailey, J., Linkman, J. (2009), “*Systematic Literature Reviews in Software Engineering: a systematic literature review*”. Information and Software Technology, Volume 51, Issue 1, pp: 7-15. <https://doi.org/10.1016/j.infsof.2008.09.009>
- Koleoso, H., Omirin, M., Adewunmi, Y., Babawale, G. (2013), “*Applicability of existing performance evaluation tools and concepts to the Nigerian facilities management practice*”. International Journal of Strategic Property Management, 17(4), 361-376. doi: <https://doi.org/10.3846/1648715X.2013.861367>.
- Lai, J. H., Man, C. S. (2017), “*Developing a performance evaluation scheme for engineering facilities in commercial buildings: state-of-the-art review*”. International Journal of Strategic Property Management, 21(1), 41-57. <http://dx.doi.org/10.3846/1648715X.2016.1247304>.
- Lavy, S., Garcia, J. A., Dixit, M. K. (2010), “*Establishment of KPIs for facility performance measurement: review of literature*”. Facilities, 28 (9/10), 440-464. <https://doi.org/10.1108/02632771011057189>.
- Mohit, M. A., Azim, M. (2012), “*Assessment of residential satisfaction with public housing in Hulhumale’, Maldives*”. Procedia-Social and Behavioral Sciences, 50, 756-770. doi: <https://doi.org/10.1016/j.sbspro.2012.08.078>.
- Meir, I. A., Garb, Y., Jiao, D., Cicelsky, A. (2009), “*Post-occupancy evaluation: an inevitable step toward sustainability*”. Advances in Building Energy Research 3(1), pp:189-219. <https://doi.org/10.3763/aber.2009.0307>
- Meng, X., Minogue, M. (2011), “*Performance measurement models in facility management: a comparative study*”. Facilities, 29 (11/12), 472-484. <https://doi.org/10.1108/02632771111157141>.
- Nazeer, S. F; De Silva, N. (2016), “*TBPE scoring framework for tropical buildings*”. Built Environment Project and Asset Management, Vol. 6 Issue: 2, pp.174-186, <https://doi.org/10.1108/BEPAM-09-2014-0049>.
- Nik-Mat, N. E. M., Kamaruzzaman, S. N., Pitt, M. (2011), “*Assessing the maintenance aspect of facilities management through a performance measurement system: A Malaysian case study*”. Procedia Engineering, 20, 329-338. <https://doi.org/10.1016/j.proeng.2011.11.174>.
- Preiser, W. F. E. (1994), “*Built environment evaluation: conceptual basis, benefits and uses*”. Journal of Architectural and Planning Research, 11 (2), pp: 91–107.
- Steinke, C., Webster, L., Fontaine, M. (2010), “*Evaluating building performance in healthcare facilities: an organizational perspective*”. HERD: Health Environments Research & Design Journal, 3(2), 63-83.
- Støre-Valen, M., Lohne, J. (2016), “*Analysis of assessment methodologies suitable for building performance*”. Facilities, 34(13/14), 726-747.: <https://doi.org/10.1108/F-12-2014-0103>
- Talib, Y., Yang, R. J., Rajagopalan, P. (2013), “*Evaluation of building performance for strategic facilities management in healthcare: A case study of a public hospital in Australia*”. Facilities, Vol. 31 Issue: 13/14, pp.681-701, <https://doi.org/10.1108/f-06-2012-0042>.
- Teicholz, E. (2003), “*Rationale and challenge*”. In: Teicholz, E. (Ed.), *Facility design and management handbook*, The McGraw-Hill Companies, Inc.
- Vischer, J. C. (2008), “*Towards a user centred theory of built environment*”. Journal Building Research & Information. 36 (3) 231–240. <https://doi.org/10.1080/09613210801936472>

Numerical simulation and fire experiment in residential dormitory

R. Tabaczinski¹, C. Corrêa^{1*}, T. Ancelmo Pires¹, J.J. Rêgo Silva¹

*Contact author: cristianocorreacbmpe@gmail.com

DOI: <http://dx.doi.org/10.21041/ra.v9i1.315>

Reception: 29/05/2018 | Acceptance: 06/11/2018 | Publication: 30/12/2018

ABSTRACT

This article presents a computer-made simulation of a fire that had already been done through an experiment in a room that reproduced a bedroom of a one-family residence, which is a typical case of burned construction in the city of Recife (Pernambuco - Brazil). The experimental test of this fire has been presented by Corrêa et al. (2017), and the study presented in this article has as objective to compare the results on the development of the temperature of gases, got from the computer-made simulation with the software Fire Dynamics Simulator (FDS) with the values got by the experiment. We have found out that the temperature obtained through the model developed by the FDS were coherent with the ones obtained by experiment.

Keywords: Buildings' Fire Prevention (BFP); fire in rooms; fire in residences; computer-made fire simulation; fire dynamics simulator.

Cite as: R. Tabaczinski, C. Corrêa, T. Ancelmo Pires, J. J. Rêgo Silva (2019), "Numerical simulation and fire experiment in residential dormitory", Revista ALCONPAT, 9(1), pp. 15 – 29, DOI: <http://dx.doi.org/10.21041/ra.v9i1.315>

¹Universidade Federal de Pernambuco, Brasil.

Legal Information

Revista ALCONPAT is a quarterly publication by the Asociación Latinoamericana de Control de Calidad, Patología y Recuperación de la Construcción, Internacional, A.C., Km. 6 antigua carretera a Progreso, Mérida, Yucatán, 97310, Tel.5219997385893, alconpat.int@gmail.com, Website: www.alconpat.org

Responsible editor: Pedro Castro Borges, Ph.D. Reservation of rights for exclusive use No.04-2013-011717330300-203, and ISSN 2007-6835, both granted by the Instituto Nacional de Derecho de Autor. Responsible for the last update of this issue, Informatics Unit ALCONPAT, Elizabeth Sabido Maldonado, Km. 6, antigua carretera a Progreso, Mérida, Yucatán, C.P. 97310.

The views of the authors do not necessarily reflect the position of the editor.

The total or partial reproduction of the contents and images of the publication is strictly prohibited without the previous authorization of ALCONPAT Internacional A.C.

Any dispute, including the replies of the authors, will be published in the third issue of 2019 provided that the information is received before the closing of the second issue of 2019.

Simulação numérica e experimento de incêndio em dormitório residencial

RESUMO

Este artigo apresenta a simulação computacional de um incêndio realizado experimentalmente em um cômodo que reproduziu um dormitório de residência unifamiliar tipicamente incendiada na cidade de Recife (Pernambuco – Brasil). O ensaio experimental deste incêndio é apresentado por Corrêa et al. (2017), e o estudo discutido neste artigo tem por objetivo comparar os resultados de desenvolvimento de temperaturas dos gases obtidos através da simulação computacional com o software *Fire Dynamics Simulator* (FDS) com as aferições obtidas experimentalmente. Verificou-se que os resultados de temperaturas obtidos através do modelo desenvolvido no FDS foram coerentes com os obtidos experimentalmente.

Palavras-chave: Segurança Contra Incêndios em Edificações (SCIE); Incêndios em cômodos; Incêndios em residências; Simulação computacional de incêndios; *Fire Dynamics Simulator*.

Simulación numérica y experimento de incendio en dormitorio residencial

RESUMEN

Este artículo presenta la simulación computacional de un incendio previamente realizado como un experimento en una habitación que reproducía un cuarto de residencia unifamiliar, y ejemplo típico de construcción incendiada en la ciudad de Recife (Pernambuco - Brasil). El ensayo experimental de este incendio es presentado por Corrêa *et al.* (2017), y el estudio discutido en este artículo tiene por objetivo comparar los resultados del desarrollo de las temperaturas de los gases obtenidos a través de la simulación computacional con el software *Fire Dynamics Simulator* (FDS) con las medidas obtenidas en el experimento. Se ha verificado que los resultados obtenidos a través del modelo desarrollado en el FDS han sido coherentes con los obtenidos experimentalmente.

Palabras-clave: Seguridad Contra Incendios en Edificaciones (SCIE); Incendios en habitaciones; Incendios en residencias; Simulación computacional de incendios; *Fire Dynamics Simulator*.

1. INTRODUCTION

Fires are tragic events that happen frequently in Brazil and around the world, possessing a great destructive potential of patrimony and lives. According to the study carried out by Corrêa et al. (2015) on the occurrence of fires in the city of Recife (Pernambuco – Brazil) in years 2011-2013, about 33% of the occurrences of these events were in buildings. Of this percentage, about 40% corresponds to residential buildings, and the great majority of these events, approximately 75%, occur in single-family homes. According to the authors, this fact is worrying, since in Brazil this type of building does not have preventive normative guidelines on Fire Safety, showing the need for investment in research in this area of knowledge.

Studies of the behavior and development of fires in buildings are of importance to assist researchers in understanding this phenomenon. With these studies, it's possible, among others, to estimate temperatures and predict the movement of smoke in burned buildings before the occurrence of the incident, helping in the development of strategies aimed at protecting the life of its occupants and the patrimony.

The computer simulation is a tool that presents great potential in the aid of studies on Building Fire Prevention (BFP), providing the researcher with a better understanding of the behavior of this phenomenon. Nowadays, the use of this tool is a common practice among researchers in this area around the world. However, in Brazil, the use of software for this purpose is still not widespread, a fact that results in a scarce availability of literature to aid in their understanding and use (Tabaczenski, *et al.*, 2017a).

In sum, fire simulation software ‘scan be based on the zone model, such as *software OZone*, developed by *University of Liège*, and the *Consolidated Model of Fire and Smoke Transport (CFAST)*, developed by *National Institute of Standards and Technology* from United States of America (NIST/EUA), or, based on computational fluid dynamics model, as the *software Fire Dynamics Simulator (FDS)*, also developed by NIST, and the *SMARTFIRE*, developed by *University of Greenwich*.

From the fire simulation software, the SDS is the most used in technical-scientific research, and consequently the richest in available literature. Since the beginning of dissemination, in the year of 2000, it has been widely used in BFP studies worldwide. In Brazil, the first publications of research carried out with the aid of this software date back to the year of 2008 and, gradually, it has gained space in the technical-scientific environment as a tool to support studies aimed at both diagnosis and for predictions of buildings in a situation of fire.

Due to insufficient knowledge of the properties of materials (mainly combustible materials), and of complete pyrolysis and combustion behavior of these materials, there is still a need for improvements in simulation techniques in this software. Therefore, full-scale experimental fire tests are of importance to improve knowledge about the behavior of this phenomenon, allowing the comparison of measured measurements with the numerical results, in order to improve the precision of the developed models (Byström *et al.*, 2012).

In order to demonstrate some of the potential uses of SDS in aid of BFP studies, this study aims to develop a computer model capable of reproducing the development of temperatures in the first minutes of a fire experimentally performed by Corrêa *et al.* (2017), in a room that represented a dormitory belonging to single-family residences typically burned in the city of Recife.

1.1 Bibliographic Review

In the world panorama, several studies of SCIE have been using experimental tests to calibrate the models of computational simulation of fires developed in the FDS (McGrattan *et al.*, 2013; WANG *et al.*, 2016; YU LONG-XING *et al.*, 2018). Byström *et al.* (2012), carried out an experimental fire test with wood pieces under low ambient temperature in a two-story concrete building and later developed a computational model of this experiment in the FDS. The experimental results of the development of temperatures were compared with the results of the numerical simulations, showing that the developed model presented results consistent with those obtained experimentally. Yuen *et al.* (2014), conducted some experimental fire tests in a fully furnished dormitory and later developed a computational model of this scenario in the FDS. The analysis of the results showed that the computational model was able to provide predictions of temperature, heat flow, and propagation of fire and smoke consistent with those obtained experimentally.

Among the studies carried out in Brazil, a predominance of prognostic analyzes is noticed and there is a lack of experimental studies that can help in the validation of the developed computational models. Despite this, some studies have used experimental tests found in the literature to calibrate the models developed in the FDS. (Tabaczinski *et al.*, 2017a)

Centeno *et al.* (2015) developed a computational model of a confined pool fire in a residential environment, based on an experimental study found in the literature. With this study, the authors observed that the temperature profile obtained with the FDS agreed with the experimental results, demonstrating the software's ability to reproduce the fire studied.

Tabaczinski *et al.* (2017b) developed a computational model of a fire in a subdivision representing an office, based on an experimental essay found in the literature. With this study the authors verified that the knowledge and application of the thermal properties not only of the combustible materials but also of the incombustible materials involved in a computational simulation in the FDS is of importance to obtain results consistent with the real situations. Therefore, the results obtained showed that, when properly calibrated, the models developed in the software can return reliable predictions of the development of gas temperatures in fire scenarios.

2. EXPERIMENTAL STUDY

The experimental study is presented by Corrêa *et al.* (2017). In this study, an analysis of the development of temperatures resulting from a fire in a room belonging to the ground floor of the Fire Fighting Training Workshop was carried out, within the Center for Teaching and Instruction of the Fire Brigade of Pernambuco. This room was adapted to reproduce a dormitory similar to those belonging to single-family dwellings typically burned in the city of Recife, according to the survey of Corrêa *et al.* (2016).

The fire load of this dormitory was materialized through the furniture and objects determined in the research of Corrêa *et al.* (2016), based on the mapping of fires in buildings in this city during the triennium of 2011-2013 conducted by Corrêa *et al.* (2015). Figure 1 shows the internal dimensions and furniture of this dormitory.



Figure 1. Dormitory burned in the study conducted by Corrêa *et al.* (2017).

These furniture and objects had their dimensions and weight measured to, through the calorific potential of the predominant materials in their composition, determine the value of the fire load present in the dormitory. The calorific value of the materials was obtained through the CBMSC IN 003 (2014) and, with this, it was concluded that the fire load present in this dormitory was 499,56 MJ/m² (Corrêa *et al.*, 2017).

The structure of this dormitory, as well as of the whole building, is reinforced concrete; the floor is simple concrete and the pre-shaped slab is lined with ceramic tiles and concrete cover. The walls of the dormitory are made of non-structural ceramic bricks, externally lined with cement mortar and internally with different materials, such as: cement slab (walls P1 e P4), plaster mortar (wall P2) e cement mortar (wall P3) (Corrêa *et al.*, 2017).

The ignition of the fire occurred through a paraffin device for igniting fireplaces positioned under the lower bed of the bunk. For temperature gauging, 24 K type thermocouples were installed, distributed in the furniture, center and walls of the compartment as shown in Figure 2.

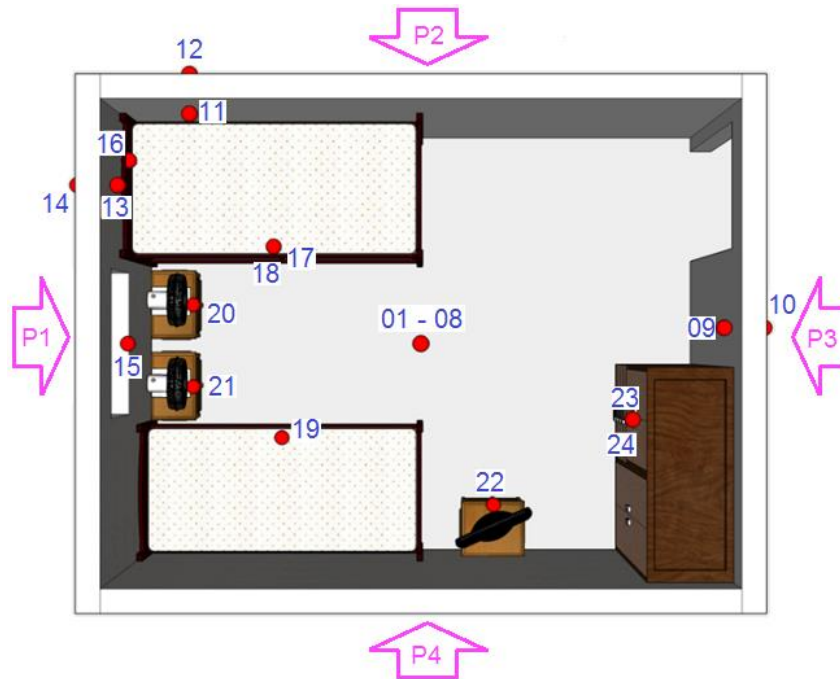


Figure 2. Distribution of the thermocouples in the compartment tested by Corrêa *et al.* (2017).

During the 48-minute experimental test, the window belonging to the burning dormitory was fully opened while the door remained closed for the first few minutes, causing the fire to be controlled by ventilation and to develop combustion and exhaust cycles. At 18 minutes, in order to prevent the natural extinction of the fire, the compartment door was opened, providing a cross ventilation, bringing the heat flow quickly to the compartment adjacent to the test. However, despite this strategy, there was no generalization of the fire, instead, after a few more cycles of combustion and exhaustion it went into decline until a fire fighting team of the fire department entered the environment promoting the extinguishing of the flame's remnants and wall cooling (Corrêa, *et al.* 2017).

3. COMPUTATION MODEL DEVELOPED IN THE FDS

The development of the computational model in FDS was done in order to reproduce in the best possible way the experimental test carried out by Corrêa *et al.* (2017). The input parameters and strategies adopted to develop the model were based on the event's chronology, geometry and specificities of the building, observation of environmental conditions and relevant technical standards.

The FDS is a CFD model-based fire simulation software that, among other things, allows the achievement of gas temperatures and solid objects, as well as graphically represent the behavior of fire propagation and smoke movement throughout the simulated building. In this software it is possible to simulate several rooms at the same time, allowing to perform analyzes not only in the room that is set on fire but also in the adjacent ones. Thus, to perform a closer analysis of reality, all the ground floor of the building used to carry out the experimental study was considered in the computational model developed in the FDS. Figure 3 shows the schematic diagram of the ground floor of the building where the experimental test took place.

Table 1. Thermal properties of non-combustible materials used in computational simulations.

Material	Density (kg/m ³)	Thermal conductivity (W/m.K)	Specific heat (kJ/kg.K)	Emissivity
Ceramic Brick	1400	0.90	0.92	0.90
Plaster Mortar	1200	0.70	0.84	0.90
Cement Mortar	2000	1.15	1.00	0.90
Concrete	2300	1.75	1.00	0.90
Steel	7800	55.00	0.46	0.70

Analogously to the experimental study, the computational simulation of the walls of the dormitory was considered with different internal coatings. Due to the impossibility of representing the roughness resulting from the cementitious slab, this was described in the software as being a layer of cement mortar with a smaller thickness than the other layers composed by this material. The thicknesses and materials that made up the layers of walls, ceiling and floor are shown in Table 2. From this table, Layer 1 is the inner layer, Layer 2 is the middle layer and Layer 3 is the outer layer to the compartment. The other walls of the building were assumed with the same characteristics of the wall P3. It should be noted that these thicknesses are independent of the dimensions of the mesh adopted.

In the absence of parameters indicated by Corrêa *et al.* (2017) and, due to the difficulty of obtaining thermal properties of all the combustible materials present in the experimental test, to model the fire in the room was considered a simplified strategy where the fire load was materialized by wooden rafters, distributed in the environment according to the distribution of the experimental objects, whose thermal properties were: density, thermal conductivity and specific heat, with respective values of 400 kg/m³, 0.12 W/m.K and 1.34 kJ/kg.K, defined according to the instructions of ABNT NBR 15220-2 (2005); Emissivity, with adopted value of 0.9; calorific power of 17500 kJ/kg, defined according to the indications of NP EN 1991-1-2 (2010); ignition temperature of 210 °C, according to the study by Figueroa & Moraes (2009); heat release rate of 100 kW/m², according to the study of Rocha (2014).

Table 2. Thickness and materials of walls layers, roof and soil of simulated compartment.

Side	Layer 1		Layer 2		Layer 3	
	Thickness (cm)	Material	Thickness (cm)	Material	Thickness (cm)	Material
Wall P1	2.5	Cement Mortar	10.0	Ceramic Brick	2.5	Cement Mortar
Wall P2	2.5	Plaster Mortar	10.0	Ceramic Brick	2.5	Cement Mortar
Wall P3	2.5	Cement Mortar	10.0	Ceramic Brick	2.5	Cement Mortar
Wall P4	1.0	Cement Mortar	10.0	Ceramic Brick	2.5	Cement Mortar
Roof	7.0	Ceramic Brick	3.0	Concrete		
Floor	10.0	Concrete				
Door	0.03	Steel				

The geometry of the model developed for computational fire simulation in FDS is shown in Figure 4.

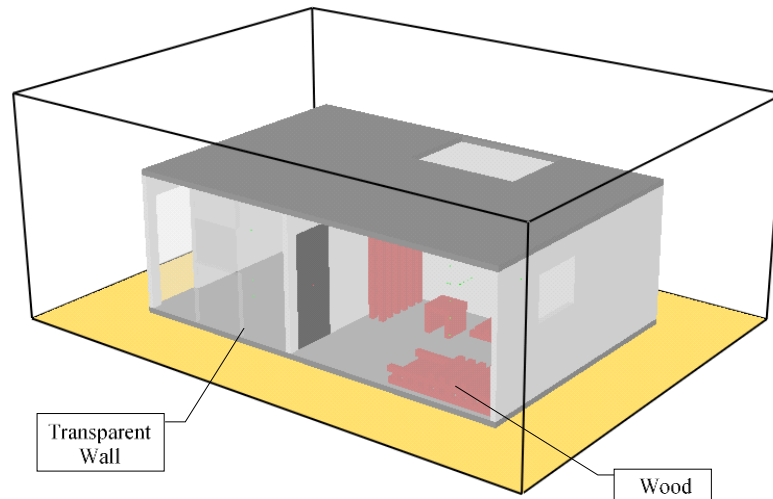


Figure 4. Model developed in FDS.

In simulations of fires in the FDS, it is necessary to define a gaseous fuel reaction that will act as a substitute for all potential fuel sources. If this reaction is not defined in the standard software library, the user can specify the chemical formulation of the fuel along with the CO, soot, and other related parameters. (McGrattan *et al.*, 2016). In the model developed in this study, the wood fuel was represented by the chemical formulation $\text{CH}_{1.7}\text{O}_{0.74}\text{N}_{0.002}$, yields of carbon monoxide and soot of 0.004 kg/kg e 0.015 kg/kg respectively. These yields are expressed in amount of carbon monoxide and soot emitted per unit mass of fuel consumed (Weinschenk *et al.*, 2014).

To account for the ignition of the fire that occurred through the paraffin device in the experimental test of Corrêa *et al.* (2017), a burner was used similarly to the device in the experimental test. This burner was deactivated after 150 seconds, releasing approximately 0.06% of the total fire load, and had the function of only starting the fire. As a result, the increase in temperature generated a chain reaction, causing the fire to spread through the burning of the wooden rafters that combust after reaching their respective ignition temperature.

To obtain readings of the temperatures developed during the fire, some meters positioned similarly to the thermocouples were inserted in the experimental test (see Figure 2). The following thermocouples: 01 – 08 (gas in the center of the room), 09 e 10 (internal and external faces of the wall P3), 11 e 12 (inner and outer faces of wall P2), and, 13 e 14 (internal and external faces of the wall P1).

As in the experimental test, in this computational simulation the window of the burned dormitory was considered open during the whole simulation, while the door was opened only at 18 minutes. During this time, between the start of the fire and the opening of the door, in the experimental test the maximum temperatures varied between 600 °C and 800 °C. Under these temperature conditions the integrity of human life would have already been corrupted. Thus, in the comparison of the obtained results, this study was stopped at the initial minutes of the fire until the door opening, as shown below.

4. RESULTS

As in the experimental test, in the computer simulation performed through the FDS software (up to 18 minutes) there was no generalization of the fire (Flashover). This was due to the depletion of oxygen in the environment, since with the closed door there was no cross ventilation that could provide enough supply of the combustion agent for fire development. In this way, as can be observed in the Figure 5, the fire was restricted to the wooden rafters that represented the bunk present in the experimental test. In this figure the smoke was concealed for the purpose of visualizing the fire only.

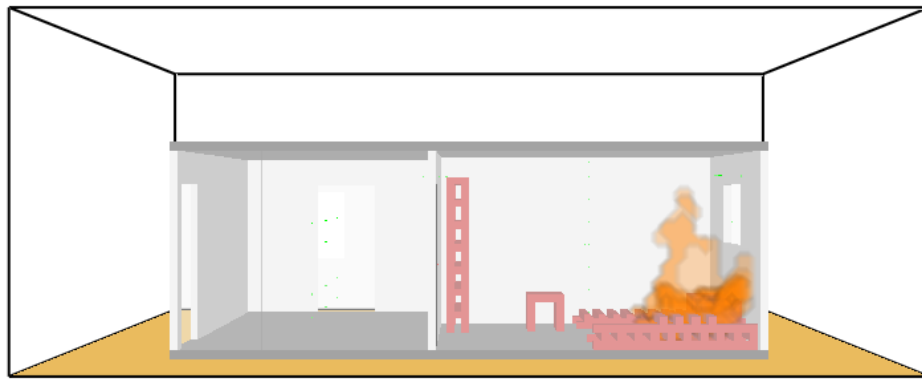


Figure 5. FDS computational simulation - Fire propagation.

As in the experimental test, it was observed that in less than 5 minutes the room was totally taken up by smoke, as can be observed in the Figure 6.

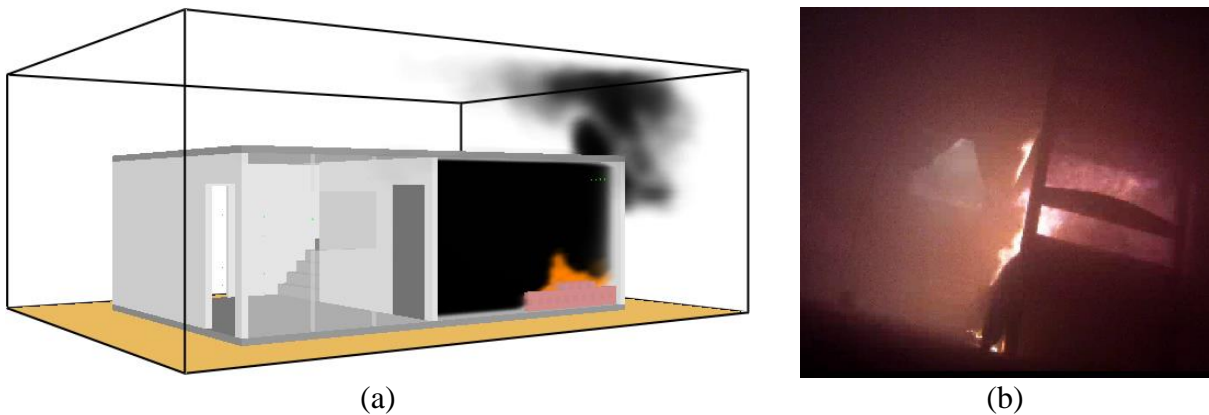


Figure 6. Spread of smoke within 4 minutes of fire: (a) Computer simulation in FDS; (b) Experimental test by Corrêa *et al.* (2017).

In the computational simulation the combustion and exhaust cycles were not observed as in the experimental test presented by Corrêa *et al.* (2017). Despite this, in general it was observed that the temperatures obtained with the developed model were close to the average temperatures obtained in the experimental test. Figure 7 shows the temperatures of the gases obtained through the thermocouple 08, positioned just below the compartment ceiling (top layer), the computer simulation in the FDS and the experimental test.

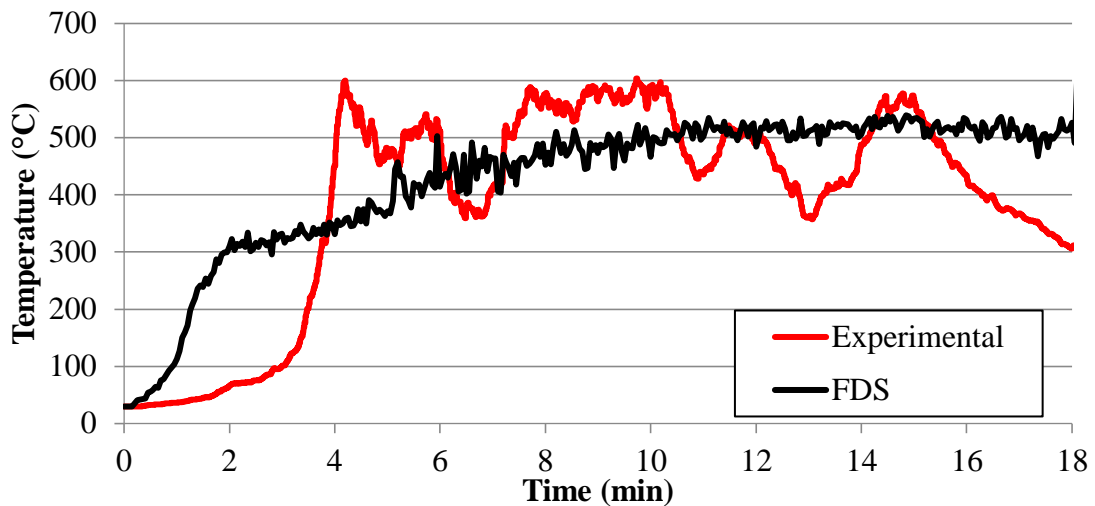


Figure 7. Gas temperatures in the upper layer of the compartment (thermocouple 08).

In the computational simulation, there is a rapid growth of temperatures up to 2 minutes, reaching 300 °C, after that the growth occurs more slowly until reaching the level of 500 °C at 6 minutes. In the experimental test this sudden growth occurs between 2 and 4 minutes until the dormitory is taken up by the smoke promoting a gas saturation in the environment, after which the combustion and exhaust cycles begin, culminating in peaks up to 600°C and valleys up to 360°C in temperature. This behavior is repeated at all measuring points in the center of the room. Figure 8 shows the temperatures of gases obtained through thermocouple 04, positioned at a height of 120 cm from the floor of the compartment (intermediate layer).

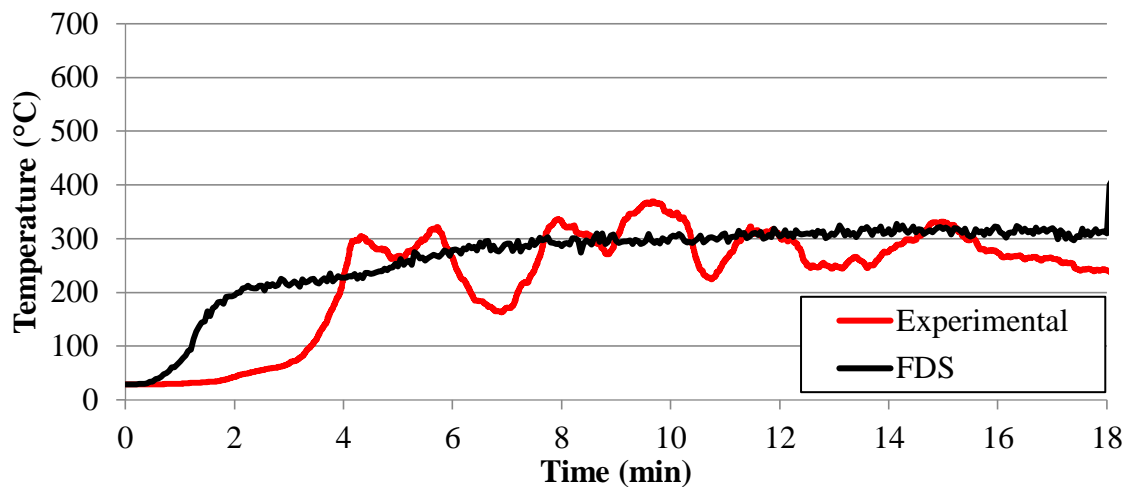


Figure 8. Gas temperatures in the intermediate layer of the compartment (thermocouple 04).

In the middle layer of the compartment the differences in results: experimental and computational become more discreet. It is observed that in the experimental test the maximum temperature is reached at 10 minutes with 360 °C. In this same moment in the computational simulation the measured temperature is of 300 °C.

In the lowest layer of the compartment the values are reversed. At this point, the temperatures measured through the computational simulation become larger than those measured experimentally, yet the difference between these values always remains between 50 °C and 100 °C. Figure 9 shows the temperatures of gases obtained through thermocouple 01, positioned at a height of 30 cm from the floor of the compartment (lower layer).

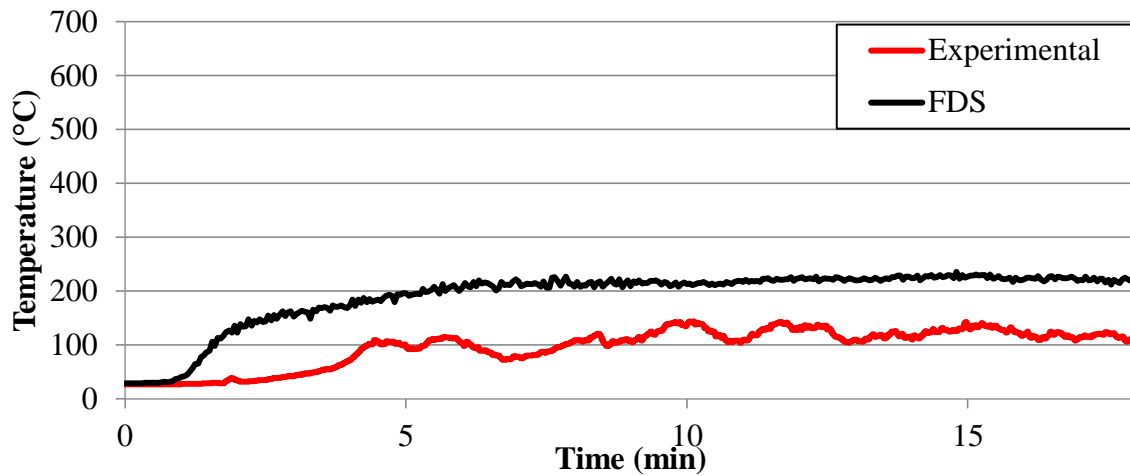


Figure 9. Gas temperatures in the lower layer of the compartment (thermocouple 01).

As seen through the Figure 7, Figure 8 and Figure 9, the computational simulation presented results of more homogeneous temperatures along the height of the compartment. From these results, it is possible to draw some temperature profiles obtained in the center of the studied compartment, as shown in Figure 10.

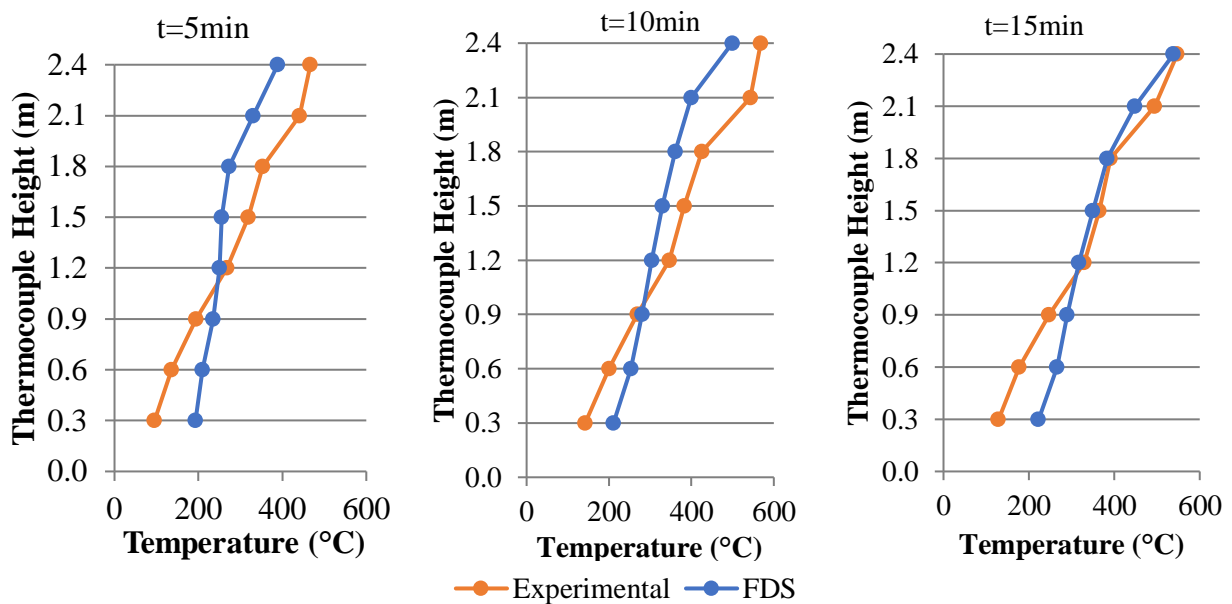


Figure 10. Temperature profiles in the center of the room (thermocouples 01 to 08).

It is observed that, in the lower layers of the dormitory, the results of temperatures obtained through the computational simulation were generally higher than those obtained experimentally. In the upper layers this behavior is inversely, that is, the results obtained experimentally were generally higher than those obtained through the computational simulation.

Although the computational simulation provides a less expressive temperature gradient, it is evident the difference between the analyzed heights. At 15 minutes of simulation, the lowest layer of the compartment (30 cm from the floor) is 220 °C, while the uppermost layer (close to the ceiling, 240 cm from the floor) is 540 °C, behavior resulting from the convection of hot gases into the environment.

Figure 11 shows the temperature profile in the XZ plane of the computational domain in the center of the flared dormitory at 15 minutes of simulation.

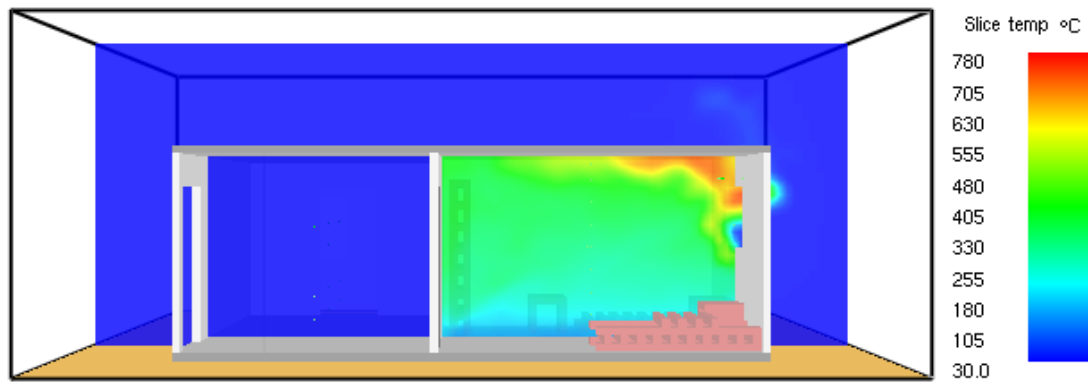


Figure 11. Temperature profile in the XZ plane in the center of the dormitory (Time = 15 min).

Through this profile it is possible to visualize the temperature gradient developed in the entire XZ plane in the dormitory due to the convection of the gases in the environment. It is evident that the maximum temperatures occur close to the window that was open. In this same place you can also see a small entrance of fresh air coming from outside the building.

As for the measured temperatures on the wall faces, due to measurement uncertainties, thermocouples were positioned analogously to the experimental test, providing the gauging of temperatures that were actually absorbed by the walls through the thermal radiation of the fire, and, in addition thermocouples were placed a few centimeters apart from their faces, allowing the measurement of temperatures in the gases close to them.

In the analysis of the results, it was verified that the temperatures captured in the computational simulation that more closely approximated those obtained experimentally were the ones measured in the gases near the walls, and not in the face of the same ones. Figure 12 shows the development of measured temperatures in the wall P3, whose inner coating was cement mortar.

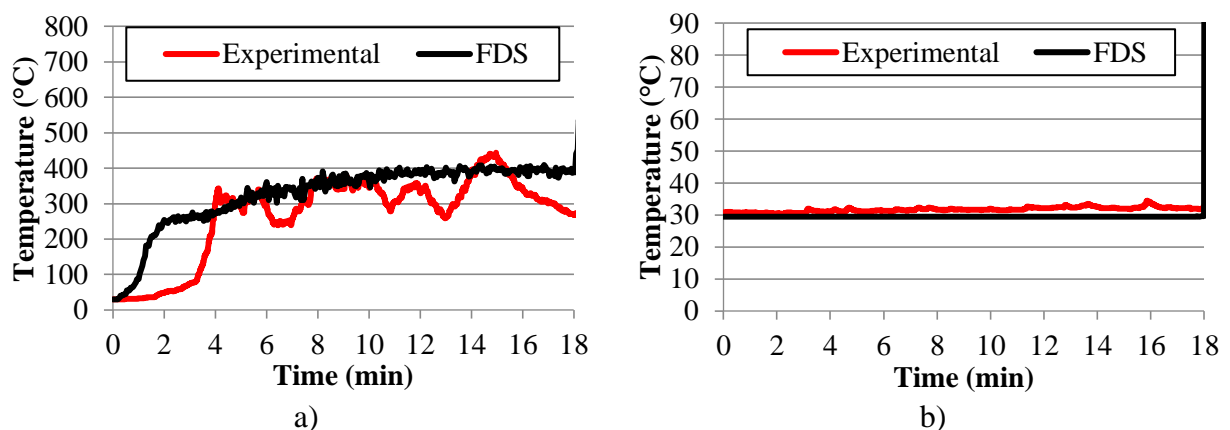


Figure 12. Temperatures measured on the wall P3: (a) internal face (thermocouple 09); (b) external face (thermocouple 10).

In the inner face of the wall (face exposed to fire), the maximum temperatures developed were 400 °C, value very close to that obtained experimentally. In the external face of the wall, the measured temperatures, both computationally and experimentally, did not exceed 35 °C.

Figure 13 and Figure 14 show the development of measured temperatures in the walls P2 and P1, whose internal coating was gypsum mortar and cement slab respectively.

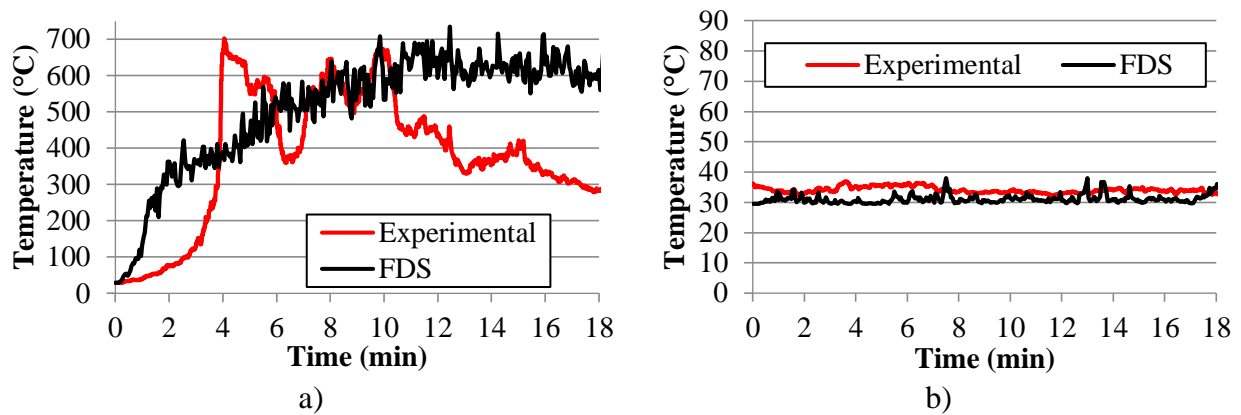


Figure 13. Temperatures measured on the wall P2: (a) internal face (thermocouple 11); (b) external face (thermocouple 12).

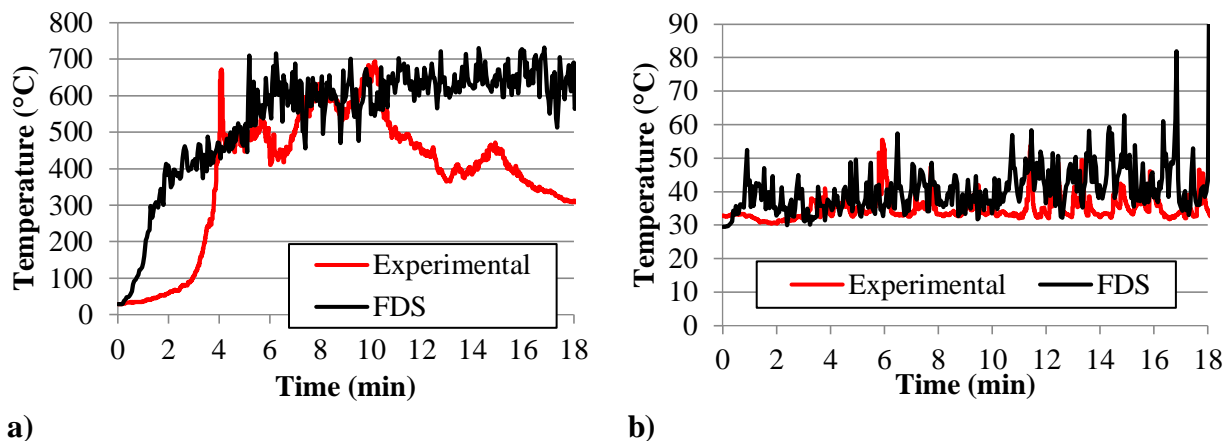


Figure 14. Temperatures measured on the wall P1: (a) internal face (thermocouple 13); (b) external face (thermocouple 14).

On the inner faces of the walls (faces exposed to fire), the maximum temperatures developed were approximately 700 °C, value very close to that obtained experimentally. In these measurements there is a greater oscillation in the results on the outer faces of the walls, especially on the wall P1. Vvm. This fact is justified by the thermocouples being positioned near the dormitory window. Thus, due to the incidence of the wind in the place, this meter gauged the temperatures coming from the convection of the gases that left the dormitory.

In the external face of the wall P2, the measured temperatures, both computationally and experimentally, did not exceed 38 °C. In wall P1 the difference between the results was slightly higher: In the experimental test, the maximum temperature recorded was 65 °C, while in computer simulation this value was 82 °C.

5. CONCLUSIONS

This study presented the computational simulation of a fire in dormitory of single-family homes typically burned in the city of Recife (Pernambuco, Brazil), whose experimental trial was presented by Corrêa *et al.* (2017).

The computational simulation was performed through the FDS software and had as objective the analysis of the development of temperatures in the dormitory set fire. In view of the results presented, the following conclusions can be:

- As in the experimental test, there was no generalization of the fire due to oxygen depletion in the environment;

- The computational simulation did not present cycles of combustion, intense gas production and exhaustion as in the experimental test. The occurrence of this behavior raised two hypotheses: (1) the admission of simplified strategies for model development does not contemplate all the phenomena that occurred in the experimental test, due to the absence of oxygen and excess smoke in the compartment. It should be emphasized that in the FDS there is the possibility of insertion of numerous physical-chemical properties of the materials, which allow a more accurate characterization of these in a computational simulation, however, these properties are difficult to obtain, making such refinement also difficult to execute; (2) the FDS combustion model is not suitable for scenarios in which there is no oxygen in the compartment, leading to the computational simulation under this condition to develop a behavior different from the experimental test;
- In the lower layers of the dormitory, the temperature results obtained through the computational simulation were generally higher than those obtained experimentally. In the upper layers, the experimental results were generally higher than those obtained through computational simulation;
- The maximum temperatures developed in the fire occurred near the dormitory window, which is the only source of supply of fire retardant in the initial 18 minutes of the experimental test;
- In the center of the dormitory, the highest temperature measured was 530 °C close to the ceiling (240 cm from the floor), at 15 minutes of simulation;
- On the walls, the highest measured temperatures were approximately 730 °C after 10 minutes of simulation, on the inner faces of walls P1 and P2. This behavior was already expected, since these were the closest to the initial focus of the fire;
- Despite the simplified strategy adopted, the developed temperatures were close to the average temperatures obtained in the experimental test, showing that, despite not faithfully reproducing the behavior of the actual fire, the developed model was able to represent results consistent with the temperatures developed during the fire.

6. ACKNOWLEDGEMENT

The authors thank the Coordination of Improvement of Higher Education Personnel (CAPES) for the promotion of this research.

7. REFERENCES

- Associação Brasileira de Normas Técnicas (2005), *ABNT NBR 15220-2:Desempenho térmico de edificações - Parte 2: Métodos de cálculo da transmitância térmica, da capacidade térmica, do atraso térmico e do fator solar de elementos e componentes de edificações*. Rio de Janeiro.
- Byström, A., Cheng, X., Wickström, U., Veljkovic, M. (2012), *Full-scale experimental and numerical studies on compartment fire under low ambient temperature*. Building and Environment, v.51, p. 255-262.
- Centeno, F. R., Cassol, F., Rodrigues, E. E. C. (2015), *Validação de modelagem numérica empregando o Software Fire Dynamics Simulator para um ambiente habitacional em situação de incêndio*. In: 3º Congresso Ibero-Latino-Americano sobre Segurança Contra Incêndios (3º CILASCI), Porto Alegre – RS (Brasil).
- Corrêa, C., Silva, J. J. R., Oliveira, T. A. C. P., Braga, G. C. (2015), *Mapeamento de Incêndios em Edificações: um estudo de caso na cidade do Recife*. Revista de Engenharia Civil IMED, Passo Fundo – RS (Brasil), v.2 n.3, p. 15-34.

- Corrêa, C., Silva, J. J. R., Pires, T. A., Braga, G. C., Melo, I. A. V. (2018), *Edifício Modal: Uma representação para o Estudo de Incêndios na cidade de Recife*. Revista Cientec, Recife – PE (Brasil), v.10, n.2, p.01-10.
- Corrêa, C., Braga, G. C., Junior, J. B., Silva, J. J. R., Tabaczinski, R., Pires, T. A. (2017), *Incêndio em compartimento de residência na Cidade do Recife: Um estudo experimental*. Revista ALCONPAT, 7(3), p. 215-230
- Figuroa, M. J. M., Moraes, P. D. (2009), *Comportamento da madeira a temperaturas elevadas*. Ambiente Construído, Porto Alegre – RS (Brasil), v. 9, n. 4, p. 157-174.
- Instituto Nacional de Meteorologia – INMET (2017), *Estações automáticas - gráficos*. Brasil. Disponível em: <http://www.inmet.gov.br/portal/index.php?r=home/page&page=rede_estacoes_auto_graf>. Acessado em: 20 mar. 2017.
- McGrattan, K. B., McDermott, R. J., Weinschenk, C. G., Forney, G. P. (2013), *Fire dynamics simulator, technical reference guide*. Special Publication (NIST SP) – 1018, <https://dx.doi.org/10.6028/NIST.sp.1018>
- McGrattan, K., Hostikka, S., McDermott, R., Floyd, J., Weinschenk, C., Overholt, K. (2016), *Fire Dynamics Simulator – User’s Guide: Sixth Edition*. NIST – Special Publication 1019: National Institute of Standards and Technology – NIST & Technical Research Centre of Finland – VTT, Maryland (EUA).
- Norma Portuguesa (2010), *NP EN 1991-1-2: Acções em estruturas Parte 1-2: Acções gerais Acções em estruturas expostas ao fogo*. Caparica (Portugal).
- Rocha, M. A. F. (2014), *Determinação experimental de propriedades de combustão de madeiras maciças brasileiras*. Dissertação de Mestrado em Engenharia Civil, Programa de Pós-graduação em Engenharia Civil, Universidade Federal do Rio de Janeiro – UFRJ, Rio de Janeiro – RJ (Brasil), pp. 147.
- Tabaczinski, R., Corrêa, C., Santos, M. M. L., Pires, T. A. C., Silva, J. J. R. (2017), *Aplicação do Software Fire Dynamics Simulator (FDS) no Estudo da Segurança Contra Incêndios (SCI) no Brasil*. Revista Flammae, Recife – PE (Brasil), v.3, n.7, p.87-116, 2017.
- Tabaczinski, R., Pires, T. A. C., Silva, J. J. R., Negreiros, R. (2017), *Simulação computacional de um incêndio natural compartimentado: validação com um estudo experimental*. In: 4º Congresso Ibero-Latino-Americano sobre Segurança Contra Incêndios (4º CILASCI), Recife – PE (Brasil).
- Wang, X., Fleischmann, C., Spearpoint, M. (2016), *Assessing the influence of fuel geometrical shape on fire dynamics simulator (FDS) predictions for a large-scale heavy goods vehicle tunnel fire experiment*. Case Studies in Fire Safety, v. 5, p. 34-41.
- Weinschenk, C. G., Overholt, K. J., Madrzykowski, D. (2014), *Simulation of an Attic Fire in a Wood Frame Residential Structure -Chicago, IL*. NIST – Technical Note 1838: National Institute of Standards and Technology (EUA), pp. 39.
- Yu, L.-X., Beji, T., Maragkos, G., Liu, F., Weng, M.-C., Merci, B. (2018), *Assessment of Numerical Simulation Capabilities of the Fire Dynamics Simulator (FDS 6) for Planar Air Curtain Flows*. Fire Technology, Volume 54, Issue 3, pp 583–612, <https://doi.org/10.1007/s10694-018-0701-7>
- Yuen, A. C. Y., Yeoh, G. H., Alexander, R., Cook, M. (2014), *Fire scene reconstruction of a furnished compartment room in a house fire*. Case Studies in Fire Safety, v.1, p. 29-35.

Influence of anchorage on flexural strength of beams strengthened with CFRP sheets

M. P. Ferreira^{1*} , M. H. Oliveira² , A. F. Lima Neto³ , L. S. Tapajós⁴ ,
A. J. C. Nascimento⁵ , M. C. Freire³ 

*Contact author: mpinaf@gmail.com

DOI: <http://dx.doi.org/10.21041/ra.v9i1.269>

Reception: 29/09/2017 | Acceptance: 18/10/2018 | Publication: 30/12/2018

ABSTRACT

In order to evaluate the influence of anchorage on the flexural strength of beams strengthened with Carbon Fiber Reinforced Polymer (CFRP) sheets, the experimental results of 126 tests in the literature and of an unprecedented series with 4 reinforced concrete beams, tested by these authors, were analyzed. The parameters affecting the performance and the strength of the beams are evaluated, and the design criteria of fib Bulletin 14 (2001) and ACI 440-2R (2008) are discussed. It was observed that, even with auxiliary devices in the PRFC anchorage, premature failure is possible, and that both theoretical recommendations lead to safe estimates, but excessively conservative in cases where the anchorage of the PRFC sheet is properly done.

Keywords: reinforced concrete; flexural strengthening; CFRP sheets; anchorage.

Cite as: M. P. Ferreira, M. H. Oliveira, A. F. Lima Neto, L. S. Tapajós, A. Nascimento, M. C. Freire (2018), "Influence of anchorage on flexural strength of beams strengthened with CFRP sheets", Revista ALCONPAT, 9 (1), pp. 30 – 47, DOI: <http://dx.doi.org/10.21041/ra.v9i1.269>

¹ Civil Engineering Department, Federal University of Pará, Belém, Brazil.

² Civil and Environmental Engineering Department, University of Brasília, Brasília, Brazil.

³ Nucleus of Amazonian Development in Engineering, Federal University of Pará, Tucuruí, Brazil.

⁴ Civil Engineering Department, Federal University of the West of Pará, Itaituba, Brazil

⁵ Post-graduation in Civil Engineering, Federal University of Pará, Belém, Brazil.

Legal Information

Revista ALCONPAT is a quarterly publication by the Asociación Latinoamericana de Control de Calidad, Patología y Recuperación de la Construcción, Internacional, A.C., Km. 6 antigua carretera a Progreso, Mérida, Yucatán, 97310, Tel.5219997385893, alconpat.int@gmail.com, Website: www.alconpat.org

Responsible editor: Pedro Castro Borges, Ph.D. Reservation of rights for exclusive use No.04-2013-011717330300-203, and ISSN 2007-6835, both granted by the Instituto Nacional de Derecho de Autor. Responsible for the last update of this issue, Informatics Unit ALCONPAT, Elizabeth Sabido Maldonado, Km. 6, antigua carretera a Progreso, Mérida, Yucatán, C.P. 97310.

The views of the authors do not necessarily reflect the position of the editor.

The total or partial reproduction of the contents and images of the publication is strictly prohibited without the previous authorization of ALCONPAT Internacional A.C.

Any dispute, including the replies of the authors, will be published in the third issue of 2019 provided that the information is received before the closing of the second issue of 2019.

Influência da ancoragem na resistência à flexão de vigas reforçadas com mantas de PRFC

RESUMO

Buscando avaliar a influência da ancoragem na resistência à flexão de vigas reforçadas com mantas de Polímero Reforçado com Fibra de Carbono (PRFC), foram analisados os resultados experimentais de 126 ensaios presentes na literatura e de uma série inédita, ensaiada pelos autores, com 4 vigas de concreto armado. São avaliados os parâmetros que afetam o desempenho e a resistência das vigas, e discutidos os critérios de dimensionamento do fib Bulletin 14 (2001) e ACI 440-2R (2008). Observou-se que, mesmo com dispositivos auxiliares na ancoragem do PRFC, falhas prematuras são possíveis, e também que ambas as recomendações teóricas conduzem a estimativas a favor da segurança, porém excessivamente conservadoras nos casos onde a ancoragem da manta de PRFC é feita adequadamente.

Palavras-chave: concreto armado; reforço à flexão; mantas de PRFC; ancoragem.

Influencia del anclaje en la resistencia a la flexión de vigas reforzadas con mantas de PRFC

RESUMEN

Buscando evaluar la influencia del anclaje en la resistencia a la flexión de vigas reforzadas con mantas de Polímero Reforzado con Fibra de Carbono (PRFC), se analizaron los resultados experimentales de 126 ensayos presentes en la literatura y de una serie inédita de los autores, con 4 vigas de hormigón armado. Se evalúan los parámetros que afectan desempeño y resistencia de vigas, y se discuten los criterios de dimensionamiento del fib Bulletin 14 (2001) y ACI 440-2R (2008). Se observó que, incluso con dispositivos auxiliares en el anclaje del PRFC, fallos prematuros son posibles, y que ambas recomendaciones conducen a estimaciones seguras, pero excesivamente conservadoras en los casos en que el anclaje de la manta de PRFC se realice adecuadamente.

Palabras clave: hormigón armado; refuerzo de la flexión; mantas de PRFC; fondeadero.

NOMENCLATURE

a	– shear span	f_s'	– steel strength of the compressed reinforcement
b_f	– width of the layer of CFRP	f_{ys}	– yield strength of the tensile reinforcement
b_w	– width of the beam	f_{ys}'	– yield strength of the compressed reinforcement
c	– height of the block of rectangular compression equivalent of the concrete	h	– height of the beam
c_1	– factor obtained by calibration of results (equal to 0.64 for CFRP)	k_b	– geometric factor
d	– effective beam height	k_c	– constant that considers the compacting of the concrete during the concreting
d'	– centroid position of the compressed reinforcement	l_b	– anchoring length of the CFRP sheet
f_c	– concrete compression strength	l	– clamping width
f_{ctm}	– average tensile strength of concrete	n	– number of layers of CFRP
f_{fe}	– effective strength of the CFRP	t_f	– thickness of the CFRP
f_s	– strength in the steel of the tensile reinforcement	x	– position of the neutral axis

A_f	– area of reinforcement applied to the beam	T_s	– tensile component due to the tensile reinforcement
A_s	– steel area of the tensile reinforcement	α	– reduction coefficient due to the propagation of inclined cracks
A_s'	– steel area of compressed reinforcement	β_1	– coefficient that determines the approximation of the resultant compression curve of the concrete to a rectangle according to the recommendations of ACI 440-2R (2008)
C_c	– compression component due to the concrete portion	ϵ_{bi}	– strain found in the covering of the tensile reinforcement in the beam before the strengthen
C_s	– compression component due to compressed reinforcement	ϵ_c	– concrete strain
E_f	– modulus of elasticity of the CFRP	ϵ_{cu}	– concrete ultimate strain
E_s	– modulus of elasticity of steel	ϵ_f	– carbon fiber strain
F_{cc}	– compression resulting	ϵ_{fd}	– limit value of fiber strain to be adopted in the sizing and verification of reinforcement
L	– total beam length	ϵ_{fe}	– effective strain in the CFRP
M	– moment applied during the experimental test	ϵ_{fu}	– ultimate strain observed in the polymer at the moment of failure
M_R	– resistant moment in the cross section of the beam	ϵ_s	– strain in the tensile reinforcement
M_{Rteo}	– resistant moment estimated by the recommendations	ϵ_s'	– strain in the compressed reinforcement
M_u	– experimental ultimate moment	ϵ_{ys}	– yield strain of the flexural reinforcement
M_{ACI}	– ultimate moment according to the recommendations of ACI 440-2R (2008)	r	– rate of the reinforcement of the beam before the strengthen
M_{fib}	– ultimate moment according to the recommendations of <i>fib</i> Bulletin 14 (2001)	rr	– beam reinforcement ratio after strengthen
M_{V1}	– experimental ultimate moment of the beam V1	\emptyset	– reinforcement bar diameter
$N_{fa,max}$	– maximum force that can be applied to the reinforcement of the beam	ψ	– coefficient that determines the approximation of the resulting curve of concrete compression to a rectangle, according to the recommendations of <i>fib</i> Bulletin 14 (2001)
P	– applied load in the experimental test		
R^2	– coefficient of correlation of the results		
T_f	– tensile component due to the fiber reinforcement portion		

1. INTRODUCTION

Among the techniques used for the strengthening of reinforced concrete structures, we highlight the systems that use Fiber Reinforced Polymers (FRP), for presenting low weight and high tensile and corrosion strength, and the Carbon Fiber Reinforced Polymers (CFRP) that have shown significant acceptance for more than two decades due to their high values of strength, stiffness and durability, as well as the ease of installation when compared to other types of fibers (Monti and Liotta, 2007). In the specific case of flexural reinforcement of reinforced concrete beams, several researchers show that the use of sheets of CFRP is an effective methodology, highlighting the works of Rafi et al. (2008), Khan and Fareed (2014) and Hawileh et al. (2015).

However, it is important to feature that premature failures are associated with its use. In the case of flexural reinforced beams, this brittle fracture may occur due to the detachment of the carbon fiber from the concrete substrate, which may limit the increase in strength provided by the reinforcement. This mode of brittle ruin is usually associated with deficiency in the anchorage of the reinforcement system, which makes the use of additional devices recommended, such as band clipping of CFRP sheet (see Benjeddou *et al.*, 2007; Dong *et al.*, 2011, Kim and Shin, 2011, among others).

This work presents a series of experimental tests on reinforced concrete beams strengthened with CFRP sheets, carried out with the objective of evaluating the influence of the anchorage in the reinforcement structural performance. In addition, a large database was set up, with experimental results selected from the work of different authors. This database is used to discuss the influence of different parameters on the performance of reinforcement with CFRP sheets and to evaluate the performance of theoretical predictions of strength obtained using the recommendations presented by ACI 440-2R (2008) and fib Bulletin 14 (2001).

2. CFRP STRENGTHENED BEAMS

2.1 Failure modes

Teng *et al.* (2003) state that beams strengthened to flexure with CFRP sheets may exhibit brittle failure modes, for instance: by exhaustion of the strength of the CFRP (see Figure 1a); detachment of the reinforcement at the interface with the concrete (see Figure 1b); and separation of the reinforcement together with the concrete covering of the flexural reinforcement (see Figure 3c). The failure of the CFRP sheet can occur in weakly reinforced beams by flexure, being a brittle mode of failure since the CFRP presents linear-elastic behavior until the failure. The detachment of the sheet may occur due to lack of the anchorage of reinforcement, excessive cracking of the beam or, faults in its bonding process. The separation of concrete cover layer can be caused by shear strengths at the interface between concrete and CFRP due to the difference between the moduli of elasticity of these materials, which can be amplified by the corrosion of the bending reinforcement.

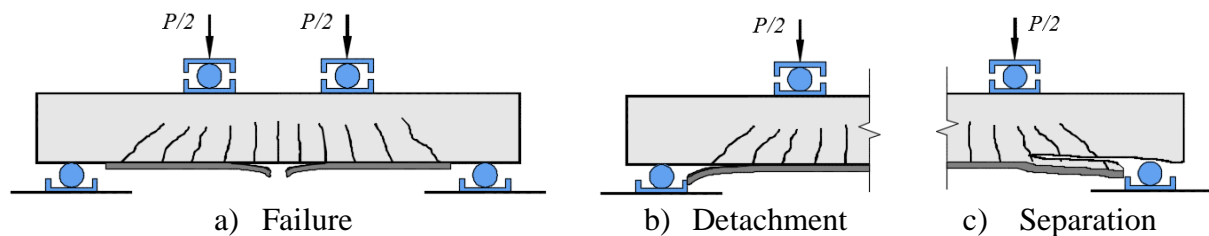


Figure 1. Failure modes of beams strengthened to flexure with CFRP.

2.2 Flexural Strength

The behavior of a reinforced concrete beam strengthened with CFRP and subjected to bending can be expressed according to the diagram of Figure 2. In this analysis, it's considered that the ratio of the reinforced beam framework is equivalent to the sum of the initial reinforcement rate with contribution from the reinforcement, as presented in (1).

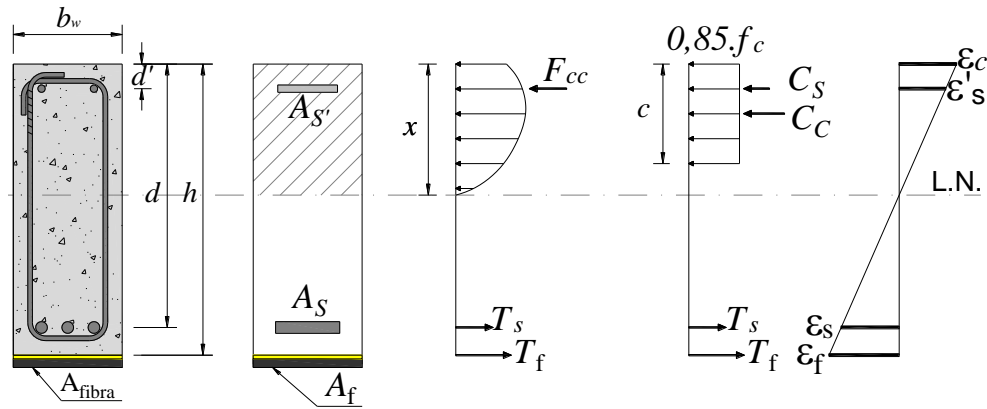


Figure 2. Stress-strain diagram of a beam strengthened with CFRP.

$$\rho_r = \rho + \frac{A_f \cdot E_f}{b_w \cdot h \cdot E_s} \quad (1)$$

Where: ρ is the rate of the reinforcement of the beam before the strengthening; A_f is the area of reinforcement applied to the beam; E_f is the modulus of elasticity of the CFRP; E_s is the modulus of elasticity of steel; b_w is the width of the beam; h is the height of the beam.

2.2.1 ACI 440-2R (2008)

The American code ACI 440-2R (2008) presents recommendations for the sizing of reinforcement using CFRP. To determine the flexural strength of reinforced concrete beams reinforced with carbon fiber sheets, (2) - (10) are used.

$$\epsilon_{fd} = 0,41 \cdot \sqrt{\frac{f_c}{n \cdot E_f \cdot t_f}} < 0,9 \cdot \epsilon_{fu} \quad (2)$$

$$\epsilon_{fe} = \epsilon_{cu} \cdot \left(\frac{h-x}{x} \right) - \epsilon_{bi} \leq \epsilon_{fd} \quad (3)$$

$$f_{fe} = E_f \cdot \epsilon_{fe} \quad (4)$$

$$\epsilon_s' = \epsilon_{cu} \cdot \left(\frac{x-d'}{x} \right) \quad (5)$$

$$\epsilon_s = \epsilon_{fe} \cdot \left(\frac{d-x}{h-x} \right) \quad (6)$$

$$f_s' = E_s \cdot \epsilon_s' \leq f_{ys}' \quad (7)$$

$$f_s = E_s \cdot \epsilon_s \leq f_{ys} \quad (8)$$

$$x = \frac{(A_s \cdot f_s) + (A_f \cdot f_{fe}) - (A_{s'} \cdot f_s')}{\beta_1 \cdot 0,85 \cdot f_c \cdot b_w} \quad (9)$$

$$M_R = A_s \cdot f_s \cdot \left(d - \frac{\beta_1 \cdot x}{2} \right) + 0,85 \cdot A_f \cdot f_{fe} \cdot \left(h - \frac{\beta_1 \cdot x}{2} \right) + A_s' \cdot f_s' \cdot \left(\frac{\beta_1 \cdot x}{2} - d' \right) \quad (10)$$

Where: ε_{fd} is the limit value of fiber strain to be adopted in the sizing and verification of reinforcement to avoid premature fiber failure; n is the number of layers of CFRP; t_f is the thickness of the CFRP; ε_{fu} is the ultimate strain observed in the polymer at the moment of failure; ε_{fe} is the effective strain in the CFRP; x is the position of the neutral axis; ε_{bi} is the strain found in the covering of the tensile reinforcement in the beam before the strengthen; f_{fe} is the effective strength of the CFRP; d is the effective beam height; ε_s' is the strain in the compressed reinforcement; f_s' is the strength in the steel of the compressed reinforcement; d' is the centroid position of the compressed reinforcement; ε_s is the strain in the tensile reinforcement; f_s is the strength in the steel of the tensile reinforcement; A_s is the steel area of the tensile reinforcement; A_s' is the steel area of compressed reinforcement; β_1 is a coefficient that determines the approximation of the resultant compression curve of the concrete to a rectangle, being 0.85 for concrete with f_c values lower than 28 MPa and there being a linear decrease of 0.05 for each 7 MPa above that limit of strength, the minimum value for such a coefficient, according to ACI 318 (2014), is 0.65; M_R is the tough moment in the cross section of the beam.

2.2.2 *fib* Bulletin 14 (2001)

The *fib* Bulletin 14 (2001) presents recommendations for the dimensioning of flexural reinforced beams with CFRP and adopts a calculation philosophy like that adopted by ACI 440-2R (2008). The same equations presented by the ACI are used in this document, differentiating only the following parameters: the coefficient β_1 in it is called of ψ and equals to 0.8, independent of the class of strength of the concrete; and the strain limit of the fiber, which is calculated by (11), whose parameters are found by means of (12) - (14).

$$\varepsilon_{fd} = \frac{N_{fa,max}}{E_f \cdot A_f} \quad (11)$$

$$N_{fa,max} = \alpha \cdot c_1 \cdot k_c \cdot k_b \cdot b_w \cdot \sqrt{E_f \cdot t_f \cdot f_{ctm}} \quad (12)$$

$$k_b = 1,06 \sqrt{\frac{2 - \frac{b_f}{b_w}}{1 + \frac{b_f}{400}}} \geq 1 \quad (13)$$

$$f_{ctm} = 0,33 \cdot \sqrt{f_c} \quad (14)$$

Where: $N_{fa,max}$ is the maximum force that can be applied to the reinforcement of the beam (expressed in N); α is a reduction coefficient due to the propagation of inclined cracks, adopted as 0.9; c_1 is equal to 0.64; k_c is a constant that considers the compacting of the concrete during the concreting, being this value equal to 1 when the strengthening is applied in the underside of the beam and 0.67 in the upper face; k_b is a geometric factor; f_{ctm} is the average tensile strength of concrete, as expressed in Eurocode 2 (2004); b_f is the width of the layer of CFRP.

3. EXPERIMENTAL PROGRAM

3.1 Characteristics of the beams

Tests were carried out on 4 reinforced concrete beams strengthened with CFRP sheets, having as variables the sheet anchorage length and width in order to evaluate their influence on both the performance and the strength of the beams. It was tested 1 reference beam without reinforcement and 3 reinforced beams with carbon fiber sheet. The rates of steel reinforcement and CFRP were kept constant. Table 1 and Figure 3 show the main characteristics of the beams. The strains in the flexural reinforcement, the reinforcement sheet and the clamping were monitored with electrical extensometers, as shown in Figure 4. Figure 5 shows the test system of the beams.

Table 1. Characteristics of the tested beams.

Beam	l (mm)	l_b (mm)	b_f (mm)	A_f (mm ²)	t_f (mm)	E_f (GPa)	ϵ_{fu} (%)
V1	-	-	-	-	-	-	-
V2	100	285	120	19.92	0.166	230	2.1
V3		385					
V4	150						

$b_w = 120$ mm; $h = 200$ mm; $d = 166$ mm; $A_s = 101$ mm²; $f_c = 20$ MPa; $a = 400$ mm

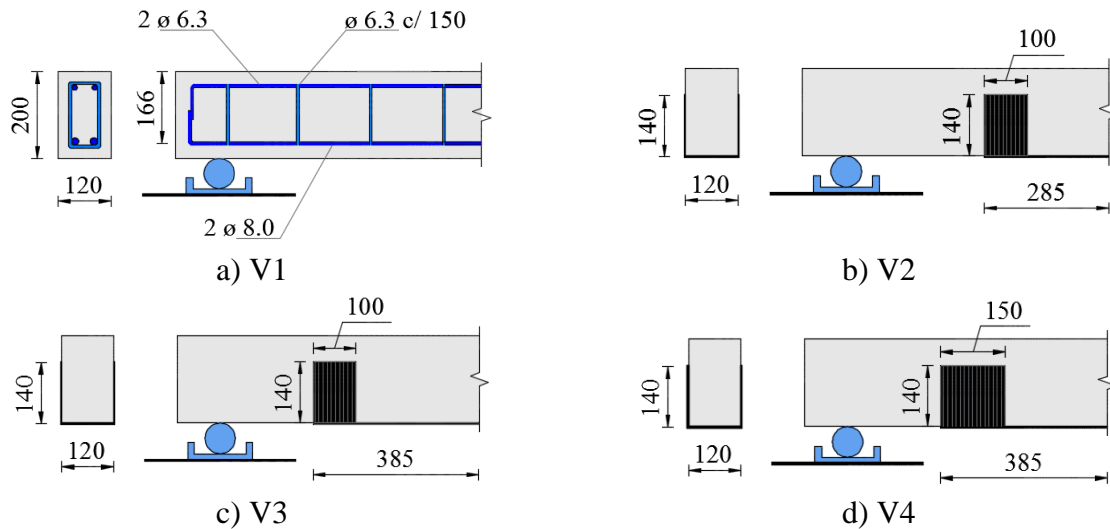


Figure 3. Characteristics of tested beams.



Figure 4. Monitoring of beams.

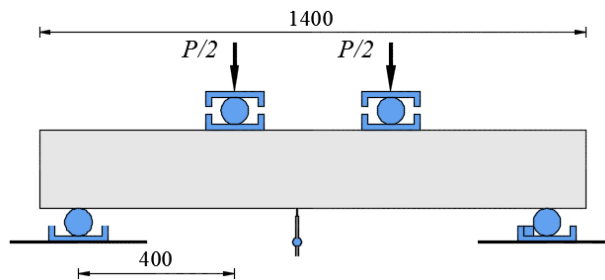


Figure 5. Test system of beams.

3.2 Discussion of Results

The failure mode of each of the beams tested can be visualized in Figure 6. It was observed that the reference beam failed by flexure after its longitudinal reinforcement reached high levels of strain (Figure 6a). In the V2 beam the concrete was pulled out in the zone adjacent to the clamping (Figure 6b). The V3 beam lost its strength after the fiber detachment occurred in part of the clamping contact zone (Figure 6c). However, the V4 beam failed after the detachment of the concrete covering in the region of the flexure span (Figure 6d).

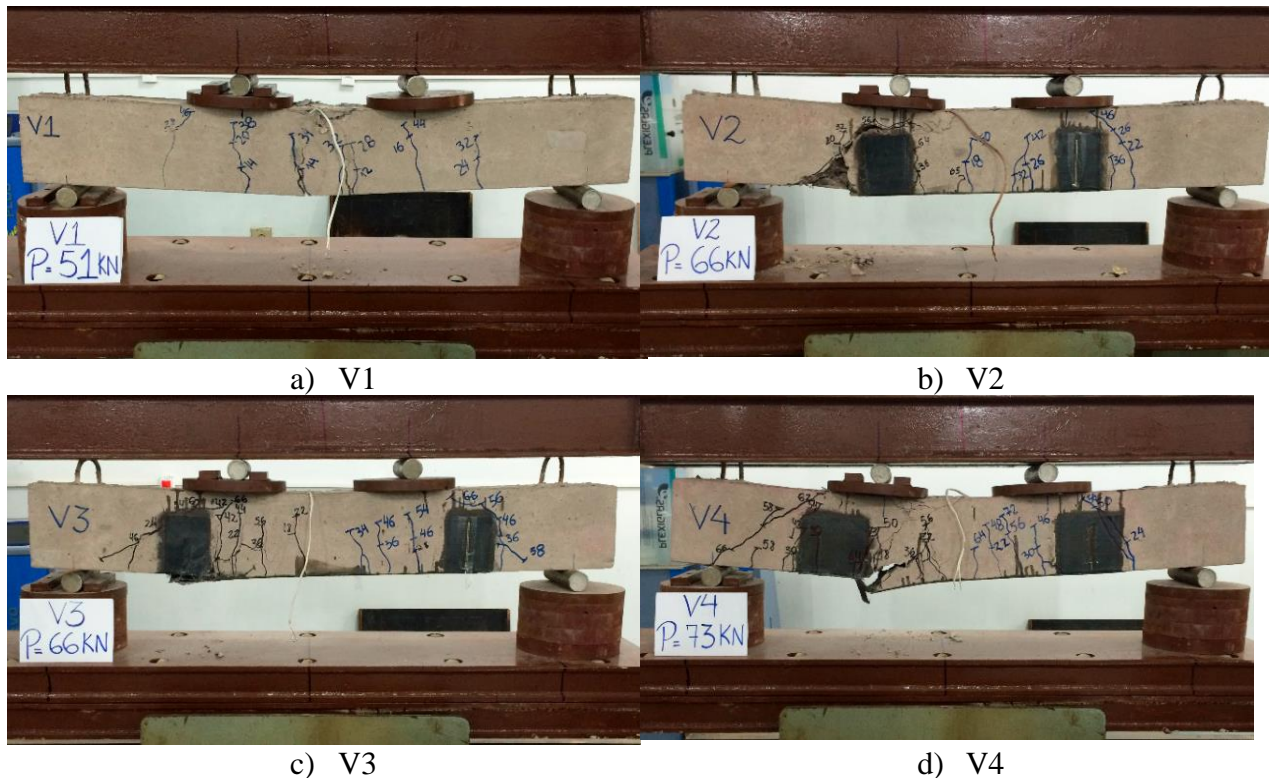


Figure 6. Failure surface of tested beams.

Figure 7 shows the results of strains measured in the flexural reinforcement and at different points of the PRFC. It is noticed that, in all the beams, the flexural reinforcement reached the yielding, as shown in Figure 7a. The strains in the flexural reinforcement were smaller in the beams with the sheet of CFRP for the same load levels, since the reinforcement contributed in the tensile part of the piece. In addition, it was observed that the resistant behavior of the beams with the sheet was more brittle than that of the non-reinforced beam, since after reaching the maximum strength, the readings were interrupted by the failure of the part, whereas in the beam V1, if the maximum load was reached, this loading level remained associated to a high level of strain. Figure 7b shows that

both the anchoring length of the fiber and the clamping width influenced the ultimate strain of the CFRP measured in the tests, varying from 3.5 ‰ for the beam V2 to approximately 4.2 ‰ for the beams V3 and V4. In all cases, it should be noted that these values are higher than theoretically predicted by the ACI, which would be 1.9 ‰. It should be emphasized that none of the beams failed with the exhaustion of the tensile strength of the sheet of CFRP. Figure 7c shows that in all the beams the level of strain at the end of the reinforcement was smaller than that measured in the middle of the span, where the moment is maximum and that in the case of the beam V2, which failed due to the detachment of the fiber in this region, the strain limit measured was practically the same as that suggested by the manufacturer of 2.1 ‰. In Figure 7d it is possible to notice that the level of strain developed in the region of the clamping was small and that in beam V3 it clearly begins to separate before the failure.

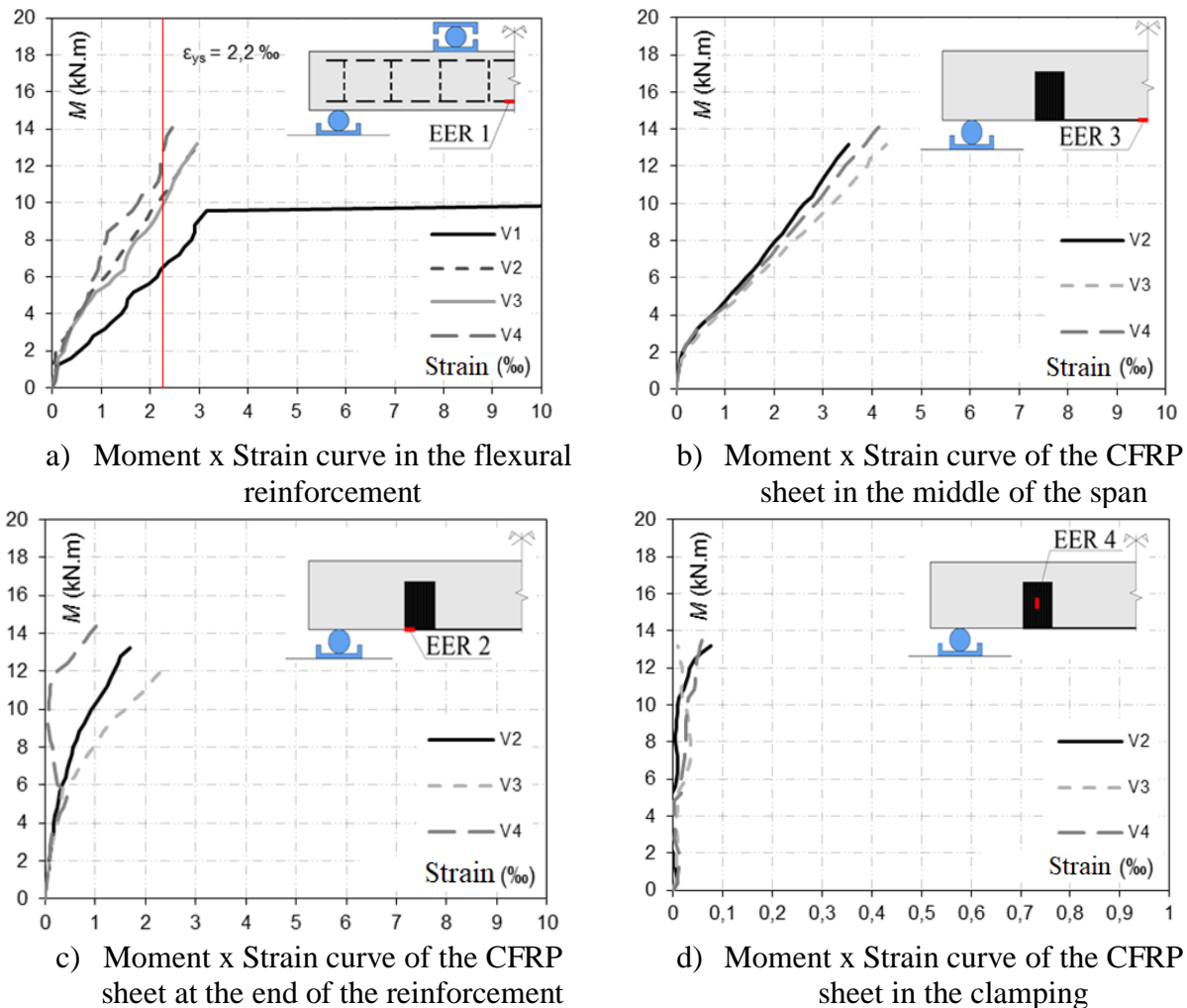


Figure 7. Results of the beams tests.

Figure 8 shows the vertical displacement curve of the beams, measured in the middle of the span. It is possible to notice that the reinforced beams presented a very similar response, showing greater rigidity than the reference beam, which failed by flexure in a ductile manner and showed large displacements when reaching the moment of yield of its flexural reinforcement. As seen, all the reinforced beams failed abruptly, with failure occurring in different regions of the CFRP.

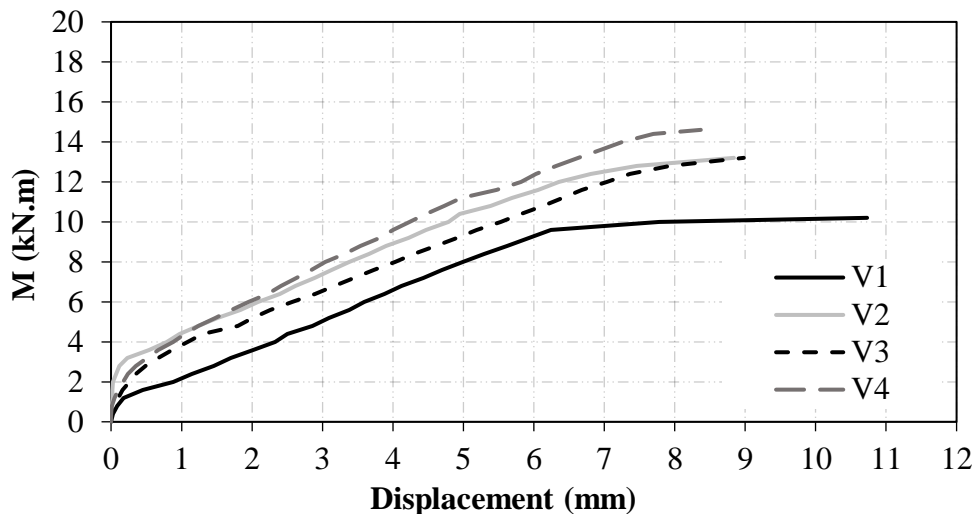


Figure 8. Moment-displacement curves of the tested beams.

Table 2 presents the final loads of the tested beams and compares the strength of the reinforced beams with the sheet of CFRP with the reference beam (V1), in order to determine the increment of strength generated by the reinforcement. In addition, the experimental strength of the beams is compared with theoretical estimates obtained following the recommendations of the ACI and *fib*14. From these results, it was observed that the increase of the anchoring length of the beam V3 in relation to the beam V2 did not result in an increase of strength, and that the increase of the clamping width was responsible for the greater strength of the beam V4 in relation to the beam V3. It was also observed that the use of ACI would result in predictions of strength against safety for beams V2 and V3, while *fib*14 presented results in favor of safety.

Table 2. Ultimate loads of the beams.

Beam	M_u (kN.m)	M_u/M_{V1}	M_u/M_{ACI}	M_u/M_{fib}
V1	10.2	1.00	-	-
V2	13.2	1.29	0.94	1.14
V3	13.2	1.29	0.94	1.14
V4	14.6	1.43	1.04	1.26

4. DATABASE

4.1 Methodology of collection and analysis of data

In addition to the experimental program, a database was collected with the results of 126 tests of 20 authors, involving flexural reinforced beams with the sheet of CFRP. As a criterion for the choice of beams, only those that failed by bending, without initial loading and externally bonded reinforcement, were selected. The objective of this data analysis is to evaluate the influence of the main variables on the flexural strength of reinforced beams with CFRP.

The analysis of the database involves the comparison of the experimental results with the theoretical estimates obtained using the ACI and *fib* 14. Thus, it was calculated the values of average, coefficient of variation and standard deviation of the ratio between the experimental ultimate moment and the theoretical resistant moment (M_u/M_{Rteo}), and finally, the percentage of safety results ($M_u/M_{Rteo} < 1$) was evaluated. In order to evaluate the precision of the theoretical models, graphs are presented that compare the moment of experimental failure (M_u) by the function of the predicted resistant moment (M_{Rteo}), in order to analyze if the tendency of the obtained results approaches the ideal condition ($M_u = M_{Rteo}$).

As previously noted, the performance of the reinforcement with sheet of CFRP is directly related to the quality of fiber anchoring to concrete. Therefore, the beams of the database were divided into 3 groups: group 1 for situations where the bonding of the sheet stretched from the center of the beam to the support or beyond; the group 2 with beams in which the glue of the sheet did not extend to the support; and the group 3 with beams in which external devices were used to aid in reinforcement anchorage, such as screws or restrainers. It should be noted that this type of anchorage is considered by several authors as the most favorable for anchoring the CFRP sheet, since that the device is made of this same material.

Another method used was the Collins (2001) criterion, known as *Demerit Points Classification* (DPC), in which the values of M_u/M_{Rteo} were classified in ranges from "extremely dangerous" to "extremely conservative", with performance of the theoretical model defined as a number resulting from the sum of the products from M_u/M_{Rteo} by their corresponding score, according to the classification. Table 3 presents a summary of the characteristics of the beams of the database, as well as the symbology used by the authors to identify the figures. Table 4 shows a summary of the variables related to the reinforcement with carbon fiber sheet of the beams of the database. Table 5 presents the parameters related to Collins DPC (2001).

Finally, were prepared graphs which relate the experimental strength of the beams to the predicted theoretical failure (M_u/M_{Rteo}) according to the number of layers of CFRP sheets, as well as the reinforcement ratio after strengthening in relation to the initial reinforcement (ρ_f/ρ). The purpose of these charts is to analyze if the hypotheses adopted by the theoretical models present adequate correlation with the existing experimental evidence.

Table 3. Characteristics of the database beams.

Author	No. of beams	b_w (mm)	h (mm)	d (mm)	a (mm)	A_s (mm ²)	f_{ys} (MPa)	f_c (MPa)
Beber (2003)	12	150	300	272	833	245	706	32
Beber <i>et al.</i> (2000)	8	120	250	219	783	157	565	33
David <i>et al.</i> (2003)	4	150	300	267	933	307	500	39
Esfahani <i>et al.</i> (2007)	6	150	200	164	600	402-626	350-406	24
Breña <i>et al.</i> (2003)	9	203	356-406	318-368	1065-1220	395	440	35-37
Rusinowski <i>et al.</i> (2009)	5	200	300	262	1300	402	527	64-70
Toutanji <i>et al.</i> (2006)	7	108	158	127	560	142	427	49
Barros <i>et al.</i> (2007)	6	120	170	141-145	300	39-99	627-788	44
Gamino (2007)	14	75	150	120	550	62	640	45
Zhang <i>et al.</i> (2006)	4	120	250	224	750	226-402	335	23
Spadea <i>et al.</i> (2000)	2	140	300	266	1800	402	435	30
Alagusundaramoorthy <i>et al.</i> (2003)	12	230	380	342	1830	981.75	414	31
Ferrari (2007)	3	170	350	300	950	254.4	548	35-38
Dias <i>et al.</i> (2002)	5	120	180	160	720	100.5	533	41
Balaguru e Kurtz (2001)	3	200	300	255	1000	258	447	47
Vieira <i>et al.</i> (2016)	8	120	245	220	800	157-245	500	44
Bilotta <i>et al.</i> (2015)	2	120	160	135	925	157	590	21
Garcez (2007)	2	150	300	270	950	245.4	578	41.4
Juvandes (1999)	9	75-150	150	130	605-650	14-226	192-507	20-45
Chahrour e Soudki (2005)	5	150	250	219	750	402.1	400	39

Table 4. Strengthening variables of the beams.

Author	No. of beams	No. of layers	b_f (mm)	t_f (mm)	A_f (mm ²)	E_f (GPa)	e_{fu} (‰)
Beber (2003)	12	1-6	50-150	0.1-1.4	10-140	240	12-14
Beber <i>et al.</i> (2000)	8	1-10	120	0.011	1.3-13.2	230	15
David <i>et al.</i> (2003)	4	2-4	50	1.2	120-240	150	15
Esfahani <i>et al.</i> (2007)	6	1-2	100-150	0.176	17.6-52.8	237	12
Breña <i>et al.</i> (2003)	9	1-2	50-100	0.165-1.2	16.5-104	62-230	12-16
Rusinowski <i>et al.</i> (2009)	5	1-2	50-120	1.4	140-168	155-300	9-15
Toutanji <i>et al.</i> (2006)	7	3-6	102	0.165	50.5-101	110	6
Barros <i>et al.</i> (2007)	6	1-3	9.6-80	0.1-1.4	13.4-40.3	158.8-240	15-17
Gamino (2007)	14	1-2	75	0.11-0.13	8.2-16.5	230-235	15
Zhang <i>et al.</i> (2006)	4	1-2	120	0.11	13.3-26.6	235	14.27
Spadea <i>et al.</i> (2000)	2	1	80	1.2	96	152	15.1
Alagusundaramoorthy <i>et al.</i> (2003)	12	1-3	76-203	1.4-4.7	36.4-975	48-228	11.5-15
Ferrari (2007)	3	1-3	16.5	0.17	2.8-8.4	50	13
Dias <i>et al.</i> (2002)	5	1-2	20-70	0.1-1.4	15.5-28	200-240	11-15
Balaguru e Kurtz (2001)	3	2-5	152	0.071	21.6-54	200	6
Vieira <i>et al.</i> (2016)	8	2-5	100	0.166	33.2-83	230	21
Bilotta <i>et al.</i> (2015)	2	1-2	40	1.4	56-112	171	12
Garcez (2007)	2	1-2	150	0.165	247-49	227	15
Juvandes (1999)	9	1	50	1.2	60	155	19
Chahrour e Soudki (2005)	5	1	100	1.2	120	155	19

Table 5. Collins criterion.

M_{exp}/M_{Rteo}	Classification	Penalty
< 0.50	Extremely Dangerous	10
(0.50 - 0.65)	Dangerous	5
(0.65 - 0.85)	Low Safety	2
(0.85 - 1.15)	Proper Safety	0
(1.15 - 2.00)	Conservative	1
≥ 2.00	Extremely Conservative	2

4.2 Discussion of Results

Figure 9 shows the graphs that confront the experimental strength of the database with the theoretical predictions, including in red, the experimental results tests of this research. It was observed that the two theoretical models presented similar performance in relation to the average of the results, but with *fib* 14 showing greater dispersion and higher percentage of results against safety. Moreover, the tested beams fit well in the trend of results observed for the larger universe generated by the database.

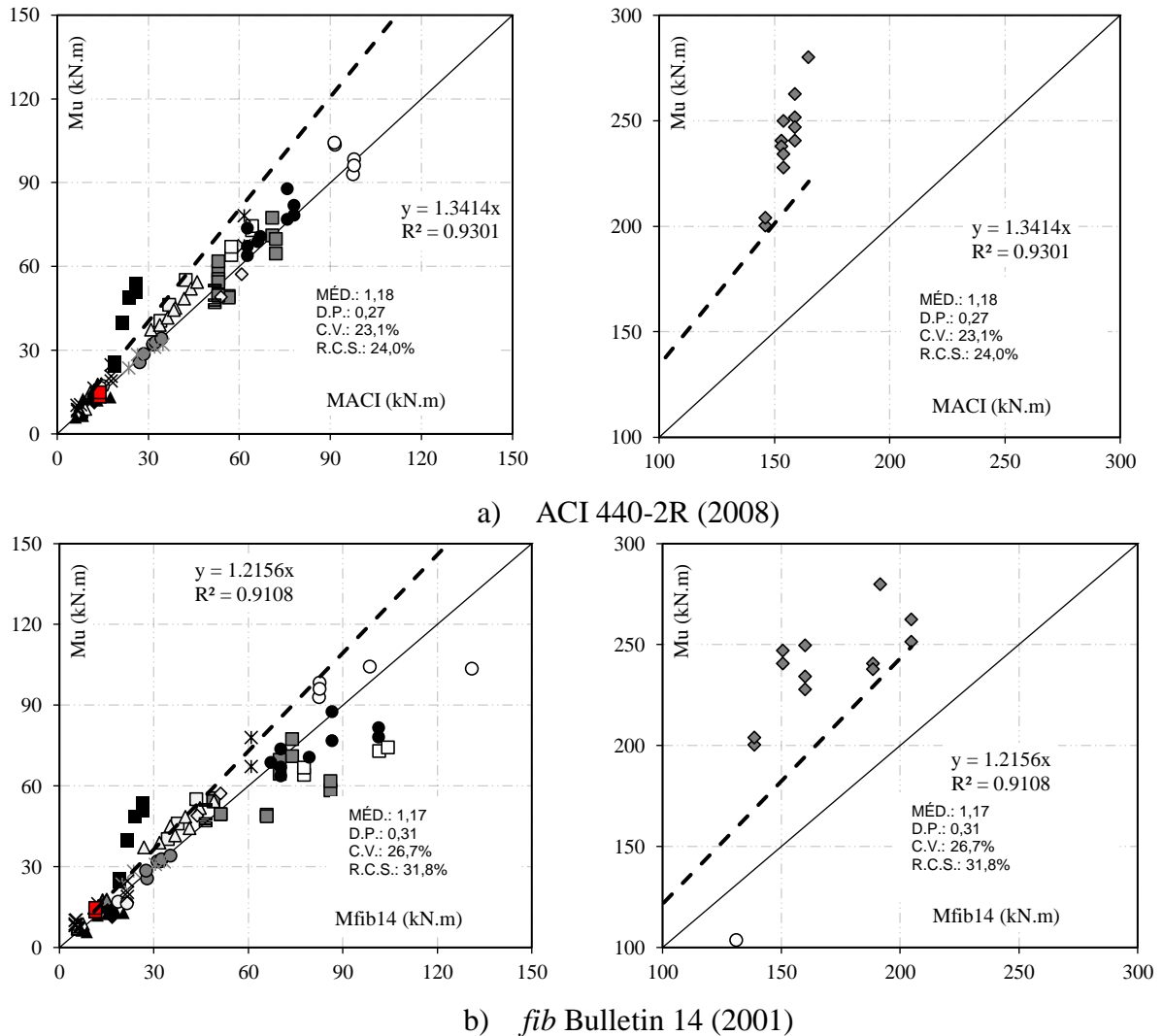


Figure 9. Analysis of the theoretical model's accuracy.

In order to evaluate the influence of the type of anchorage of the reinforcement with CFRP in the performance of the theoretical predictions, Figure 10 divides the general data presented in Figure 9, classifying them by type of anchorage in 3 distinct groups. For group 1, ACI presented an average closer to 1.0, as well as a lower dispersion of results and approximately the same number of values against safety, when compared with *fib* 14. In group 2, this behavior was reversed, and *fib* 14 showed lower average, but still with greater dispersion and greater percentage of results against the safety. For the beams of group 3 the theoretical methods presented similar performance, with the ACI showing again less dispersion.

As seen, using Collins criterion (2001), it is possible to establish scores for the two recommendations, based on the sample space of the collected database, as shown in Figure 11. It is observed that the ACI presents a lower penalty according to the criterion adopted.

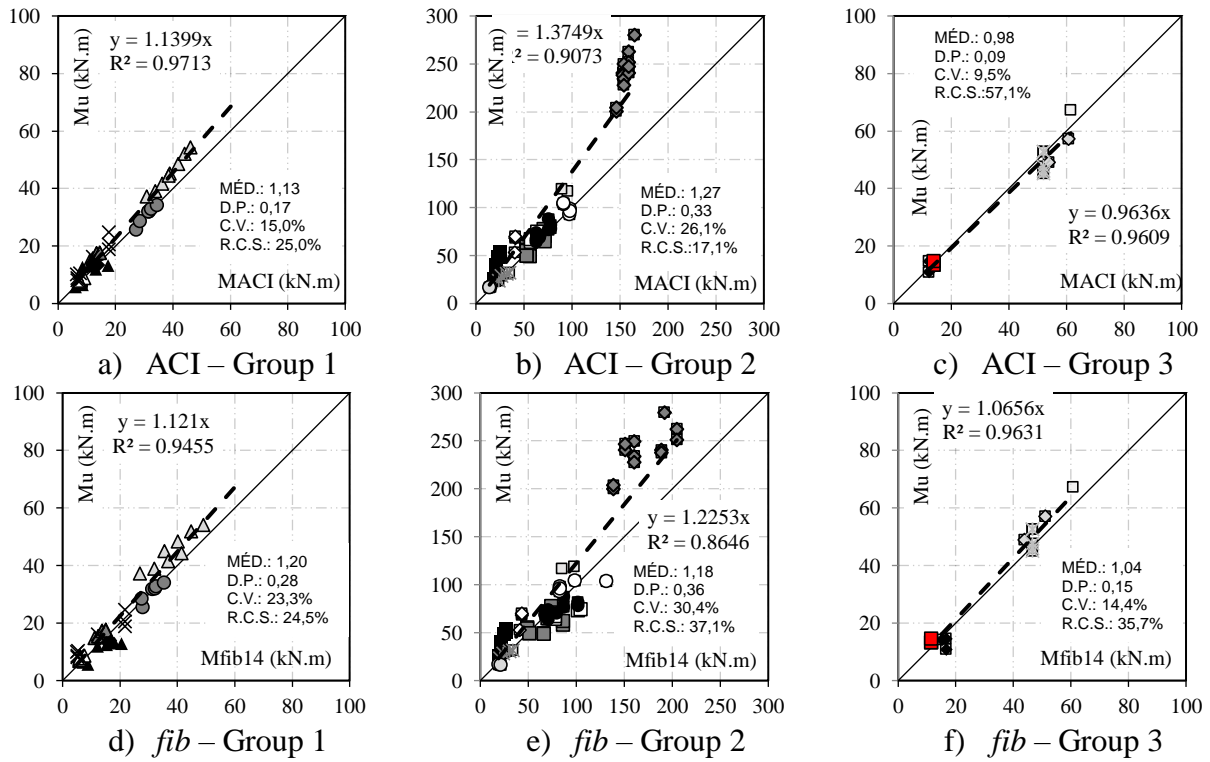


Figure 10. Analysis of the theoretical models accuracy in relation to the anchorage type.

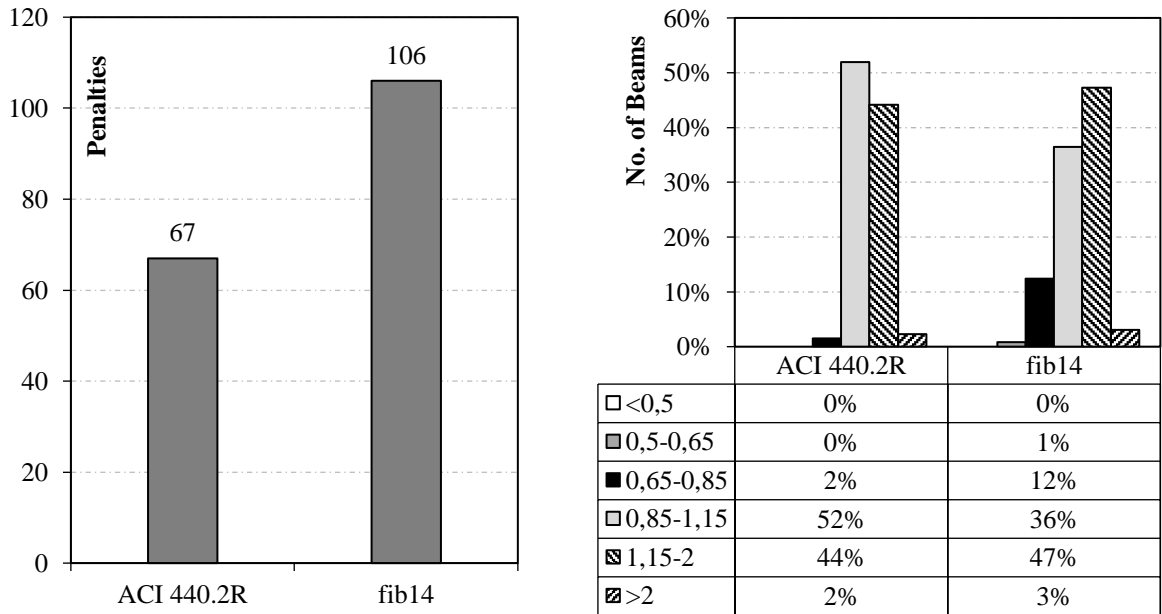


Figure 11. Result of the Collins criterion (2001).

Figure 12 analyzes the influence of the number of layers of CFRP on both reinforcement performance and theoretical methods. It is noticed that there is a trend of more conservative results as the amount of layers increases, which is justified by the fact that both recommendations limit the strain of CFRP. For the ACI, this trend is slightly higher, since in its equation the number of layers is used, which penalizes the strength estimation of reinforced beams with a high number of layers. In contrast, in *fib* 14 this factor is not considered.

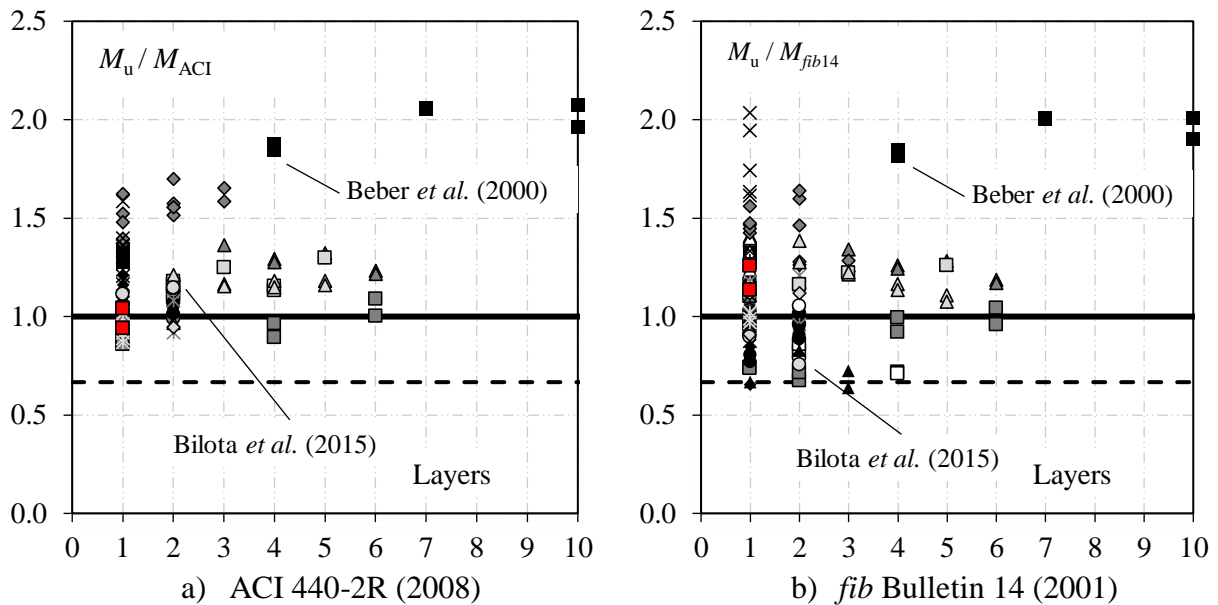


Figure 12. Influence of the number of strengthening layers.

Figure 13 shows the influence of the proportion between the reinforcement ratio after the strengthening and the flexural reinforcement ratio (ρ_r/ρ). There is a trend of less conservative results as ρ_r/ρ increases, and for values above 1.4, ACI tends to stabilize this trend, avoiding estimates of strength against safety. However, the same was not observed for *fib* 14, whose predictions approached the dashed line, which expresses the limit of the design strength.

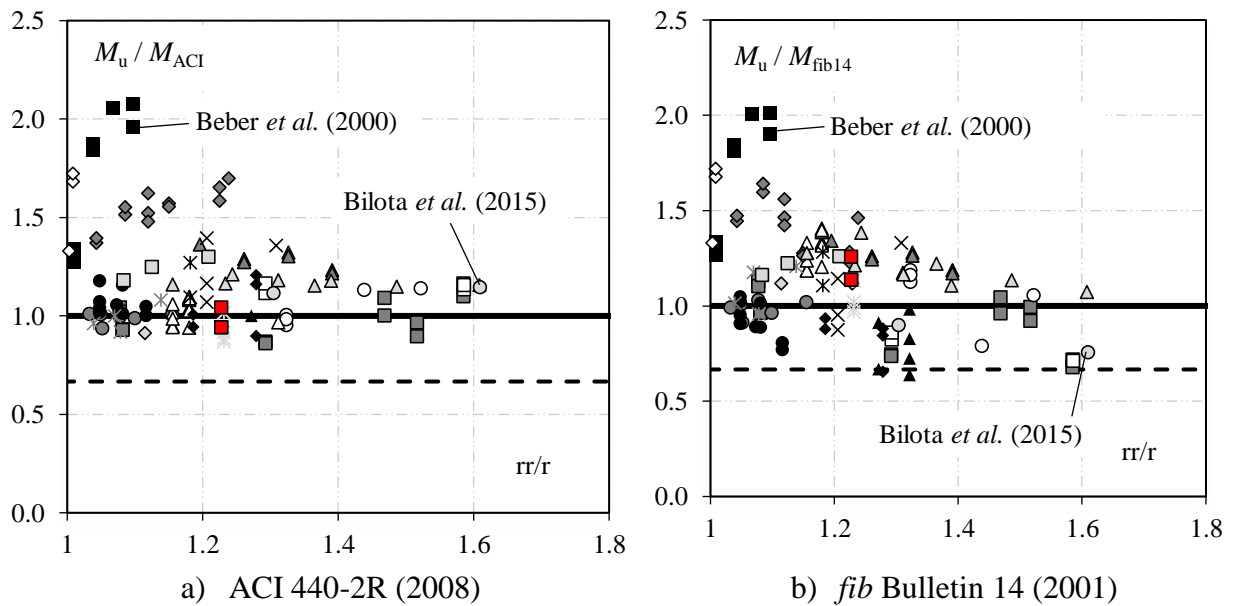


Figure 13. Influence of the reinforcement ratio increase (ρ_r/ρ)

Figures 12 and 13 show that the number of layers of CFRP is not necessarily a parameter that should be penalized in the prediction of strength of flexural reinforced beams with sheets of CFRP as defined by the ACI. This is evident from, for example, the results of Beber *et al.* (2000), who tested beams with up to ten layers of CFRP sheets and obtained good performance, and those of Bilota *et al.* (2015), whose beams tested had only one or two layers of CFRP and showed much lower performance. By analyzing Figure 13, the beams of Beber *et al.* (2000) present low values of ρ_r/ρ while those of Bilota *et al.* (2015) presented extreme values within the beams of this

database, evidencing that ρ_r/ρ is a fundamental parameter to be taken into consideration in the design.

5. CONCLUSION

In order to observe the influence of reinforcement anchorage with CFRP on the behavior of beams resisting to flexure, an experimental study was carried out, involving tests on 4 reinforced concrete beams, varying the anchorage criteria of the carbon fiber sheets. In addition to the experimental approach, a database with results from several authors was used to evaluate the influence of different parameters on the strength of reinforced beams to flexion with CFRP sheets. These data were also used to discuss the performance of the theoretical methods proposed by *fib* Bulletin 14 (2001) and ACI 440-2R (2008).

As for beam tests, it was observed that the clamping width had a greater influence on the flexural strength of the reinforced beams with CFRP sheet, since the V4 beam presented the greatest strength in relation to the others, even though the anchoring length was identical to the one of the beam V3. The beams V2 and V3 presented the same values of strength, although the beam V3 presented a greater length of anchorage between them. Another important point is that, even with the strength additions of the reinforced beams in relation to the reference, the beams with CFRP sheet have failed prematurely. Finally, it was observed that the limit values of strain of the CFRP sheet assumed by the manufacturer are very conservative in face of the experimental results recorded in this research.

As for the evaluation of the theoretical models, it is verified that both the *fib* 14 and the ACI presented conservative results in relation to the M_u/M_{Rteo} ratio, which in practice should guarantee predictions of strength in favor of safety in most cases. It was also observed that the procedure of reducing reinforcement efficiency by means of limitations on CFRP strains, although generally in favor of safety, may become excessively conservative in cases of reinforcement where CFRP anchorage is performed properly. Finally, it is emphasized that among the evaluated parameters that affect the flexural strength of beams with CFRP sheets, it is worth noting that the ratio ρ_r/ρ was more relevant than the number of layers of CFRP sheets, considering the data of this database.

6. ACKNOWLEDGMENTS

For the support on this and other researches, the authors thank: the Federal University of Pará (UFPA); to the Nucleus of Amazonian Development in Engineering (NDAE); to the Nucleus of Applied Structural Modeling (NUMEA); to the University Campus of Tucuruí (CAMTUC); to Eletrobras Eletronorte; to VIAPOL Ltda for donating the reinforcement material used in the experiments; and the development agencies CNPq, CAPES and FAPESPA.

7. REFERENCES

- Alagusundaramoorthy, I., Harik, I. E., Choo, C. C. (2003), *Flexural Behavior of R/C Beams Strengthened with Carbon Fiber Reinforced Polymer Sheets or Fabric*. ASCE - Journal of Composites for Construction. 7 (4):292-301. [https://doi.org/10.1061/\(ASCE\)1090-0268\(2003\)7:4\(292\)](https://doi.org/10.1061/(ASCE)1090-0268(2003)7:4(292))
- American Concrete Institute. (2014), *ACI Committee 318-M. Building Code Requirements for Structural Concrete and Commentary*. Farmington Hills, Michigan.
- American Concrete Institute. (2008), *ACI Committee 440-2R. Guide for the design and construction of externally bonded FRP systems for strengthening concrete structures*. Farmington Hills, Michigan.

- Balaguru, P., Kurtz, S. (2001), *Comparison of inorganic and organic matrices for strengthening of RC beams with carbon sheets*. Journal of Structural Engineering, 127:35-42.
- Barros, J. A. O., Dias, S. J. E., Lima, J. L. T. (2007), *Efficacy of CFRP-based techniques for the flexural and shear strengthening of concrete beams*. Cement and Concrete Composites. Volume 29, Issue 3, Pages 203-217. <https://doi.org/10.1016/j.cemconcomp.2006.09.001>
- Beber, A. J. (2003), “*Comportamento Estrutural de Vigas de Concreto Armado Reforçadas com Compósitos de Fibra de Carbono*”. Tese de Doutorado, Universidade Federal do Rio Grande do Sul, p. 289.
- Beber, J. A., Campos Filho, A., Campagnolo, J. L. (2000), “*Estudo Teórico-Experimental de Vigas de Concreto Reforçadas com Tecidos de Fibra de Carbono*”. IV Simpósio EPUSP sobre estruturas de concreto, São Paulo.
- Benjeddou, O., Ouezdou, M. B., Bedday, A. (2007), *Damaged RC beams repaired by bonding of CFRP laminates*. Construction and Building Materials. Volume 21, Issue 6, Pages 1301-1310. <https://doi.org/10.1016/j.conbuildmat.2006.01.008>
- Bilotta, A., Ceroni, F., Nigro, E., Pecce, M. (2015), *Efficiency of CFRP NSM strips and EBR plates for flexural strengthening of RC beams and loading pattern influence*. Composite Structures, 124:163-175. <http://dx.doi.org/10.1016/j.compstruct.2014.12.046>
- Breña, S. F., Bramblett, R. M., Wood, S. L., Kreger, M. E. (2003), *Increasing Flexural Capacity of Reinforced Concrete Beams Using Carbon Fiber-Reinforced Polymer Composites*. ACI Structural Journal. 100:36-46.
- Chahrour, A., Soudki, K. (2005), *Flexural Response of Reinforced Concrete Beams Strengthened with End-Anchored Partially Bonded Carbon Fiber-Reinforced Polymer Strips*. ASCE Journal of Composites for Construction. 9 (2):170-177. [https://doi.org/10.1061/\(ASCE\)1090-0268\(2005\)9:2\(170\)](https://doi.org/10.1061/(ASCE)1090-0268(2005)9:2(170))
- Collins, M. P. (2001), “*Evaluation of shear design procedures for concrete structures*”. A Report prepared for the CSA technical committee on reinforced concrete design.
- David, E., Ragneau, E., Buyle-Bodin, F. (2003), *Experimental analysis of flexural behavior of externally bonded CFRP reinforced concrete structures*. RILEM Materials and Structures. 38:238-241.
- Dias, S. J. E., Juvandes, L. F. P., Figueiras, J. A. (2002), *Comportamento de Vigas de Betão Armado Reforçadas à Flexão com Sistemas Compósitos de CFRP*. Unidireccionais. Engenharia Civil UM. 14:15-28.
- Dong, J. F., Wang, Q. Y., Qiu, C. C., He, D. (2011), *Experimental study on RC beams strengthened with CFRP sheets*. Advanced Materials Research. 213:548-52.
- Dong, J. F., Wang, Q. Y., Zhu, Y. M., Qiu, C. C. (2010), *Experimental study on RC beams strengthened with externally bonded FRP sheets*. Journal of Sichuan University (Engineering Science Edition). 42:197-203.
- Esfahani, M. R., Kianoush, M. R., Tajari, A. R. (2007), *Flexural behavior of reinforced concrete beams strengthened by CFRP sheets*. Engineering Structures. 29:2428-2444. [10.1016/j.engstruct.2006.12.008](https://doi.org/10.1016/j.engstruct.2006.12.008)
- Eurocode 2 (2004), *Design of Concrete Structures—Part 1-1: General Rules and Rules for Buildings*. Brussels, Belgium.
- Ferrari, V. J. (2007), “*Reforço à Flexão de Vigas de Concreto Armado com Manta de Polímero Reforçado com Fibras de Carbono (PRFC) Aderido a Substrato de Transição Constituído por Compósito Cimentício de Alto Desempenho*”. Tese de Doutorado, Escola de Engenharia de São Carlos da Universidade de São Paulo, p. 310.
- fib Bulletin 14 (2001), *Externally Bonded FRP Reinforcement for RC Structures*. FIB, Lausanne.
- Gamino, A. L. (2007), “*Modelagem física e computacional de estruturas de concreto reforçadas com CFPR*”. Tese de doutorado, Escola politécnica da universidade de São Paulo, p. 259.

- Garcez, M. R. (2007), “*Alternativas para Melhoria no Desempenho de Estruturas de Concreto Armado Reforçadas pela Colagem de Polímeros Reforçados com Fibras*”. Tese de Doutorado, Universidade Federal do Rio Grande do Sul, p. 241.
- Hawileh, R. A., Nawaz, W., Abdalla, J. A., Saqan, E. I. (2015), *Effect of flexural CFRP sheets on shear strength of reinforced concrete beams*. Composite Structures. 122:468-476. <https://doi.org/10.1016/j.compstruct.2014.12.010>
- Juvandes, L. F. P. (1999), “*Reforço e reabilitação de estruturas de betão usando materiais compósitos de “CFRP”*”. Tese de Doutorado, Faculdade de Engenharia da Universidade do Porto, p. 302.
- Khan, A. R., Fareed, S. (2014), *Behaviour of reinforced concrete beams strengthened by CFRP wraps with and without end anchorages*. Procedia Engineering. 77:123-130. <https://doi.org/10.1016/j.proeng.2014.07.011>
- Kim, H. S., Shin, Y. S. (2011), *Flexural behaviour of reinforced concrete (RC) beams retrofitted with hybrid fiber reinforced polymers (FRPs) under sustaining loads*. Composite Structures. 93:802-11.
- Monti, G., Liotta, M. A. (2007). *Tests and design equations for FRP-Strengthening in shear*. Construction and Building Materials. 21:799-809. <https://doi.org/10.1016/j.conbuildmat.2006.06.023>
- Rafi, M. M., Nadjai, A., Ali, F., Talamona, D. (2008), *Aspects of behavior of CFRP reinforced concrete beams in bending*. Construction and Building Materials. 22:277-285. <https://doi.org/10.1016/j.conbuildmat.2006.08.014>
- Rusinowsky, P., Taljsten, B., Sand, B. (2009), “*Peeling Failure at the Cut-off End of CFRP Strengthened RC Beams*”. Proceedings of the 9th International Symposium of the Fiber-Reinforced Polymer Reinforcement for Reinforced Concrete Structures, Sydney.
- Spadea, G., Bencardino, F., Swamy, R. N. (2000), *Optimizing the performance characteristics of beams strengthened with bonded CFRP laminates*. Materials and Structures. 33:119-126.
- Teng, J. G., Smith, S. T., Yao, J., Chen, J. F. (2003), *Intermediate crack-induced debonding in RC beams and slabs*. Construction and Building Materials. 17:447-462. [10.1016/S0950-0618\(03\)00043-6](https://doi.org/10.1016/S0950-0618(03)00043-6)
- Toutanji, H., Zhao, L., Zhang, Y. (2006), *Flexural behavior of reinforced concrete beams strengthened with CFRP sheets bonded with an inorganic matrix*. Engineering Structures, 28:557-566. [10.1016/j.engstruct.2005.09.011](https://doi.org/10.1016/j.engstruct.2005.09.011)
- Vieira, M. M., Santos, A. R. S., Mont’Alverne, A. M., Bezerra, L. M., Montenegro, L. C. S. and Cabral, A. E. B. (2016), *Experimental analysis of reinforced concrete beams strengthened in bending with carbon fiber reinforced polymer*. IBRACON Structures and Materials Journal. 9 (1) pp. 123:152. <http://dx.doi.org/10.1590/S1983-41952016000100008>
- Zhang, A., Jin, W., Li, G. (2006), *Behavior of preloaded RC beams strengthened with CFRP laminates*. Journal of Zhejiang University SCIENCE A. 7:436-444. <https://doi.org/10.1631/jzus.2006.A0436>

Contribution to the reinforced concrete beams degraded by fire: Comparative analysis between structural reinforcement with carbon fibers and steel sheets

Y. S. Simões^{1*} , C. F. R. Santos¹ 

* Autor de Contacto: yaghosimoes@usp.br

DOI: <http://dx.doi.org/10.21041/ra.v9i1.259>

Reception: 25/09/2018 | Acceptance: 29/10/2018 | Publication: 30/12/2018

ABSTRACT

This article aims to compare two techniques of structural reinforcement, carbon fiber and steel sheets, used for the recovery of reinforced concrete elements degraded by fire. It simulates the deterioration of a beam in a fire situation from a thermal numerical modeling and then the mentioned reinforcements are calculated. The carbon fiber required a smaller area compared to that for the steel sheet, due to its high mechanical resistance. As limitations, it is mentioned that the study is preliminary and involves only a thermal analysis of the beam, not considering the loading and its implications. It is concluded that the carbon fiber presents greater advantages with respect to reinforcement of beams.

Keywords: reinforced concrete beam; structural reinforcement; carbon fiber; bonded-in steel sheets.

Cite as: Y. S. Simões, C. F. R. Santo (2019), "*Contribution to the reinforced concrete beams degraded by fire: Comparative analysis between structural reinforcement with carbon fibers and steel sheets*", Revista ALCONPAT, 9 (1), pp. 48 -64, DOI: <http://dx.doi.org/10.21041/ra.v9i1.259>

¹ Escola de Engenharia de São Carlos - EESC/USP.

Legal Information

Revista ALCONPAT is a quarterly publication by the Asociación Latinoamericana de Control de Calidad, Patología y Recuperación de la Construcción, Internacional, A.C., Km. 6 antigua carretera a Progreso, Mérida, Yucatán, 97310, Tel.5219997385893, alconpat.int@gmail.com, Website: www.alconpat.org

Responsible editor: Pedro Castro Borges, Ph.D. Reservation of rights for exclusive use No.04-2013-011717330300-203, and ISSN 2007-6835, both granted by the Instituto Nacional de Derecho de Autor. Responsible for the last update of this issue, Informatics Unit ALCONPAT, Elizabeth Sabido Maldonado, Km. 6, antigua carretera a Progreso, Mérida, Yucatán, C.P. 97310.

The views of the authors do not necessarily reflect the position of the editor.

The total or partial reproduction of the contents and images of the publication is strictly prohibited without the previous authorization of ALCONPAT Internacional A.C.

Any dispute, including the replies of the authors, will be published in the third issue of 2019 provided that the information is received before the closing of the second issue of 2019.

Contribuição às vigas de concreto armado degradadas pela ação do fogo: Análise comparativa entre o reforço estrutural com fibras de carbono e chapas metálicas

RESUMO

Esse artigo tem como objetivo comparar duas técnicas de reforço estrutural, fibra de carbono e chapa metálica, utilizadas para recuperação de elementos de concreto armado degradados pela ação do fogo. Simula-se a deterioração de uma viga em situação de incêndio a partir de uma modelagem numérica térmica e, em seguida, são calculados os reforços mencionados. A fibra de carbono exigiu uma menor área em comparação àquela para chapa metálica, em função de sua elevada resistência mecânica. Como limitações, cita-se o fato de o estudo ser preliminar e envolver apenas uma análise térmica da viga, não sendo considerado o carregamento atuante e suas implicações. Conclui-se que a fibra de carbono apresenta maiores vantagens no que diz respeito ao reforço de vigas.

Palavras-chave: viga de concreto armado; reforço estrutural; fibra de carbono; chapa metálicas coladas; incêndio.

Contribución a las vigas de hormigón armado degradadas por la acción del fuego: Análisis comparativo entre el refuerzo estructural con fibras de carbono y chapas metálicas

RESUMEN

Este artículo tiene como objetivo comparar dos técnicas de refuerzo estructural, fibra de carbono y chapa metálica, utilizadas para la recuperación de estructuras de hormigón armado degradados por el fuego. Se simula un deterioro de una viga en situación de incendio a partir de un modelaje numérico térmico y, en seguida, se calculan los refuerzos mencionados. La fibra de carbono exigió un área menos en comparación con la chapa metálica, debido a su elevada resistencia mecánica. Este es un estudio preliminar que envolvió solamente un análisis térmico de una viga, sin tener en cuenta el cargamento actuante y sus implicaciones. Se concluye que la fibra de carbono presenta mayores ventajas en lo que se refiere al refuerzo de vigas.

Palabras clave: viga de hormigón armado; refuerzo estructural; fibra de carbono; chapa metálica; pegadas; incendio.

1. INTRODUCTION

The design of a structural project is a very complex task since, in addition to the steps of launching, designing and detailing the structural elements, the designers must foresee measures that avoid or hinder the occurrence of pathological manifestations. In general, structures are designed for a 50-year life. For this to be achieved, preventive actions must be taken, which prevent the resistant capacity of the structural elements from being lost in the short term. An example of preventive action corresponds to the waterproofing of the exposed surface of the structural component to the external environment. It acts as a mechanical barrier that prevents the entry of harmful substances or even substances that result in chemical reactions whose products are damaging, inside the structural elements.

In elements of reinforced concrete, a type of very common pathological manifestation that promotes the degradation of the structural element is the spalling. It may occur at room temperature due to corrosion of the submerged framework inside the concrete, for example (Stukovnik et al.,

2014). In this context, Wang et al. (2013) define that the deterioration of reinforced concrete structures occurs in two stages. In the first one, there is the degradation of the protective barrier of the reinforcement, allowing the aggressive agents to enter the element. In this process, called depassivation, the structural element does not lose its resilient capacity. Regarding the second step, the deterioration of the structural element itself occurs, in which the process of corrosion of the reinforcement is initiated, followed by the spalling of the concrete surface and, later, the collapse of the structural element.

In addition to the aggressive agents, actions like fire and explosions can also lead to degradation of structures. Currently, due to the increase in the number of cases of residential buildings in a fire situation, many designers have admitted that the design of structures at room temperature, although essential, is not enough to meet the structural safety criteria. Thus, the structural elements must also be designed to meet the required fire resistance time (Kobes et al., 2010).

In everyday life, the risk of fire is imminent. It may be caused by a short circuit of an appliance, improper electrical wiring or gas leakage. In the context of the study of structures submitted to fire, it is essential to know the curve that characterizes the evolution of the temperature of the gases over time, responsible for heating the structural element. It should be noted that no fire is the same as the other, since there are many parameters involved to determine the temperature evolution of the structural element, such as: degree of ventilation of the structure, type and amount of fire load. In this regard, it becomes difficult to define an average temperature and time that residential buildings commonly reach when they are in a fire situation. Thus, the technical standards allow the adoption of a standard heating curve for the construction of models in experimental analysis. This is the standard fire model; whose standardization allows the treatment of the fire in a simpler and more approximate way.

On reinforced concrete structures, concrete acts as a thermal barrier reducing the flow of heat to steel. This is because concrete presents better thermal properties compared to other materials, such as low thermal conductivity and high specific heat, which decrease heat propagation into the cross section. In any case, because there is a heating, both materials tend to lose rigidity and mechanical resistance. Ingham (2009) explains the mechanisms of microstructural degradation of concrete in a fire situation. When the temperature of the material reaches about 100°C, the free water present in the aggregates and in the matrix evaporates, increasing the capillary porosity. At this moment, there is a small loss of resistance of the material. When the temperature rises and reaches 300°C, there is a loss of water bound to the cement matrix. Up to 600°C, the aggregates undergo thermal expansion and there is an increase of internal tension. Between 600°C and 800°C the carbonate constituents undergo decarbonation and, in the range of 800°C to 1200°C, the components disintegrate, and the concrete is calcined.

Kodur and Agrawal (2016) studied the mechanisms of failure in structural elements under fire. They explain that the deterioration of a structure is due to both the disintegration of parts of the concrete (spalling) and consequent elevation of the temperature in the steel bars, as well as the appearance of permanent deformations induced by the heating of the materials.

According to Deeny et al. (2008), the spalling that occurs in structures exposed to fire can have three origins. The first origin relates to the collapse of the aggregate near the heated surface, the second one to the disintegration of the corners of the concrete and the third to the fragile rupture of the heated surface due to the appearance of internal stresses from the evaporation of the free water. While the first origin is responsible only for surface damage and therefore does not affect the resistant capacity of the material, the second and third ones promote disintegration of concrete parts, leading to loss of mechanical strength (Khoury, 2000; Hertz, 2003).

After the fire it is necessary to evaluate if there was damage in the resistant capacity of the structural elements. If it has occurred, it should be checked the extent of it and thus choose either to destroy the structure or to recover the structural elements. The latter alternative can be achieved using

structural reinforcement techniques, in order to restore the bearing capacity of the degraded structure (Reis, 1998). Among the current reinforcement techniques and those of particular interest for this work are the bonding of steel sheets and that of carbon fiber reinforced polymers on the concrete surface. Both were chosen because they present little increase of the useful section of the structural element and do not require, in the constructive process, concreting (Obaidat, 2011). Despite the research done so far, with authors such as Lin and Zhang (2013), Firmo et al. (2015) and Jiangtao et al. (2017), who investigated the behavior of several types of reinforcement when exposed to high temperatures, none of them present reinforcement design for fire-retarded reinforced concrete structures. In addition to the behavior of the structural elements under high temperatures, it is important that the designer knows how to dimension the structural reinforcement for the situation described. Thus, this work proposes a comparative study between the two types of reinforcement previously mentioned, to be used in reinforced concrete beams degraded by the action of the fire and designed subject to flexure. Therefore, the thermal gradient was defined inside the beam, from a numerical modeling and the necessary reinforcement was calculated so that the structure returned to the resistant capacity for which it was dimensioned.

2. STRUCTURAL REINFORCEMENT

2.1. Reinforcement with carbon fibers

According to Fard (2014), the use of carbon fibers as structural reinforcement is more advantageous than the adoption of bonded-in steel sheets. This is due to the high rigidity and mechanical strength of the carbon fibers, which, together with their low specific mass, promotes an increase in the bearing capacity of the structure without adding its final weight. Moreover, corrosion resistance also represents an advantage of carbon fibers over bonded-in steel sheets. Among the disadvantages of using carbon fibers are the high cost and low performance of the fibers when subjected to fire.

In general, the carbon fiber reinforcement system is composed of two main elements: the carbon fiber, which is the element responsible for the mechanical resistance of the system, and the epoxy matrix (Figure 1), formed by epoxy resin resulting from the combination of epichlorohydrin and biphenol. The epoxy matrix is responsible for the transfer of the tensile stresses in the structure to the carbon fibers, being made by both friction and adhesion (Machado, 2007). The matrix involves all the carbon fibers present in the reinforcement, providing both mechanical strength and resistance to the aggressive agents that can deteriorate the fibers. Fard (2014) points out that the surface must be clean, free of powdery materials and the finish should be planned in order to prevent loss of adhesion between the resin and the concrete surface.

Regarding the executive process, the carbon fiber application system consists of five stages. Initially, the concrete surface is prepared by inserting a primer layer, whose function is to form a stable base free of dust and contaminants. Afterwards, the surface is regularized leaving it free of protrusions for later application of the carbon fiber. Then, the epoxy resin is applied followed by the carbon fiber blanket and the resin again. Finally, in order to protect the parts exposed to the sun against UV radiation, a finishing layer is made with acrylic paint.

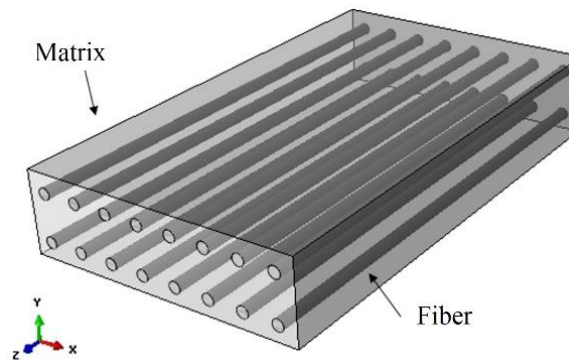


Figure 1. Epoxy matrix and carbon fibers (Obaidat, 2011)

Regarding the arrangement of the described system, the fibers should be oriented in the direction of the tension lines that they fight. Machado (2002) describes that fibers besides having a high tensile strength, have good shear strength, albeit to a lesser extent than the previous one. For the latter situation, the reinforcement is positioned in the regions of the supports in order to counter the shear stress.

According to Chowdhury et al. (2008) and Raouf and Bournas (2017), one of the main concerns in the use of carbon fiber reinforcement in structural elements is related to their combustibility. At high temperatures, the resin responsible for attaching the carbon fiber blanket to the concrete tends to degrade, generating toxic smoke and increasing the size of the flames. Wang et al. (2003), Forter and Bisby (2005) and Chowdhury et al. (2008) point out that when the temperature in the reinforcement reaches that corresponding to the glass transition of the resin, around 93°C, the degradation of its mechanical properties begins. In addition to the mechanical resistance, the authors verified that, for temperatures higher than the glass transition of the resin, there was a reduction of the adhesion between the reinforcement and the concrete.

There is no definition in the literature about the temperature at which the total degradation of the mechanical properties of the reinforcement occurs, commonly called critical temperature. Chowdhury et al. (2008) points out that it occurs between 300°C and 400°C, which corresponds to the combustion temperature of the resin. On the other hand, for Kumahara et al. (1993) and Wang et al. (2003) this critical temperature is around 250°C. Despite these heterogeneous values, Tanano et al. (1997) found that the critical temperature depends on the resin composition used in the reinforcement. These authors identified in their tests two critical temperatures depending on the type of resin used, 250°C and 860°C.

Another advantage of carbon fiber reinforcement is its residual strength after exposure to high temperatures. Forter and Bisby (2005) found that when the reinforcement is exposed to a temperature of up to 300°C and then cooled to room temperature, it recovers its mechanical strength and stiffness.

2.2. Reinforcement by the addition of bonded-in steel sheets

The other object of study of this work corresponds to the technique of reinforcement by bonding thin steel sheets to the concrete surface. Its principle consists basically in the creation of a structural system composed of concrete-glue-steel, in which thin steel sheets are bonded, by means of epoxy resin and/or screws, to the surface of the concrete, significantly increasing the resistance of the element stresses, bending moment and shear stress.

Souza (2008) and Adorno et al. (2000) state that the bonding of the sheets to the structure can be done by means of epoxy resin applied in the area of contact between the element and the sheet (Figure 2a), or by metal screws with epoxy resin injection in the holes (Figure 2b), where the former is the most widely adopted solution in the market. This is due to both the greater ease of execution and the lower probability to be further weakened, due to holes, an already degraded structure. It is

emphasized that the epoxy adhesive is of extreme importance for the process, because it is through it that the stress transfer takes place, causing the old part and the reinforcement to act as a single body in a situation of perfect adhesion. (Reis, 2001).

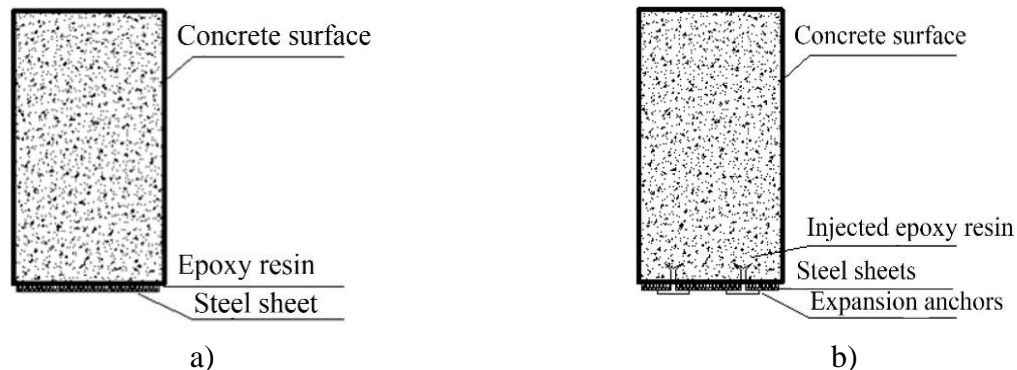


Figure 2. Reinforcement with steel sheet: a) fastening with resin; b) fastening with resin application into holes

Like any material, its use has advantages and disadvantages. As benefits, the efficiency and the low cost stand out and associated with the fast and simple execution are a good alternative when it is necessary to reinforce the structure in a short time. Furthermore, it results in little interference in the architecture, since the reinforced section has only small geometric changes, which generates a great acceptance in the market. The disadvantages are the steel corrosion, low fire resistance, the need for struts and the difficulty to handle it, due to the weight and commercial sizes of the sheets. Branco (2012) recommends the application of fire and corrosion protection after the design of the reinforcement, since the steel sheets are not resistant to these pathologies and, besides that, the epoxy adhesive deteriorates at temperatures higher than 60°C.

3. DESIGN OF THE STRUCTURAL REINFORCEMENT SUBJECT TO FLEXURE

In a similar way to the flexural theory of reinforced concrete beams described in the Brazilian Standard (NBR) 6118:2014, the structural reinforcement calculation consists of a balance of the internal forces so that the resistant moment of the element is greater or equal to the present bending moment. Figure 3 shows the balance of forces and deformations for a reinforced concrete beam with strengthening at the bottom.

The calculation begins with the definition of the type of crack that the reinforced concrete element will present in the rupture. Hence, it is necessary to adopt the relation between the depth of the neutral axis (x) and the useful height of the element (d), since this parameter determines if it will be a fragile or ductile failure. For reinforced concrete elements with f_{ck} up to 50 MPa, NBR 6118:2014 limits this value to 0.45 for the structure to show collapse with prior notice. Thus, the tensile stresses of the concrete (F_c), of the positive steel (F_s) and negative steel (F'_s) and of the structural reinforcement are calculated, applying the weighting coefficients defined by the international standards.

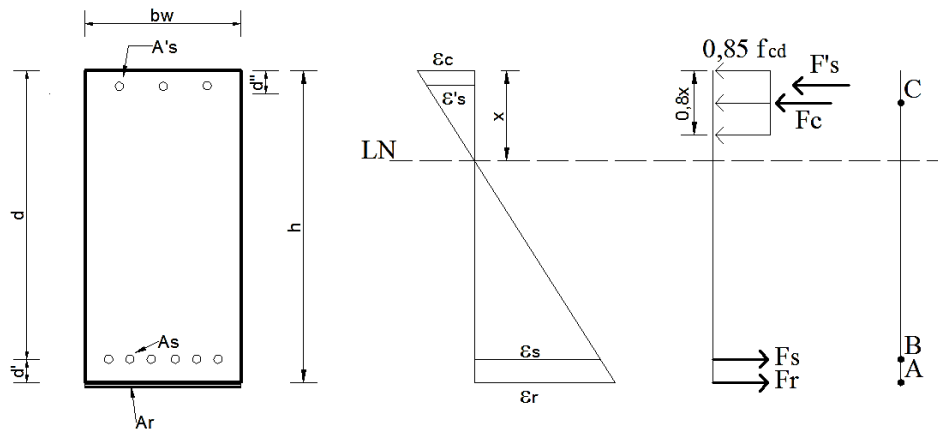


Figure 3. Equilibrium of forces and deformations in a reinforced concrete beam

In which:

b_w - Beam base;

h - Beam height;

d - Distance from the most compressed fiber to the center of gravity of the positive reinforcement;

d' - Distance from the most compressed (tensioned) fiber to the center of gravity of the negative reinforcement (positive);

x - Distance from the most compressed fiber to the neutral axis;

A_s - Area of positive reinforcement (tension);

A'_s - Area of negative reinforcement (compression);

A_r - Area of reinforcement;

ε_c - Concrete deformation;

ε_s - Positive reinforcement deformation;

ε'_s - Negative reinforcement deformation;

ε_r - Reinforcement deformation;

F_c - Resultant force from the compressed section of the concrete.;

F_s - Resultant force from the tensioned section of the positive reinforcement;

F'_s - Resultant force from the tensioned section of the negative reinforcement;

F_r - Resultant force from the tensioned section of the reinforcement.

After calculating the tensile stresses of the materials, it is performed the sum of the bending moment in relation to the reinforcement application (point A of Figure 3), where the reinforcement and glue thickness are neglected for their fastening. The bending moment found at this point is valid for any other location of the beam and will be pertinent to the designing if it presents a value greater than or equal to the requested one. However, if this value is much larger than the requested bending moment, the crack mode and the position of the neutral axis initially settled are not adequate because they do not lead to an economical solution.

If the value found is acceptable, it is set the resistant bending moment in relation to the cross-section points B and C in Figure 3. As in point A, these values should be matched to the requested bending moment. The equations for calculating the moments at points A, B and C are described below.

$$M_A = F_c (h - 0,4x) + F'_s (h - d') - F_s (h - d) \quad (1)$$

$$M_B = F_c (d - 0,4x) + F'_s (d - d') + F_r d' \phi \quad (2)$$

$$M_C = F_s (d - 0,4x) + F'_s (0,4x - d') + F_r \phi (h - 0,4x) \quad (3)$$

The coefficient ϕ represents the reduction factor applied only when the reinforcement is the carbon fiber. It is adopted $\phi = 0.85$, as suggested by ACI 440.2R: 2008. From equations (2) and (3) we find two values for the force of reinforcement (F_r) which, by equilibrium, must be equal. This force will be used to calculate the required reinforcement area, from equations (4) and (5).

$$A_r = \frac{F_r}{f_r} \quad (4)$$

$$f_r = \varepsilon'_r \cdot E_r \leq f_{ru} \quad (5)$$

In which:

f_r - It is the tensile strength of the reinforcement;

E_r - It is the elasticity modulus of the reinforcement, provided by the material manufacturer;

ε'_r - It is the deformation of the reinforcement material, found by:

$$\varepsilon'_r = \varepsilon_r - \varepsilon_{bi} \leq \varepsilon_{ru} \quad (6)$$

Such as:

ε_r - It is the deformation of the reinforcement found by the linear behaviour of the deformations according to the position of the neutral axis (x);

ε_{bi} - It is the pre-existing deformation in the steel located at the bottom of the beam, the result of its previous loading, as described by Machado (2002).

Also, according to Machado (2002), to know the level of tension, which will be reinforced during its application, it is necessary to identify the existing deformation in the structure to be reinforced.

Therefore, the pre-existing deformation in the lower face of the beam (ε_{bi}) is verified. This deformation can be calculated from its permanent load when the element is strutted during the application of the reinforcement, or its entire working load, in case the strutting is not chosen. It is worth mentioning that, if the calculated resistant moment of the structural element is lower than the requested one, the position of the neutral axis is changed, and the process described above is restarted. It is, therefore, an iterative method.

4. MATERIALS AND METHODS

The study consists, initially, in the numerical representation of a beam with a span of 6.0m and cross section shown in Figure 4, degraded by the action of fire. Next, the two types of reinforcements studied here, steel sheets and carbon fibers, will be designed with the purpose of recovering the initial resistant capacity of the beam.

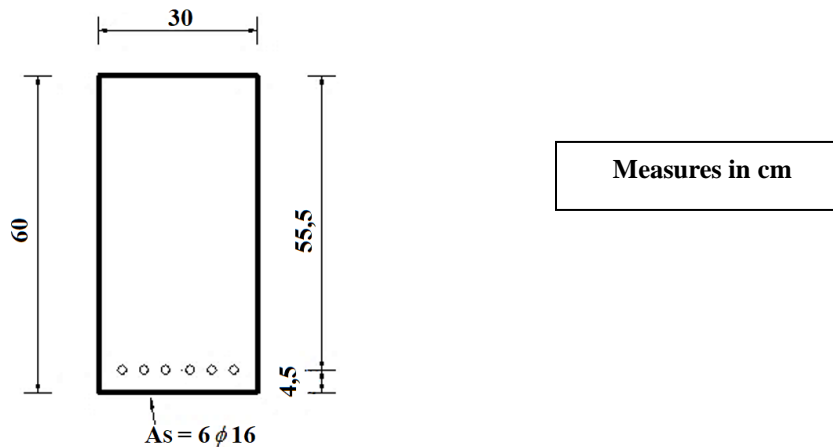


Figure 4. Cross section of reinforced concrete beam under study

The concrete adopted for the beam under study has f_{ck} equal to 30 MPa and steel of type CA50, whose modulus of elasticity is equivalent to 210 GPa. According to the calculation methods presented in NBR 6118:2014, the structural element was designed to resist a requested bending moment of 265.7 kN.m. Attention is drawn to the kind of crack that the beam presents. It lies in the deformation domain 2, where the steel has a maximum deformation of 1%, while that of the concrete ranges from zero to its limit, which is equal to 0.35%.

In order to represent the fire's action on the beam, a numerical model was developed using the ABAQUS computational code, which allows the solution of engineering problems, including structures at high temperatures, based on the Finite Element Method theory.

The behavior of a reinforced concrete beam under fire is complex and goes beyond the reduction of the mechanical properties (strength and stiffness) of steel and concrete. There is, for example, the previously described phenomenon of spalling, which causes the cross section to lose part of the concrete thickness when it reaches the temperature range 375-425 ° C (Deeny et al., 2008). In addition, during the fire, since the steel and the concrete present different coefficients of thermal expansion, there may be longitudinal cracks in the contact between these materials.

Considering the situation presented above, for the case study presented in this work we will adopt some simplifications for the design of the reinforcement, which are described below:

1. The thermal numerical modeling will be used only to obtain the temperature field formed in the cross section. From the thermal gradient caused by the low thermal conductivity of the concrete, an average temperature representative of the beam heating will be calculated, which will be used to calculate the reduction of the mechanical properties of the materials.
2. A displacement of 1.5 cm in thickness shall be considered throughout the cross section of the reinforced concrete beam to represent the spalling.
3. The reinforcement will be calculated for the new cross section, admitting the decrease of the mechanical properties of concrete and steel. The requested moment that the degraded element must support corresponds to the one for which it was initially designed, that is, 265.7 kN.m.
4. The post-fire behavior of the reinforced concrete beam shall not be considered in the analysis.
5. It is assumed the perfect adhesion between the concrete, the framework and the reinforcement to be used.
6. It is not allowed changes in the ultimate deformations of concrete and steel (0.35% and 1%, respectively) with the elevation of temperature.
7. No additional deformation, cracking or any other manifestation will be taken into account for the calculation of reinforcement.
8. The effect of the thermal action on the shear strength of the reinforced concrete beams will not be considered. It is known that in normal situations, the force that takes these structural elements

to failure is the flexure. Therefore, the calculation of the reinforcement presented here will be only to combat this force.

The following items will describe in detail the thermal numerical modeling and the calculation of the reinforcement for the beam under study.

5. CASE STUDY

5.1. Thermal numerical modeling

ABAQUS adopts the principle of the conservation of energy to perform its thermal analysis. Regarding the method of analysis, the transient sort was adopted in this work, in which the thermal properties of the materials and the temperature distribution vary over time. The boundary conditions required to perform a thermal analysis refer to the three mechanisms of heat transfer: convection, radiation and conduction.

The convection and radiation are inserted in the model with the commands "Surface film condition" and "Surface radiation", respectively, which are available in the Interaction function of the computational code. The application of these phenomena occurs through the creation of a surface in the structural element and insertion of the quantities, the convection coefficient (α_c) for the first mechanism, and the resulting emissivity of the material (ϵ) and Stefan-Boltzmann constant ($5,67 \times 10^{-8} \text{ W/m}^2 \text{ K}^4$) for the second. Regarding conduction, it is provided for the numerical analysis the density, specific heat and thermal conductivity for concrete and steel. The value adopted for the resultant emissivity of the concrete was 0.7, and for the convection coefficient, $25 \text{ W/m}^2 \text{ }^\circ\text{C}$.

The modeling was carried out based on the parameters and properties of the materials described in the Brazilian standard (NBR 1500, 2012) and European standard (EUROCODE 2 Part 1-2 (2004)) that deal with the behavior of reinforced concrete at high temperatures. The heating curve used to heat the structural element corresponds to the standard fire curve provided by ISO 834-1:1999. In this context, the thermal action with duration of 60 minutes was applied on the four faces of the beam with the objective of simulating a uniform heating.

This time corresponds to the minimum time that a beam, when present in a residential environment, must withstand fire, as provided in NBR 14432: 2000. With respect to the creation of the numerical model, the finite element of the solid type, DC3D8, was used to represent the concrete, and the bar element, DC1D2, for modeling the reinforcement. The insertion of the reinforcement in the concrete was done through the command *embedded region* that indicates to the computer code that they are positioned inside the concrete and both materials have perfect adherence. In the mesh generation, a refinement study was made, from which an automatic process was chosen which sought finite elements with a size equal to 30 mm.

It is important to note that in the computational codes, thermal numerical modeling is performed separately from the modeling in which the load of the structural element is considered. The analysis called thermo-structural, characterized by being the one in which a structural element is in a fire situation, is made by associating the results of each of the previously mentioned steps. Hence, naturally, in the numerical modeling performed in this article, which is the thermal analysis case, the possible effects caused by the load on the beam are not considered, so the reduction coefficients of the mechanical and thermal properties of the concrete and steel are not modified and correspond to those mentioned in the Brazilian and European standards. The thermal numerical results are described below.

5.1.1 Description of the thermal field

Using the parameters described above it was possible to obtain the thermal field formed in the cross section of the studied beam. In order to characterize the temperature advance along the section, six measurement points of this magnitude (T1 to T6) were selected and are indicated in Figure 5a that

presents the discretized beam. Based on this assumption, the evolution of the temperatures of these points is shown in Figure 5b.

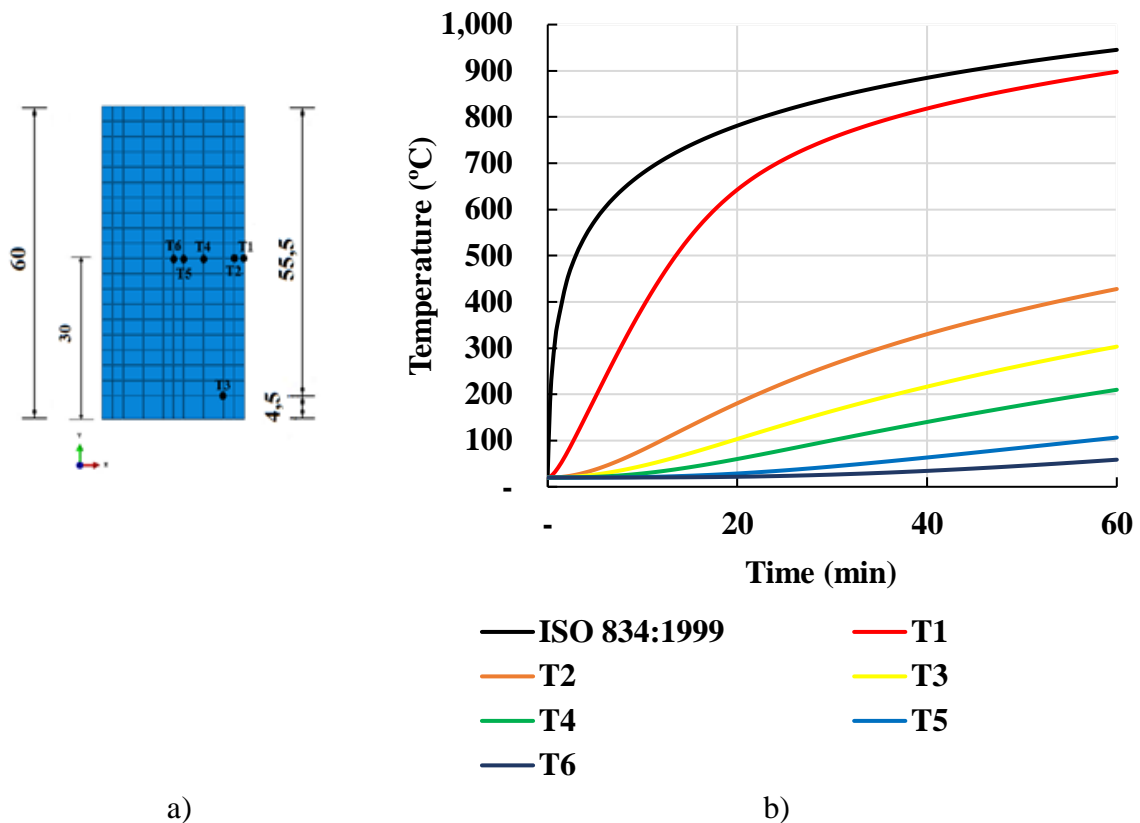


Figure 5. a) Position of temperature measuring points in the cross section; b) Evolution of the temperatures of the measuring points

As can be seen in Figure 5b, the reinforced concrete beam, even heated on all four sides, presented a non-uniform thermal field along the cross section, so that as it approached its geometric center, smaller the temperatures became. This is due to the low thermal conductivity of the concrete and the robustness of the section that promotes a differential heating of the structural element. The foregoing conclusion can be seen in Figure 6, in which the temperature variation developed in the section is illustrated for a time of 60 minutes exposure to fire.

It is important to emphasize that, as the numerical analysis was developed using the parameters (thermal properties and gas heating curve) provided by current fire standards, there will be no validation of these numerical models. This is because the experimental tests can hardly be calibrated by the normative parameters, since the heating curve usually obtained in tests differs from that of the standard fire. Moreover, since this is only a comparative study between types of reinforcement, the simplification above does not invalidate the purpose of this work.

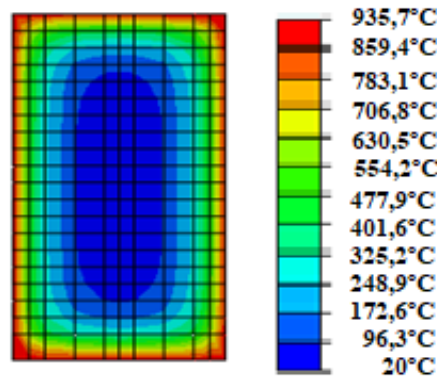


Figure 6. Temperature variation in the cross section

5.2. Resistant capacity of the degraded beams

In the previous item, the reinforced concrete beam was modeled to represent its behavior in a fire situation. After obtaining the thermal field, it was possible to calculate the average temperature of the cross section that results in the reduction of the mechanical properties of steel and concrete. Prior to this calculation, as well as for the determination of the resistant capacity of the deteriorated element, a 1.5 cm thick layer of concrete was removed in every cross section for spalling representation, being the new section shown in Figure 7.

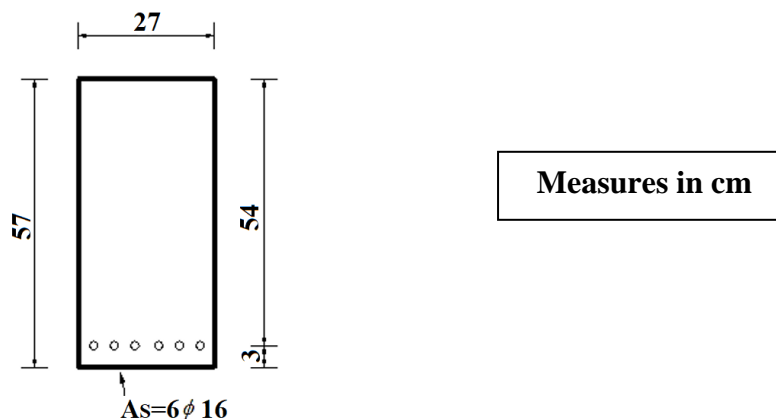


Figure 7. Cross section of degraded reinforced concrete beam

The average temperature for each section material, obtained in the thermal analysis, was 394.7°C for the concrete and 358,5°C for the steel. Based on the coefficients of the compressive strength reduction of the concrete ($k_{c,\theta}$), the yield stress ($k_{s,\theta}$) and the modulus of elasticity ($k_{Es,\theta}$) of the steel as a function of temperature described in NBR 15200: 2012 (Table 1) it was possible to reduce the mechanical properties of the materials.

To simplify the problem, the temperature of 400°C in both materials will be considered to reduce the mechanical properties described above. In view of this, concrete is now considered with $f_{ck} = 22,5\text{MPa}$ and steel, $f_y = 470\text{MPa}$ and $E_s = 147\text{GPa}$.

Based on the calculation method presented by NBR 6118:2014, it can be concluded that the beam has lost 12% of its pure flexure resistant capacity, i.e., the degraded section will only withstand a requesting bending moment of 233,7 kNm which is now in deformation domain 3. As described in the initial hypothesis, the beam was subjected to a requesting bending moment of 265.7 kNm, it will need structural reinforcement.

Table 1. Coefficients of reduction of steel and concrete mechanical properties

Temperature	Concrete	Steel	
	$k_{c,\theta}$	$k_{s,\theta}$	$k_{Es,\theta}$
20	1	1	1
100	1	1	1
200	0.95	1	0.9
300	0.85	1	0.8
400	0.75	0.94	0.7
500	0.6	0.67	0.6

Source: ABNT NBR 15200:2012 (Adapted).

5.3. Structural reinforcement design

In this item the necessary area of the structural reinforcement (carbon fiber and bonded-in steel sheet) is determined so that the degraded beam will again support the requested moment for which it was dimensioned. Therefore, initially the preexisting deformation in the steel (ε_{bi}), as a result of its initial loading, must be calculated as described in the reinforcement calculation methodology. Assuming that the permanent load corresponds to 80% of the total load acting on the beam and that it is a distributed single load, the requested moment of the calculation, due to this load, will correspond to 212.56 kNm. Thus, from the equilibrium equations and Hooke's Law, provided by the resistance of materials, it is calculated the deformation that the steel will have in the degraded beam which in this study was equivalent to 0.25%.

Following the methodology described in item 4, in the next items will be presented the calculation of the required area for the two types of reinforcements studied. In order to obtain the most economical situation in which the resistant moment (M_{Rd}) approaches the requested one (M_{Rd}), the position of the neutral axis was changed until it was reached the equilibrium equations.

5.3.1 Carbon fibers

The carbon fiber used in the development of this study corresponds to that provided by the company MasterBrace "BASF", it is called LAM 170/3100 "BASF", it has a square mesh of 120 mm wide, a thickness of 1.4 mm and a modulus of elasticity of 170 GPa. In Table 2, the design of the reinforcement with carbon fiber is shown in a simplified form.

Table 2. Design of carbon fiber reinforcement

x (cm)	F_c (kN)	F_s (kN)	F_r (kN)	σ_{fc} (kN/cm ²)	A_s (cm ²)	$F_s + F_r$ (kN)	M_{Rd}
14,00	413,10	492,89	2579,04	140,25	18,39	3071,93	197,56
15,00	442,61	492,89	2088,41	124,10	16,83	2581,30	210,94
16,00	472,11	492,89	1607,04	109,97	14,61	2099,93	224,10
17,00	501,62	492,89	1134,93	97,50	11,64	1627,82	237,02
18,00	531,13	492,89	672,07	86,42	7,78	1164,96	249,72
19,00	560,64	492,89	218,47	76,50	2,86	711,36	262,17
20,00	590,14	492,89	93,58	67,58	1,38	586,47	274,38

In which,

x - Position of the neutral axis;

F_c - Concrete resistant force;

F_s - Steel resistant force;

F_r - Reinforcement resistant force;

σ_{fc} - Tension to which the reinforcement is subject;

A_s - Required area of reinforcement;

$F_s + F_r$ - Sum of horizontal resistant forces of the steel and the reinforcement which, by equilibrium, must be equal to that corresponding to the resistant force of the concrete;

M_{Rd} - Resistant moment of the reinforced beam.

With the data presented in Table 2 it can be inferred that the position of the neutral axis, for an economic design associated with a correct balance of horizontal forces (resistant force of the concrete equal to the sum of steel and reinforcement resistant forces), is located between 19 and 20 cm. Analyzing this range of values, it is accepted that the value of $x = 19,85$ cm is the one that best meets the quoted criterion. For this value, the required reinforcement area is 1.35 cm^2 and the resistant moment is approximately 270 kNm.

As the carbon fiber has a width of 120 mm in each lamina and it has a thickness of 1.4 mm, only one layer of this reinforcement will be adopted along the whole span of the beam.

5.3.2 Bonded-in steel sheets

The laminated steel sheet used in this study corresponds to ASTM A 572 Grade 50, 4 mm thick, for structural works. According to NBR 8800:2008, sheet A 572, with a thickness of less than 100 mm and grade 50, has a yield stress of 345 MPa and a tensile stress equivalent to 450 MPa. Similar to item 5.3.1, Table 3 demonstrates the design for the bonded-in steel sheet.

Table 3. Design of bonded-in steel sheet reinforcement

x (cm)	F_c (kN)	F_s (kN)	F_r (kN)	A_s (cm ²)	$F_s + F_r$ (kN)	M_{Rd}
14,00	413,10	492,89	2192,19	73,07	2685,07	197,55
15,00	442,61	492,89	1775,15	59,17	2268,04	210,94
16,00	472,11	492,89	1365,99	45,53	1858,87	224,10
17,00	501,62	492,89	964,69	32,16	1457,58	237,03
18,00	531,13	492,89	571,26	19,04	1064,15	249,72
19,00	560,64	492,89	185,70	6,19	678,59	262,17
20,00	590,14	492,89	79,55	2,65	572,43	274,38

Based on the results presented in Table 3, it can be observed that the position of the neutral axis between 19 and 20 cm provides, in addition to a more economical design ($M_{Rd} = M_{sd}$), a better balance of horizontal forces. From the calculations, a value of x equal to 19.3 cm is defined. This value generates a resistant moment of approximately 265.8 kNm and a required area of reinforcement equal to 2.54 cm^2 .

In view of this, it is adopted a steel sheet with the same width of the beam and a thickness of 1 mm to be distributed along the length of the structural element.

5.3.3 Comparative analysis between carbon fiber and bonded-in steel sheet

Analyzing the presented results, it is possible to verify that the use of bonded-in steel sheet, as structural reinforcement, requires a larger area for the degraded beam to recover its resistant capacity. This is justified by the high mechanical strength of the carbon fiber.

For practical purposes, choosing the best type of reinforcement involves a number of factors, such as price, useful section increase, performance, runtime, among others. In general, the literature points to carbon fiber as the best type of structural reinforcement because, although more expensive compared to steel sheets, it has a faster execution, better performance and does not significantly increase the cross section, in addition to being corrosion resistant.

In the case study presented in this article, the increase of the cross section was similar for both reinforcements due to the low request required for the performance of the carbon fiber and the steel sheet. In view of this, and based on the available literature, it is stated that when it is necessary the expressive increase of the resistant capacity of a beam associated with a low increase of the cross section, the use of carbon fiber tends to be more advantageous when compared to the steel sheets. However, as mentioned, the choice of the best type of reinforcement should be made in a judicious way, analyzing all the parameters that influence this decision.

6. CONCLUSION

It has been developed a study about the comparison between structural reinforcement with bonded-in steel sheets and carbon fibers applied in fire-damaged reinforced concrete beams. The cited pathology reduces the mechanical properties of the steel and concrete, so that the resistant capacity for which the structural element is designed decreases, which requires the application of reinforcement.

Therefore, a case study was developed in which a reinforced concrete beam was modeled using the ABAQUS computational code and exposed to standard fire on all four faces during an exposure time of 60 min. From the obtained thermal field, it was possible to determine the average temperature that the constituent materials were submitted, approximately 400°C, which was responsible for reducing its mechanical properties.

When calculating the necessary reinforcement for the beams, it was verified that the carbon fiber generated a smaller area in comparison to the bonded-in steel sheet, since the first one presents a high mechanical resistance. In general terms, it is recognised that the carbon fiber presents greater advantages with respect to the reinforcement of beams, such as speed in the execution and a not significant increase of the height of the cross section.

7. REFERENCES

- ABNT, Associação Brasileira de Normas Técnicas (2008), “*NBR 8800: projeto de estruturas de aço e de estruturas mistas de aço e concreto de edifícios*”. Rio de Janeiro: ABNT.
- ABNT, Associação Brasileira de Normas Técnicas (2000), “*NBR 14432: exigências de resistência ao fogo de elementos construtivos de edificações – procedimento*”. Rio de Janeiro: ABNT.
- ABNT, Associação Brasileira de Normas Técnicas (2012), “*NBR 15200: projeto de estruturas de concreto em situação de incêndio – procedimento*”. Rio de Janeiro: ABNT.
- ABNT, Associação Brasileira de Normas Técnicas (2014), “*NBR 6118: projeto de estruturas de concreto – procedimento*”. Rio de Janeiro: ABNT.
- ACI, American Concrete Institute (2008), “*Guide for the design and construction of externally bonded FRP systems for strengthening concrete structures ACI 440.2R*”. Farmington Hills: ACI.
- Adorno, F. V., Dias, F. O., Silveira, J. C. O. (2015) “*Recuperação e Refuerzo de Vigas de Concreto armado*”, Trabalho de Conclusão de Curso, Universidade Federal de Goiás, Goiás, p. 70.
- Branco, F. G. (2012), “*Reabilitação e refuerzo de estruturas*”. Portugal: Instituto Superior Técnico.
- Chowdhury, E. U., Bisby, L. A., Green, M. F., Kodur, V. K. (2008), “*Residual Behavior of Fire-Exposed Reinforced Concrete Beams Prestrengthened in Flexure with Fiber-Reinforced Polymer*”.

- Sheets”. Journal of Composite for Construction, 12 (1):61-68. [https://doi.org/10.1061/\(ASCE\)1090-0268\(2008\)12:1\(61\)](https://doi.org/10.1061/(ASCE)1090-0268(2008)12:1(61))
- Deeny, S. M., Stratford, T., Dhakal R. P. (2008), “*Spalling of concrete: Implications for structural performance in fire*”, Conference Paper, University of Canterbury, New Zealand, pp. 1-5.
- EUROCODE, European Committee for Standardization (2004), “*Eurocode2 - Design of concrete structures - Part 1-2: General rules - Structural fire design*”. Brussels: EUROCODE.
- Fard, M. Y., Sadat, S. M., Raji, B. B., Chattopadhyay, A. (2014), “*Damage characterization of surface and sub-surface defects in stitch-bonded biaxial carbon/epoxy composites*”. Composites Part B: Engineering, 56:861-829. <https://doi.org/10.1016/j.compositesb.2013.09.011>
- Firmo, J. P., Arruda, M. R. T., Correia, J. R., Tiago, C. (2015), “*Flexural behaviour of partially bonded carbon fibre reinforced polymers strengthened concrete beams: Application to fire protection systems design*”. Materials and Design, 65:1064-1074. <https://doi.org/10.1016/j.matdes.2014.10.053>
- Foster, S. K., Bisby L. A. (2005), “*High Temperature residual properties of externally-bonded FRP Systems*”, in: Proceedings of the 7th international symposium on fiber reinforced polymer reinforcement for reinforced concrete structures (FRPRCS-7) ACI SP230-70, 7:1235-1252.
- Hertz, K. D. (2003), “*Limits of spalling of fire-exposed concrete*”. Fire Safety Journal, 38 (2):103-116. [https://doi.org/10.1016/S0379-7112\(02\)00051-6](https://doi.org/10.1016/S0379-7112(02)00051-6)
- Ingham, J. P. (2009), “*Application of petrographic examination techniques to the assessment of fire-damaged concrete and masonry structures*”. Materials characterization, 60(7):700-709. <https://doi.org/10.1016/j.matchar.2008.11.003>
- ISO, International Standard (1999), “*Fire-resistance tests - Elements of building construction - Part 1: General requirements*”. Geneva: ISO, p. 25.
- Jiangtao, Y., Yichao, W., Kexu, H., Kequan, Y., Jianzhuang, X. (2017), “*The performance of near-surface mounted CFRP strengthened RC beam in fire*”. Fire Safety Journal, 90:86-94. <https://doi.org/10.1016/j.firesaf.2017.04.031>
- Khoury, G. A. (2000), “*Effect of fire on concrete and concrete structures*”. Progress in Structural Engineering and Materials banner, 2:429-447. <https://doi.org/10.1002/pse.51>
- Kobes, M., Helsloot, I., de Vries, B., Post, J. G. (2010), “*Building safety and human behaviour in fire: A literature review*”. Fire Safety Journal, 45(1):1-11. <https://doi.org/10.1016/j.firesaf.2009.08.005>
- Kodur, A. K. R., Agrawal, A. (2016), “*An approach for evaluating residual capacity of reinforced concrete beams exposed to fire*”. Engineering Structures, 110:293-306. <https://doi.org/10.1016/j.engstruct.2015.11.047>
- Kumahara, S., Masuda, Y., Tanano, H., Shimizu, A. (1993), “*Tensile Strength of continuous Fiber Bar under High Temperature*”, in: International Symposium on Fiber-Reinforced Plastic for Concrete Structures, pp. 731-742.
- Lin, X., Zhang, Y. X. (2013), “*Nonlinear finite element analyses of steel/FRP-reinforced concrete beams in fire conditions*”. Composite Structures, 97:277-285. <https://doi.org/10.1016/j.compstruct.2012.09.042>
- Machado, A. P. (2002), “*Refuerzo de estructura de construcción armado com fibras de carbono*”. São Paulo: Editora Pini Ltda.
- Machado, A. P. (2007), “*Refuerzo de estructuras de concreto com fibras de carbono*”. São Paulo: Revista Técnica.
- Obaidat, Y. T. (2011) “*Structural retrofitting of reinforced concrete beams using carbon fibre reinforced polymer*”, Thesis de doctorado, Department of Construction Sciences, Division of Structural Mechanics, LTH, Lund University, Sweden, p. 88.

- Raof S. M., Bournas, D. A. (2017), “*TRM versus FRP in flexural strengtning of RC beams: Behaviour at high temperatures*”. *Construction and Builddding Materials*, 154:424-437. <https://doi.org/10.1016/j.conbuildmat.2017.07.195>
- Reis, L. S. N. (1998) “*Refuerzo de vigas de concreto armado por meio de barras de acero adicionales ou lâminas de acero e argapeso de alto desempenho*”, Dissertação de Mestrado em Engenharia de Estruturas, Escola Engenharia de São Carlos, Universidad de São Paulo, São Carlos, p.293.
- Reis, L. S. N. (2001), “*Sobre a recuperação e refuerzo de estruturas de concreto armado*”, Dissertação de Mestrado em Engenharia de Estruturas, Escola de Engenharia, Universidad Federal de Minas Gerais, Belo Horizonte, p. 114.
- Souza, A. F. V. S. (2008), “*Reparação, Reabilitação e Refuerzo de Estruturas de Betão Armado*”, Dissertação de Mestrado em Engenharia de Estruturas, Universidad do Porto, Portugal, p.114.
- Štukovnik, P., Prinčič, T., Pejovnik, R. S., Bokan Bosiljkov, V. (2014), “*Alkali-carbonate reaction in concrete and its implications for a righ rate of long-term compressive strength increase*”. *Constrution and Buildings Materials*.50:699-709. <https://doi.org/10.1016/j.conbuildmat.2013.10.007>
- Tanamo, H. et al. (1997), “*Tensile Properties at High Temperature of Continuous Fiber BARs and Deflections of contínuos Fiber Reinforced Concrete Beams under High-Temperature Loading*”, in: *The 3th Internaciona Symposium on Non-Metallic (FRP) Reinforcement for Concrete Structures*, 2:43-50.
- Wang, G., Barber, D., Johnson, P., Hui, M.-C. (2013), “*Fire safety provisions for aged concrete building structures*” in: *The 9th Asia-Oceania Symposium on Fire Science and Technology*, 62:629-638. <https://doi.org/10.1016/j.proeng.2013.08.108>
- Wang, Y. C., Wong, P. M. H., Kodur, V. (2003), “*Mechanical Properties of Fiber Reinforced Polymer Reinforcing Bars at Elevated Temperatures*”, in *ASCE – SFPE Specialty Conference on Designing Structures for Fire*, pp 183-192.

Experimental analysis of reinforced concrete beams strengthened with steel bars and epoxy structural adhesive

R. J. C. Silva^{1*} , M. B. S. Muniz¹ , F. E. S. da Silva Júnior² , É. M. F. Lima³ , C. V. dos S. Araújo⁴ .

*Contact author: ricardo.carvalho222@gmail.com

DOI: <http://dx.doi.org/10.21041/ra.v9i1.213>

Reception: 03/07/2017 | Acceptance: 01/08/2018 | Publication: 30/12/2018

ABSTRACT

This work was aimed at analyzing the efficiency of the strengthening of reinforced concrete beams with the addition of steel bars and epoxy adhesive. Five beams were produced, out of which four beams were strengthened to flexure. In two of them, “U” clips were also used to improve the anchorage of the strengthening. The tests demonstrated that the clips reduced the resistances of the beams compared to those without clips. The strengthened beams without clips yielded better results, but the largest limiting factor was the adherence between the epoxy and beam. The use of clips for solving the problem of adherence made this research original. The conclusions were based on the comparisons of the tested beams.

Keywords: strengthening; beam; reinforced concrete; jacketing.

Cite as: R. J. C. Silva, M. B. S. Muniz, F. E. S. da Silva Júnior, É. M. F. Lima, C. V. dos S. Araújo (2019), “*Experimental analysis of reinforced concrete beams strengthened with steel bars and epoxy structural adhesive*”, Revista ALCONPAT, 9 (1), pp. 65 – 78, DOI: <http://dx.doi.org/10.21041/ra.v9i1.213>

¹ Vale do Acaraú State University, Sobral, Brasil

² Federal University of Rio Grande, Rio Grande, Brasil

³ Federal University of Ceará, Fortaleza, Brasil

⁴ University of Brasília, Brasília, Brasil

Legal Information

Revista ALCONPAT is a quarterly publication by the Asociación Latinoamericana de Control de Calidad, Patología y Recuperación de la Construcción, Internacional, A.C., Km. 6 antigua carretera a Progreso, Mérida, Yucatán, 97310, Tel.5219997385893, alconpat.int@gmail.com, Website: www.alconpat.org

Responsible editor: Pedro Castro Borges, Ph.D. Reservation of rights for exclusive use No.04-2013-011717330300-203, and ISSN 2007-6835, both granted by the Instituto Nacional de Derecho de Autor. Responsible for the last update of this issue, Informatics Unit ALCONPAT, Elizabeth Sabido Maldonado, Km. 6, antigua carretera a Progreso, Mérida, Yucatán, C.P. 97310.

The views of the authors do not necessarily reflect the position of the editor.

The total or partial reproduction of the contents and images of the publication is strictly prohibited without the previous authorization of ALCONPAT Internacional A.C.

Any dispute, including the replies of the authors, will be published in the third issue of 2019 provided that the information is received before the closing of the second issue of 2019.

Análisis experimental de vigas de hormigón armado reforzadas con barras de acero y adhesivo epoxi estructural

RESUMEN

Este trabajo tuvo como objetivo analizar la eficiencia del refuerzo en vigas de hormigón armado mediante la adición de barras de acero y adhesivo epoxi. Se produjeron cinco vigas. Cuatro recibieron refuerzo a flexión, y en dos de ellas fueron adicionadas también abrazaderas “U” para mejorar el anclaje del refuerzo. Los ensayos mostraron que las abrazaderas redujeron la resistencia de las vigas, en comparación con las que no tenían. Las vigas reforzadas sin abrazaderas obtuvieron mejores resultados, pero el factor limitante más importante fue la adherencia entre el epoxi y la viga. El uso de abrazaderas para intentar resolver el problema de la adherencia dio originalidad a esta investigación. Las conclusiones se basaron en la comparación entre las vigas ensayadas.

Palabras clave: reforzamiento; viga; hormigón armado; encamisado.

Análise experimental de vigas de concreto armado reforçadas com barras de aço e adesivo estrutural epóxi

RESUMO

Esse trabalho objetivou analisar a eficiência do reforço com adição de barras de aço e adesivo epóxi em vigas de concreto armado. Foram produzidas cinco vigas. Quatro receberam reforço à flexão e em duas delas também foram utilizados grampos em “U” para melhorar a ancoragem do reforço. Os ensaios mostraram que os grampos reduziram a resistência das vigas em relação às sem grampos. As vigas reforçadas sem grampos obtiveram melhores resultados, sendo o maior limitador a aderência entre o epóxi e a viga. O uso dos grampos para tentar resolver o problema da aderência deram originalidade a essa pesquisa. As conclusões foram baseadas nas comparações entre as vigas ensaiadas.

Palavras-chave: reforço; viga; concreto armado; encamisamento.

1. INTRODUCTION

The need to rehabilitate reinforced concrete structures by strengthening may arise because of the lack of maintenance during their lifespan and their adaptation to new uses when the option of demolishing and rebuilding them is not viable. In this case, some studies were conducted regarding the strengthening of reinforced concrete structures. However, because of the ongoing development in this topic of structural engineering, there is still no specific methodology for analyzing the structural behavior of the rehabilitated beams.

According to Reis (Reis, 1998), intense studying in scientific research on the strengthening and rehabilitation of reinforced concrete structures is very important. This is mainly to define the designing rules better, understand the behavior of the strengthening of structures over time, and identifying approaches for analyzing the adhesion between the materials as well as their properties. These studies would enable determining which materials, techniques, procedures, and rules are more suitable to be used during the realization of structural rehabilitation. Therefore, the literature on the strengthening of reinforced concrete beams such as the papers by Helene (Helene, 2000), Cheong and MacAlevey (Cheong and MacAlevey, 2000), Reis (Reis, 2003), Alfaiate and Costa (Alfaiate and Costa, 2004), Altun (Altun, 2004), Santos (Santos, 2006), Lima (Lima, 2015), and Deghenhard et al. (Deghenhard et al., 2016) have been extremely important for the advancement of research in this area.

Although there are various strengthening techniques, this work will focus on the method of rehabilitation of reinforced concrete beams via the introduction of steel bars and epoxy structural adhesive (jacketing). The study of this technique, despite being antiquated, is still very important because of two simple reasons. First, it continues to be a widely used strengthening technique for small and medium works in Brazil. Second, in this research, serious problems were identified with this type of strengthening, which need further discussion.

The main objective of this work was to study the rehabilitation of reinforced concrete beams by the addition of steel bars and epoxy structural adhesive.

2. EXPERIMENTAL PROGRAM

2.1 Characteristics of the beams

For this study, the Structure and Material Research Group (GEM) of Vale do Acaraú State University (UVA) produced five reinforced concrete beams, of which four were strengthened and one beam was used as a reference (not strengthened). All the beams were produced with the same dimensions: 80 cm length (with a span of 60 cm), 15 cm height, and 10 cm width, as shown in Figure 1.

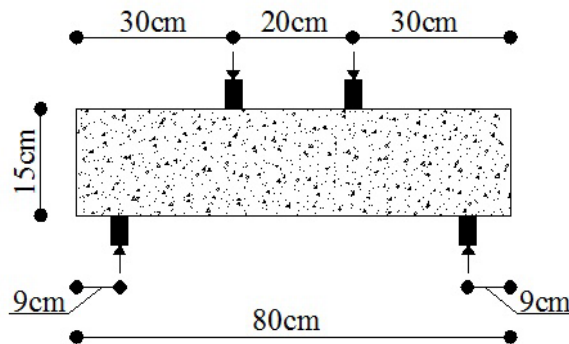


Figure 1. Dimensions of the tested beams.

The reference beam was not strengthened and is denoted as Beam E1. The other beams (E2, E3, E4, and E5) were strengthened by different approaches. All the beams had two longitudinal reinforcement bars with a diameter of 6.3 mm, and twelve transversal reinforcements (stirrups) with a diameter of 6.3 mm and 6.4 cm spacing. This arrangement of reinforcement bars was chosen so that the failure of the beams could be due to flexure. Figure 2 displays the details of the reinforcement of the five beams.

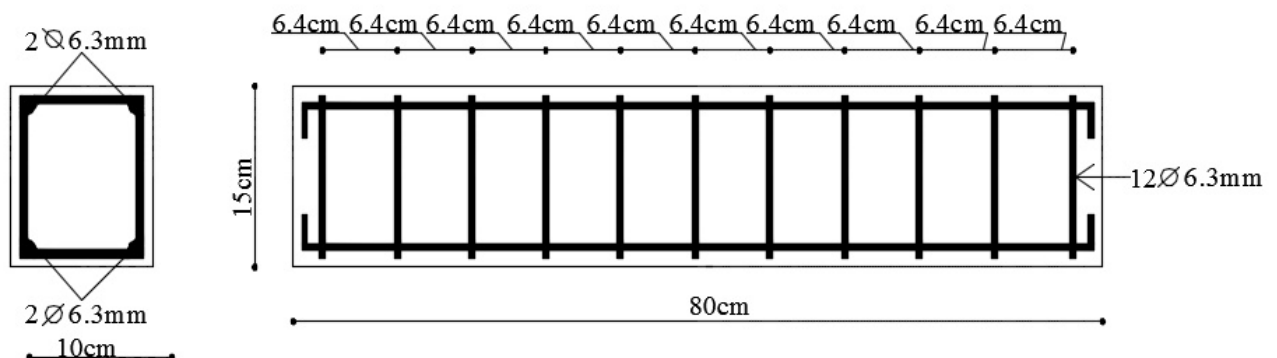


Figure 2. Details of the reinforcement of the beams.

Beam E2 was strengthened to flexure with the insertion of two bars of ϕ 6.3 mm and 50 cm length in a “tooth” formed with epoxy adhesive (Figure 3).

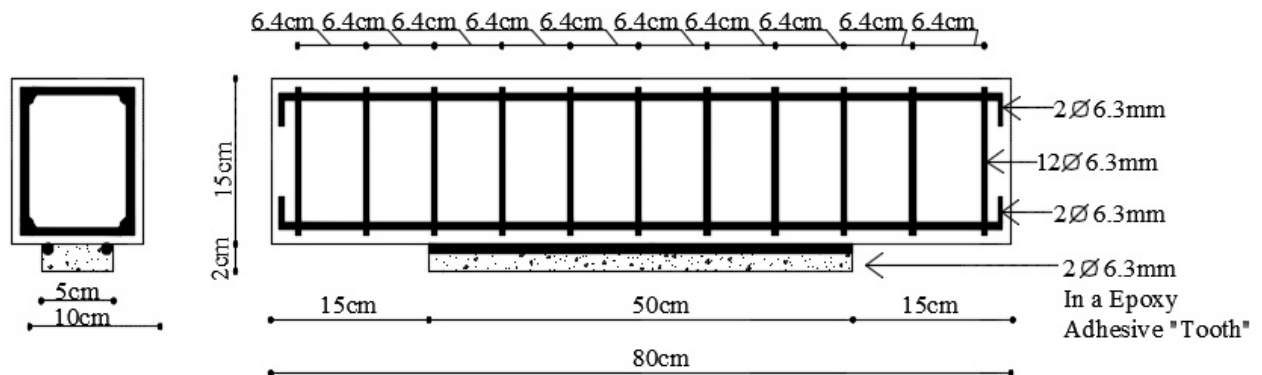


Figure 3. Details of the strengthening of Beam E2.

Beam E3 was also strengthened to flexure with the insertion of two bars of ϕ 6.3 mm and 50 cm length in a “tooth” formed with epoxy adhesive. To improve the anchorage of the strengthening bars to the substrate of the beam, seven “U” shaped clips of 7 cm height and 4.5 cm width were inserted (see later in Figure 7), which penetrated 5.5 cm into the beam (Figure 4).

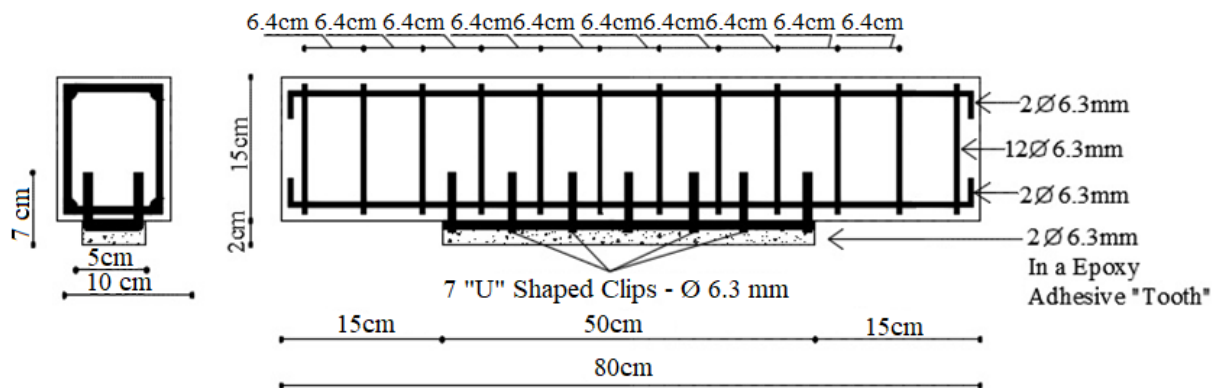


Figure 4. Details of the strengthening of Beam E3.

Beam E4 was strengthened to flexure with the insertion of two bars of ϕ 6.3 mm and 30 cm length in a “tooth” made with epoxy adhesive. The sizes of these bars were reduced to remain almost completely inside the pure flexure region (Figure 5).

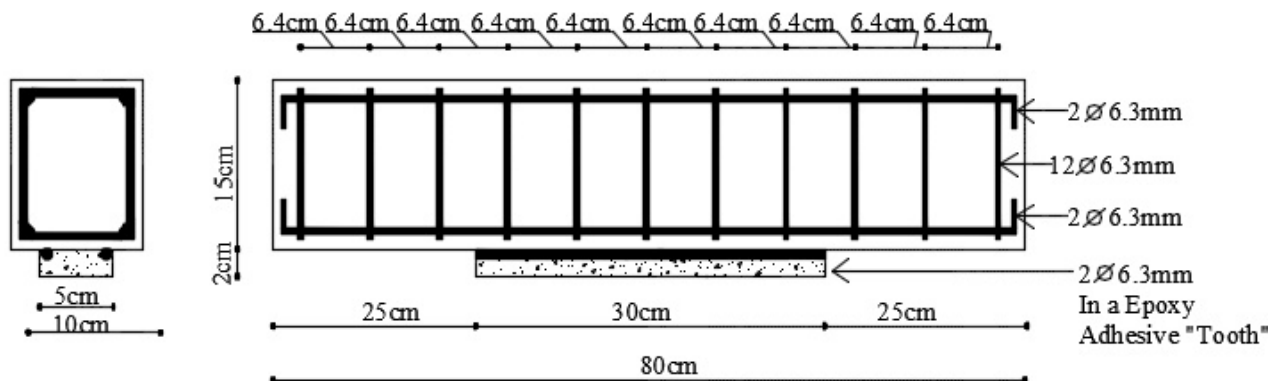


Figure 5. Details of the strengthening of Beam E4.

Table 1. Characteristics of the tested beams.

Beams	Strengthening	Bottom reinforcement	Stirrups	f_y (MPa)	E_s (GPa)	f_c (MPa)	f_t (MPa)	E_{cs} (MPa)
E1	Without Strengthening	2 ϕ 6.3 mm	12 ϕ 6.3 mm	500	210	34.91	3.20	29357.64
E2	2 ϕ 6.3 mm Length = 50 cm							
E3	2 ϕ 6.3 mm + 7U Length = 50 cm							
E4	2 ϕ 6.3 mm Length = 30 cm							
E5	2 ϕ 6.3 mm + 3U Length = 30 cm							
f_y = Yield limit of the steel according to the manufacturer; E_s = Modulus of elasticity of the steel according to the manufacturer; f_c = Average resistance to compression of concrete on the date of the test; f_t = Average resistance to tensile of concrete on the date of the test; E_{cs} = Secant modulus of elasticity of concrete calculated by NBR6118 (ABNT – NBR6118, 2014).								

Although the analyzed beams had reduced dimensions compared to real beams, it is necessary to emphasize that the aim of this work was not to determine any correlation between the reduced model and a prototype, through a dimensional analysis and laws of similarity, in a quantitative analysis. The aim was to only compare the structural behavior of the strengthened beams (E2, E3, E4, and E5) and reference beam (E1) in a qualitative analysis.

2.2 Test system

The beams built in this research underwent experimental tests performed at the Laboratory of Materials of Vale do Acaraú State University. They were submitted to the Stuttgart test, in which two concentrated forces equidistant from the supports were applied. This allowed studying the strengthening in the regions submitted to pure flexure and where shear effects (simple flexure) were also observed. Figure 8 illustrates a hydraulic press used for the tests.

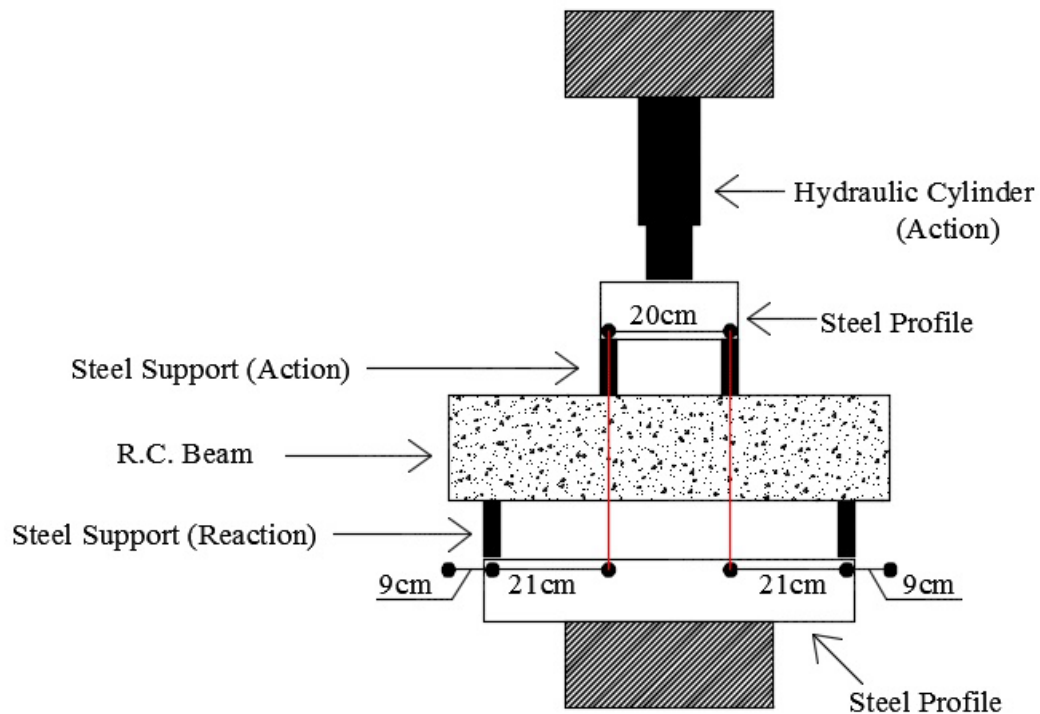


Figure 8. Details of the press used with a beam in the Stuttgart test.

The experimental tests are divided into two stages. In the first stage, beams E2, E3, E4, and E5 are subjected to a cracking load of 50 kN, which is equivalent to 60% to 80% of the failure load. The aim of this first stage was to crack the beams to simulate the need of strengthening. After removal of the 50 kN load, the beams were rehabilitated with steel bars and epoxy adhesive. The epoxy adhesive used to assist the anchor strengthening the bars to the substrate of the beam was Sikadur 31, which was not mixed with sand. The resistance to compression of Sikadur 31 at three days of age was 60 MPa, and the rehabilitation followed the manufacturer recommendations (Sika, 2015). One week after the rehabilitation, the second stage of the experimental tests began, which consisted of loading the beams through the Stuttgart test. The process was conducted with load steps of 10 kN until the beam exhibited failure. In each interval of the load applied to the beam, crack formation was examined and marked with a whiteboard marker to assist in the identification of the failure modes.

2.3 Computational model

The beams made for the experimental tests were also simulated in ANSYS software, which uses the finite element method for the discretization of structures. The computational modeling with the software was performed to replicate the conditions of the Stuttgart test performed in laboratory. Therefore, the same characteristics of the used materials were considered to obtain consistent results, which could then be correlated to the results of the experimental analysis. Figure 9 illustrates the modeling of the stirrups of Beam E1 and one of the other four beams, because of their identical rebars and spacing.

The supports and points of application of the loads were modeled with a 20 mm width, instead of 10 mm as in the tests, so that there were no stress concentrations in these regions, which could make the numerical convergence complex and cause an early failure.

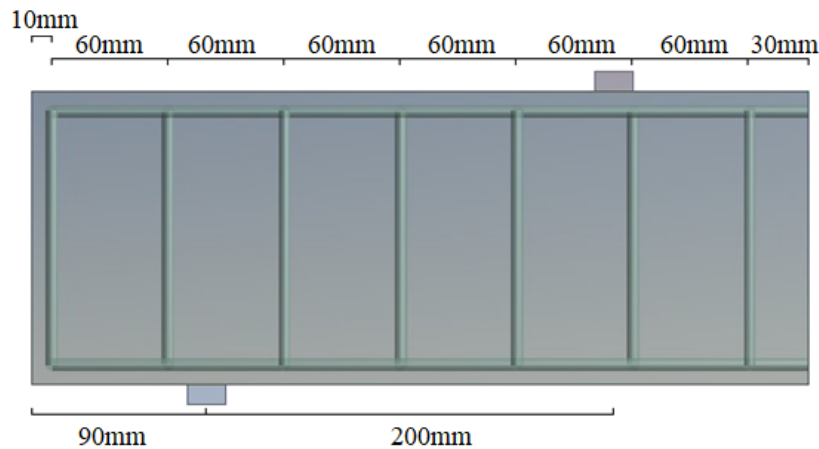


Figure 9. Modeling of the transversal reinforcement (stirrups) of beam E1.

To validate the results provided by the ANSYS software with the literature and study the effect of discretization on the precision of the results, the beams were modeled considering the individual properties of the steel and concrete materials: the modulus of elasticity, Poisson coefficient, and interactions between both the materials, as listed in Table 2.

Table 2. Properties of the Materials

Characteristics	Concrete	Steel Bars (CA-50)	Epoxy Adhesive (Sikadur 31)
Elasticity Modulus	26838 MPa ⁽¹⁾	210 GPa ⁽²⁾	4.3 GPa ⁽³⁾
Poisson coefficient	0.2 ⁽⁴⁾	0.3 ⁽⁵⁾	0.2 ⁽⁵⁾

⁽¹⁾ Secant modulus of elasticity of concrete calculated by NBR6118 (ABNT – NBR6118, 2014);
⁽²⁾ Modulus of elasticity of the steel according to the manufacturer;
⁽³⁾ Modulus of elasticity of the epoxy adhesive according to the manufacturer;
⁽⁴⁾ Poisson coefficient adopted;
⁽⁵⁾ Poisson coefficient according to the manufacturer.

Three-dimensional eight-node element Solid65 was used to model the concrete. This solid has three degrees of freedom in each node, and it is capable of cracking and crushing under tension and compression, respectively. This element considers the Willam–Warnke failure criterion for compression, and the tensioned region of the concrete is considered as an isotropic material with softening. The element is illustrated in Figure 10.

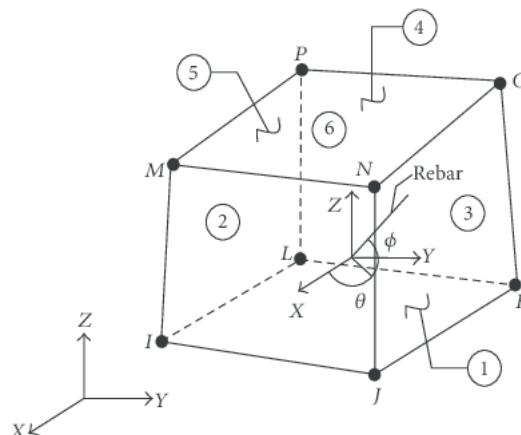


Figure 10. Geometry of element Solid65 (Ansys, 2013)

Three-dimensional element Link180 was used for modeling the reinforcements. This element has two nodes with three degrees of freedom in each node, and it is widely used to represent bars, trusses, and cables in a simplified way. This element only resists axial forces and assumes that the material exhibits the same behavior under compression and tension. An elastoplastic model is defined with a bilinear tension–strain graph as the failure criterion.

Shell element Shell181 was used to model the strengthening bars and epoxy adhesive. This type of element is mainly used for modeling jacketing with carbon fibers, but it can also be used for modeling external strengthening with steel bars. This element has four nodes with six degrees of freedom in each node and the capacity of plasticity, and its depth is considered in the analysis.

The size of the mesh was 10 mm. According to Muliterno and Pravia (Muliterno and Pravia, 2016), in nonlinear analysis, the load is divided into a series of substeps so that in each substep the stiffness matrix is updated to consider the nonlinear alterations in the structural stiffness before going to the next substep. This analysis used 500 substeps, and in each load step, the load was applied from bottom to top and a force-based convergence criterion was used. The load was applied until a magnitude error occurred, which was considered as the moment of failure. The supports were inserted into the two superior faces of the elements of reaction and defined as zero displacements in the X, Y, and Z axes. The CEINTF command was executed to combine the nodes of the beam and reinforcement, considering that there was a perfect adherence between both the materials.

3. RESULTS AND DISCUSSIONS

3.1 Loads and Failure Modes

After a visual verification of the conditions of the beams after the failure, each tested beam was correlated to the computational model and compared to the reference beam.

After all the beams achieved their ultimate load, a comparison was made between the rehabilitated and reference beams, analyzing the ultimate loads and failure modes. The most efficient strengthening method among the strengthened beams was also identified. Table 3 lists the details of the strengthening methods, ultimate load, and failure mode of each beam.

Table 3. Description of the strengthening methods, loads, and failure modes of the beams.

Beam	Strengthening	V _{ANSYS} (kN)	V _{Exper} (kN)	V _{Exper} / V _{ANSYS}	Failure Mode
E1	Without Strengthening	85.00	80.00	0.94	Flexure
E2	2 ϕ 6.3 mm (length = 50 cm) in “tooth” with epoxy adhesive	89.75	108.00	1.20	Flexure
E3	2 ϕ 6.3 mm (length = 50 cm) in “tooth” with epoxy adhesive and 7 “U” shaped clips	87.75	96.00	1.09	Shear (Compression Strut)
E4	2 ϕ 6.3 mm (length = 30 cm) in “tooth” with epoxy adhesive	90.00	116.00	1.29	Flexure
E5	2 ϕ 6.3 mm (length = 30 cm) in “tooth” with epoxy adhesive and 4 “U” shaped clips	80.00	74.00	0.93	Flexure

V_{ANSYS} = Computational failure load indicated by the Ansys software;
V_{Exper} = Experimental failure load.

3.2 Effect of the Solicitation Mode

In the experimental tests, when the beams were subjected to the second stage, Beam E2 achieved an ultimate load of 108 kN, and it was verified that it failed after the strengthening unbonded from the beam, causing failure by flexure. Comparison with the reference Beam (E1) verified that its resistance increased by 35%.

The analysis of the results of the test of Beam E3 revealed that it failed after the strengthening unbonded from the substrate of the beam. However, unlike Beam E2, it had a different failure mode due to the compression of the strut. Comparison with the reference beam verified that the mechanical resistance of Beam E3 increased by 20%.

The analysis of the results of Beam E4 verified similar to Beams E2 and E3; it failed by flexure after the strengthening unbonded from the beam. Despite the indications of a compressed strut caused by the clips, the failure mode was flexural failure. It exhibited an increase of 45% in its resistance relative to the reference beam.

Beam E5 had the same failure mode as Beams E2 and E4; it was caused by flexure after the strengthening unbonded from the beam. Compared to the reference beam, its resistance decreased by 7.85%. Figure 11 shows the tested beams after their failure.



Figure 11. Beams E1, E2, E3, E4, and E5 after failure.

The results obtained through the ANSYS software verified that the ultimate loads yielded by the software agreed to the results achieved in the experimental tests. The failure modes of the beams and variation in the results compared to the reference beam were also similar. However, there was a difference in the strengthening: in the experimental test, the strengthening debonded from the beams before they underwent failure, but in the analysis, this did not occur because the friction between the beam and strengthening was not considered. Figure 12 presents the load–displacement plot of the five beams obtained from the computational analysis.

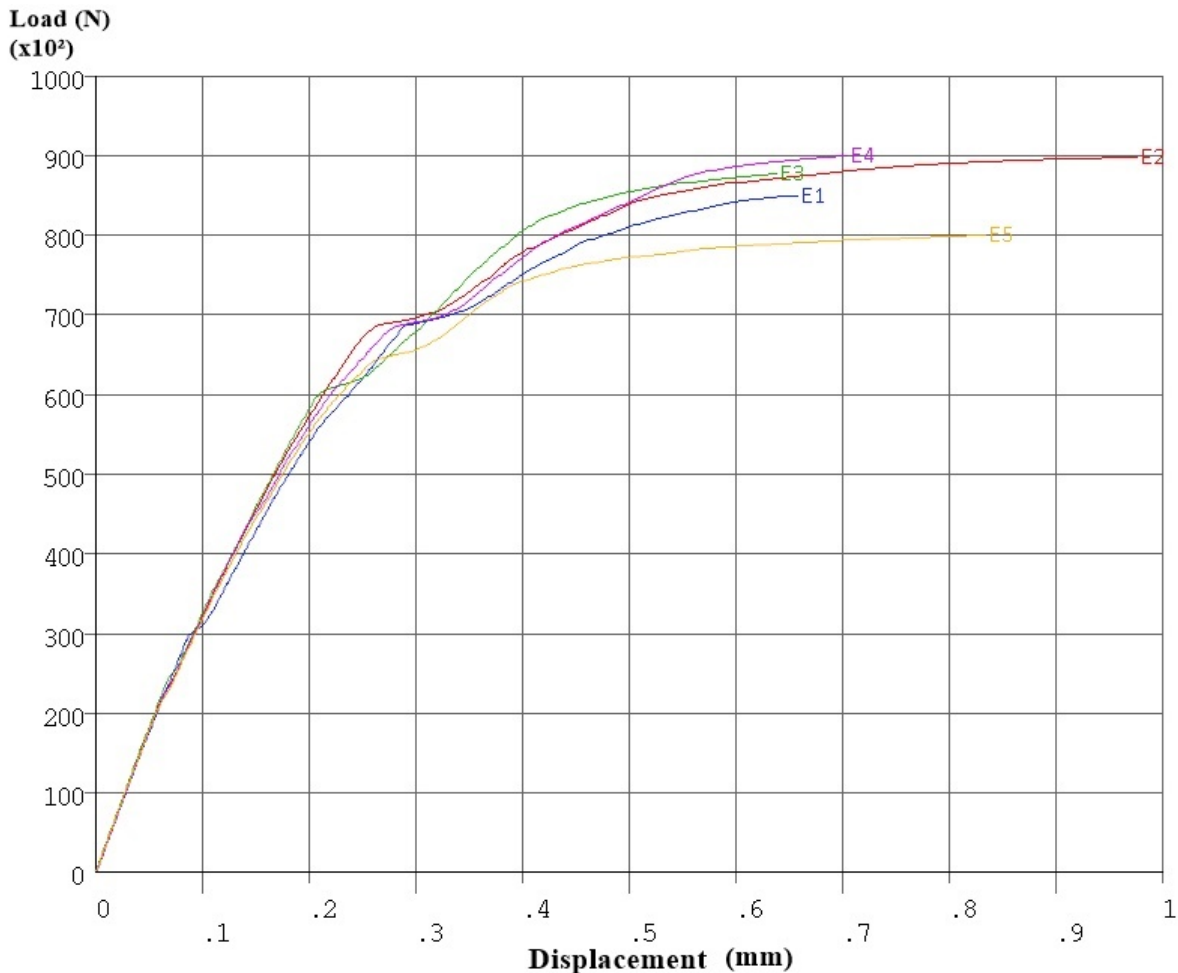


Figure 12. Load–displacement plot of all the beams on the same scale.

Dahmani, Khennane, and Kaci (Dahmani, Khennane, and Kaci, 2010) emphasized the symbology of ANSYS for the types of failure due to flexure (by flexural crack), shear (by shear crack), and compression (by crushing). These symbologies are presented as the labels in Figure 13. In addition, Dahmani, Khennane, and Kaci (2010) claimed that these symbols could also be combined depending on the type of failure. It is important to emphasize that this type of failure shown by ANSYS is a local failure, for example, the opening of a crack and a localized crushing. It alone does not provide the failure of the entire beam. A combination of these localized failures is what characterizes the failure of the beam as a whole.

The aim of the numerical analysis of the strengthened beams was to show the stress distribution in the beams after the insertion of the strengthening, to provide results for comparison with the experimental results.

The analysis of the image, as generated by ANSYS (Figure 13), exhibiting the cracked beam the instant before it underwent failure as well as the location of the clips and strengthening. This verifies that in the region where the beam is strengthened, the appearance of compression stresses is very perceptible, mainly where the first clip is inserted in the beam (from left to right). From the correlation with the experimental test, it can be noted that this is the same region where concrete is crushed (Figure 11), i.e., the region where the beam undergoes failure.

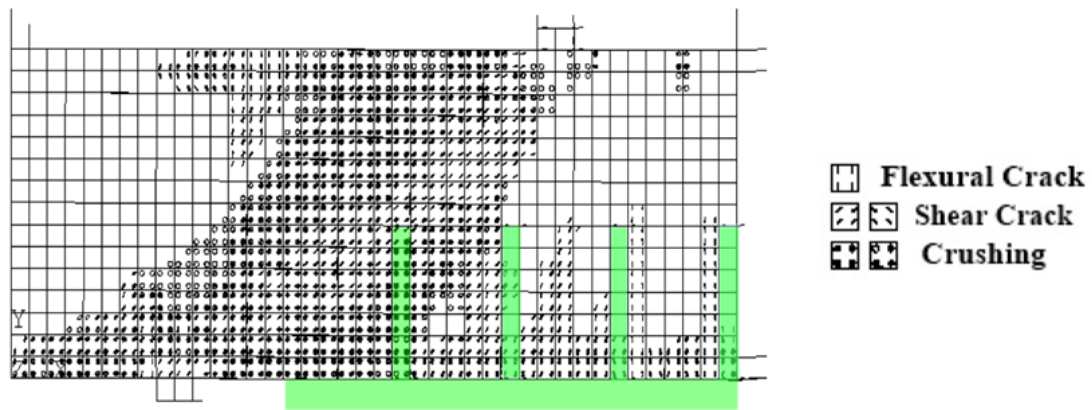


Figure 13. Crack and crushing pattern generated by ANSYS for Beam E3.

The use of clips in the strengthening of the beams, which was aimed at improving the anchorage, generated concentrations of undesirable stresses in the beams. In the analysis of this problem using the Strut and Tie Model, a secondary strut from the top of the clip to the bottom of the stirrup was observed, which overloaded the existing strut (Figure 14).

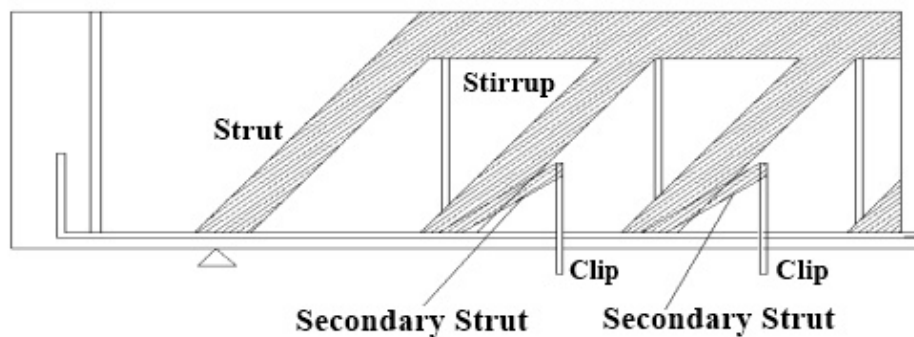


Figure 14. Strut and tie Model for Beams E3 and E5.

4. CONCLUSIONS

In this work, the analysis of the results verified that the beams with clips assisted in the anchorage between the beam and strengthening (E3 and E5). More precisely, for Beam E3, the failure mode was a compressed strut, which could be reasoned by the increase in the field of compression of the beam caused by the addition of the clips. For Beam E5, which failed under a lower load than the reference beam (E1), it was verified that after perforating the beam to insert the clips, its stiffness was reduced, thus damaging the strength of the beam.

Beam E4 experienced the highest failure load, and it was only distinguishable from Beam E2, for which the same strengthening technique was used, through its length. It can be concluded that the strengthening of Beam E2 was effective in the region of simple flexure until it unbonded from the beam and underwent failure. The strengthening of Beam E4 was effective in the region of pure flexure, which explained its higher ultimate load in comparison to Beam E2 and all the other tested beams.

The aim of the computational analysis of the strengthened beams was to show the stress distribution in the beams after the insertion of the strengthening to compare them with the real results and validate them. Thus, it can be concluded that in general, the performed analysis satisfactorily simulated the experimental tests, explaining the failure due to the diagonal compression of Beam E3.

Analysis of the strengthened and reference beams revealed that Beams E2 and E4 were under superior ultimate loads compared to the other beams. However, it can be concluded that in this study, the addition of the clips to Beams E3 and E5 damaged their strength. Moreover, the unbonding of the strengthening, which occurred in all the strengthened beams, was because the epoxy resin has an elasticity modulus significantly lower than of the other materials of the system. Therefore, when a strengthened beam was loaded, because of insufficient stiffness, the resin did not transfer all the tension that it received from the lower face of the beam. This resulted in the unbonding of the strengthening, indicating that only steel works. The scenario would be different if the materials had similar elasticity moduli. Thus, despite Beams E2, E3, and E4 having larger ultimate loads than the reference beam, the system does not operate efficiently. Therefore, it is not recommended to use this type of strengthening because it is ineffective and can be dangerous. It is important to emphasize that the conclusions of this work are limited only to the results of the tests of the five beams presented here. Other future research studies with more tests of beams and with and without strengthening are necessary for a better validation of this research.

5. REFERENCES

- Alfaiate, J., Costa, R. (2004). “*O reforço de vigas de betão armado com chapas metálicas coladas com resina*”. Métodos Computacionais em Engenharia, APMTAC, Portugal, pp 1-13. <http://hdl.handle.net/10400.1/1397>
- Altun, F. (2004) “*An experimental study of jacketed reinforced concrete beams under bending*”. Construction and Building Materials, 18 (8), pp. 611-618. <https://doi.org/10.1016/j.conbuildmat.2004.04.005>
- Ansys (2013). “*Ansys Mechanical APDL Technology Structural Analysis Guide*”. ANSYS Inc. Release 15.0, Southpointe, 498p.
- Associação Brasileira de Normas Técnicas. (2014), *NBR 6118: Projetos de Estruturas de Concreto - Procedimento*. Rio de Janeiro.
- Associação Brasileira de Normas Técnicas. (2007), *NBR 5739: Concreto - Ensaio de compressão de corpos-de-prova cilíndricos - Método de ensaio*. Rio de Janeiro.
- Associação Brasileira de Normas Técnicas. (1994), *NBR 7222: Argamassa e concreto - Determinação da resistência à tração por compressão diametral de corpos-de-prova cilíndricos - Método de ensaio*. Rio de Janeiro.
- Cheong, H. K., MacAlevey, N. (2000), “*Experimental behavior of jacketed reinforced concrete beams*”. Journal of Structural Engineering - ASCE, 126(6), pp. 692-699. [https://doi.org/10.1061/\(ASCE\)0733-9445\(2000\)126:6\(692\)](https://doi.org/10.1061/(ASCE)0733-9445(2000)126:6(692))
- Dahmani, L., Khennane, A., Kaci, S. (2010), “*Crack identification in reinforced concrete beams using ANSYS software*”. Strength of Materials Journal, 42 (2). pp. 232-240.
- Deghenhard, C. C., Teixeira, T., Vargas, A., Vito, M., Piccinini, A. C., Do Vale Silva, B. (2016), “*Análise experimental de distintas configurações de chapa metálica no reforço à flexão em vigas de concreto armado*”. Revista Alconpat, v. 6, nº 2, pp 190-201. DOI: <http://dx.doi.org/10.21041/ra.v6i2.138>
- Helene, P. R. L. (2000). “*Manual para reparo, reforço e proteção de estruturas de concreto*”. 2ª ed, São Paulo: Editora Pini, 213 p.
- Lima, E. M. F. (2015) “*Estudo teórico-experimental de vigas de concreto armado reforçadas à flexão com barras de aço em dentes de adesivo epóxi*”. Sobral. Trabalho de Conclusão de Curso - Universidade Estadual Vale do Acaraú (UVA).
- Muliterno, B. K., Pravia, Z. M. C. (2016) “*Modelo para vigas de concreto armado*”. Técnica: Revista de Tecnologia da Construção (São Paulo), v. 231, pp. 22-25.

- Reis, A. P. A. (1998). “*Reforço de vigas de concreto armado por meio de barras de aço adicionais ou chapas de aço e argamassa de alto desempenho*”. São Carlos. Dissertação (Mestrado) - Escola de Engenharia de São Carlos - Universidade de São Paulo.
- Reis, A. P. A. (2003). “*Reforço de vigas de concreto armado submetidas a pré-carregamento e ações de longa duração com aplicação de concretos de alta resistência e concretos com fibras de aço*”. São Carlos. Tese (Doutorado) - Escola de Engenharia de São Carlos - Universidade de São Paulo.
- Santos, E. W. F. (2006). “*Reforço de vigas de concreto armado à flexão por encamisamento parcial*”. Rio de Janeiro. Dissertação (Mestrado) - Coppe - UFRJ.
- Sika (2015). “*Manual Técnico – Produtos Sika*”. Osasco: Sika, 671 p.

Evaluation of the ultrasound test for estimating the depth of cracks in concrete

M. T. A. Silva^{1*} , J. H. A. Rocha² , E. C. B. Monteiro¹ , Y. V. Póvoas¹ , E. R. Kohlman Rabbani¹ 

*Contact author: marcelajtavares@hotmail.com

DOI: <http://dx.doi.org/10.21041/ra.v9i1.289>

Reception: 08/01/2018 | Acceptance: 18/10/2018 | Publication: 30/12/2018

ABSTRACT

The objective of this study is to evaluate the ultrasound test to estimate the depth of cracks in concrete, using a mathematical model published in the literature, and to verify this depth with more accurate results. Four concrete test specimens were molded for each proposed crack depth (5 cm, 10 cm, and 15 cm), simulated using zinc plates, placed during molding and removed before concrete hardening. The results show that the test is sensitive enough to detect the presence of the cracks in the concrete. The mathematical model used allowed for an estimation of the depths of most cracks, but the results are scattered and have a high margin of error for the depths of 5 cm and 15 cm. The cracks of 10-cm depth produced better results.

Keywords: ultrasound test; cracks; concrete.

Cite as: M. T. A. Silva, J. H. A. Rocha, E. C. B. Monteiro, Y. V. Póvoas, E.R. Kohlman Rabbani (2019), "Evaluation of the ultrasound test for estimating the depth of cracks in concrete", Revista ALCONPAT, 9 (1), pp. 79 – 92, DOI: <http://dx.doi.org/10.21041/ra.v9i1.289>

¹ Universidade de Pernambuco, Recife, Brasil.

² Universidad Privada del Valle, Cochabamba, Bolivia.

Legal Information

Revista ALCONPAT is a quarterly publication by the Asociación Latinoamericana de Control de Calidad, Patología y Recuperación de la Construcción, Internacional, A.C., Km. 6 antigua carretera a Progreso, Mérida, Yucatán, 97310, Tel.5219997385893, alconpat.int@gmail.com, Website: www.alconpat.org

Responsible editor: Pedro Castro Borges, Ph.D. Reservation of rights for exclusive use No.04-2013-011717330300-203, and ISSN 2007-6835, both granted by the Instituto Nacional de Derecho de Autor. Responsible for the last update of this issue, Informatics Unit ALCONPAT, Elizabeth Sabido Maldonado, Km. 6, antigua carretera a Progreso, Mérida, Yucatán, C.P. 97310.

The views of the authors do not necessarily reflect the position of the editor.

The total or partial reproduction of the contents and images of the publication is strictly prohibited without the previous authorization of ALCONPAT Internacional A.C.

Any dispute, including the replies of the authors, will be published in the third issue of 2019 provided that the information is received before the closing of the second issue of 2019.

Avaliação do ensaio de ultrassom para a estimação da profundidade de fissuras em concreto

RESUMO

Este trabalho teve como objetivo avaliar o ensaio de ultrassom para estimar a profundidade de fissuras em concreto, utilizando modelo matemático da literatura, também verificar a profundidade com melhores resultados. Foram moldados 4 prismas de concreto para cada profundidade de fissura proposta (5 cm, 10 cm e 15 cm), simuladas através de chapas de zinco, colocadas durante a moldagem e retiradas antes do concreto endurecer. Os resultados mostram que o ensaio é sensível para detectar a presença de fissuras no concreto. O modelo matemático utilizado permitiu estimar a maioria das profundidades de fissuras; mas, os resultados apresentam-se dispersos e com margem de erro elevada para as profundidades de 5 cm e 15 cm, já para 10 cm apresentou melhores resultados.

Palavras chave: ultrassom; fissuras; concreto.

Evaluación del ensayo de ultrasonido para la estimación de la profundidad de fisuras en concreto

RESUMEN

Este trabajo tuvo como objetivo evaluar el ensayo de ultrasonido para estimar la profundidad de fisuras en concreto, utilizando un modelo matemático de la literatura, además de verificar la profundidad con mejores resultados. Se moldearon 4 prismas de hormigón para cada profundidad de fisura propuesta (5 cm, 10 cm y 15 cm), simuladas a través de chapas de zinc, colocadas durante el moldeado y retiradas antes de que el hormigón endurezca. Los resultados muestran que el ensayo es sensible para detectar la presencia de fisuras en el hormigón. El modelo matemático utilizado permitió estimar la mayoría de las profundidades de fisuras; pero los resultados se presentan dispersos y con un margen de error elevado para las profundidades de 5 cm y 15 cm, ya para 10 cm se presentó mejores resultados.

Palabras clave: ultrasonido; fisuras; concreto.

1. INTRODUCTION

Cracks are the most common pathological manifestations found in concrete structures, usually appearing as a result of tensile stresses, which concrete has difficulty absorbing. Among the types of cracks that occur are those caused by thermal phenomena or by shrinkage (which are not structural hazards but may compromise sealing and performance), and those due to the lack of capacity of the structure to absorb tensile stresses, either by underestimation of the forces during sizing or by decrease of the material strength, the latter being of concern according to Silva Filho and Helene (2011). The timely detection of these defects can prevent rapid deterioration and prolong the useful life of the structures (Aggelis et al., 2010).

The evaluation of structures is usually performed through visual inspection, the results of which can be subjective because they depend on the experience of the inspector (Rocha and Póvoas, 2017). However, there are several non-destructive tests (NDTs) that allow for important information about concrete properties to be extracted (Rehman et al., 2016), and are usually used to locate and evaluate defects in hardened concrete (Lorenzi et al., 2016). Lee, Chai, and Lim (2016) consider that available methods for evaluating concrete cracks have their own limitations. The most commonly used NDT techniques for inspection of concrete structures are: ultrasound

(Aggelis et al., 2010), thermography (Bagathiappan et al., 2013), pachymetry (Maran et al., 2015), radar (Dabous et al., 2017), and sclerometry (Tomazali and Helene, 2017).

The ultrasound test can determine the modulus of elasticity and specific mass of the concrete (Pacheco et al., 2014), estimate the compressive strength with a reasonably good approximation (Bungey, Millarde Grantham, 2006), and locate and determine the size of discontinuities in the structure (Menezes et al., 2016).

Several studies have been undertaken to detect cracks and fissures in concrete using the ultrasound test (Aggelis et al., 2010; Wolf, Pirskawetz, and Zang, 2015) and others to estimate their depth (Bungey, Millard, and Grantham, 2006; Pinto et al., 2010; Souza, 2016). The study developed by In et al. (2017) used the diffuse ultrasound technique to estimate the depth of cracks in concrete pieces that simulated real beams, performing a two-dimensional simulation of finite elements. This study concluded that it is possible to estimate the depth of cracks with deviations of 1 cm in relation to the real central measurement. Seher et al. (2013) also used diffuse ultrasound combined with two-dimensional finite element simulations, for which they analyzed the wave parameters to verify the variations between cracked and uncracked elements. It can be concluded that it is possible to estimate the depth of cracks with a maximum error of 10%.

It has been demonstrated in all of the studies that the results are influenced by several factors, such as: crack depth, concrete quality, and material saturation, among others. The objective of the present article is to evaluate the ability of ultrasound method to estimate the depth of cracks in concrete structures and specifically the influence of the depth of the cracks on the results, by analyzing the time variation of the sound wave through the cracked and uncracked areas.

2. ULTRASOUND TEST PROCEDURE

The ultrasound equipment used for concrete is designed to generate longitudinal waves, also known as sound waves (Bungey, Millard, and Grantham, 2006). Those whose frequency falls within the range of 20Hz to 20,000Hz are audible to the human ear, whereas the waves below 20Hz are called infrasonic and those above 20,000Hz are known as ultrasonic. (Possani et al., 2017).

The results obtained from the test may be affected by several factors, such as the distance between the contact surfaces of the transducers; the presence of reinforcement, especially if aligned in the direction of wave propagation; the specific concrete mass, which depends on the concrete mixture and conditions; the type, specific mass and other characteristics of the aggregate; the type of cement and degree of hydration; the densification type; and the age of the concrete (Pacheco et al., 2014, Lorenzi et al, 2013, Mohamad et al., 2015).

There are several advantages to using ultrasonic tests on concrete structures, such as: the tests are non-destructive, the equipment is cheap and easy to operate, and the test can be applied at any time, as it will not contribute to deterioration of the structure. However, the test does have some limitations, because the interpretation of its results is merely qualitative in relation to the quality of the concrete. It is therefore necessary to use it in conjunction with other tests in order to obtain more conclusive results (Aggelis et al. al., 2010).

Ultrasound tests in Brazil are regulated by NBR 8802 - Hardened concrete - Determination of the propagation of ultrasonic waves (ABNT, 2013). According to this standard, there are three ways for waves to be transmitted along the surface of the concrete: direct, semidirect, and indirect, as shown in Figure 1.

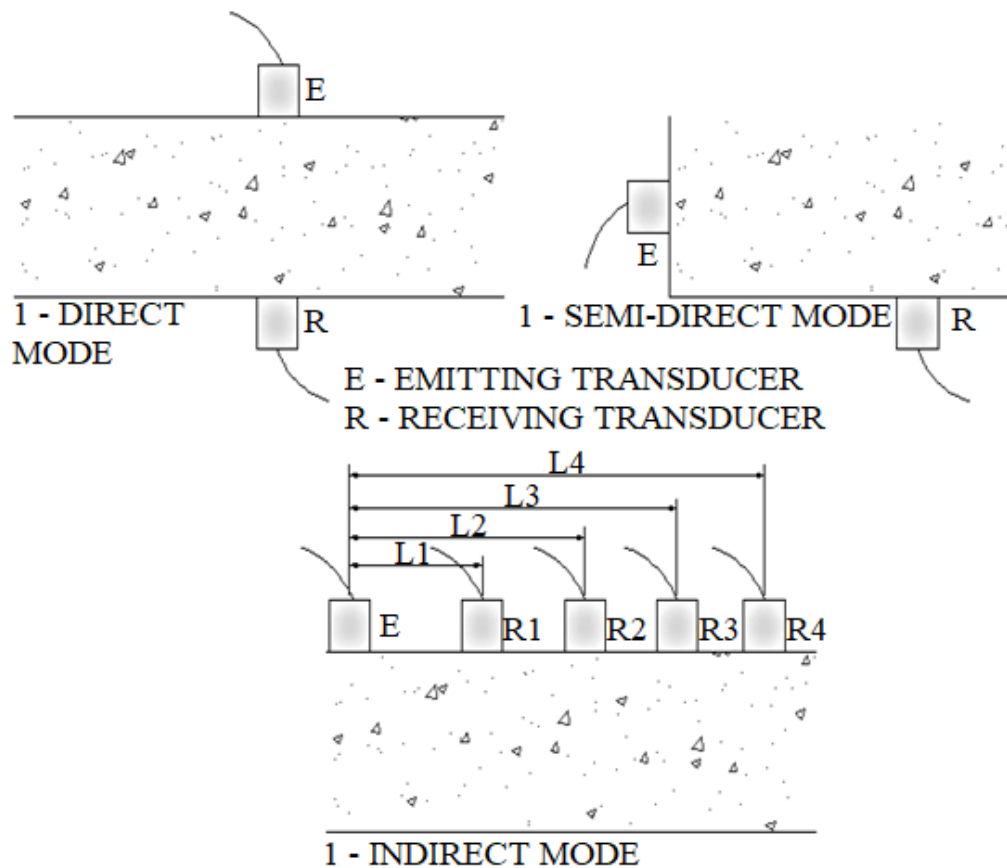


Figure 1. Transducer positioning (ABNT, 2013)

3. METHODOLOGY

To achieve the objectives of this study, concrete blocks were molded to represent real structural elements, in which cracks were induced to estimate depths using the mathematical model proposed by Bungey, Millard, and Grantham (2006). A total of 12 concrete blocks were molded, four for each of the three proposed crack depths (5 cm, 10 cm, and 15 cm). Four distances between the transducers were considered when performing the test (10 cm, 20 cm, 30 cm, and 40 cm).

To facilitate the analysis of the results, the blocks were divided into three groups (series) according to the crack depth: Series I - blocks with 5 cm deep cracks; Series II - blocks with 10 cm deep cracks; and Series III - blocks with 15 cm deep cracks.

The equipment used was the 58-E4800 UPV, with a standard frequency of 54 KHz using 50-mm diameter transducers (CONTROLS GROUP, 2017).

3.1 Test specimens

The concrete blocks had dimensions of 20 x 20 x 50 cm. The crack was induced along the axis of the block by placing a 0.95 mm thick zinc plate during the molding, which was then removed before the concrete hardened. All of the blocks were produced with the same depth, because research in the literature showed no influence on the results caused by the depth. Figure 2 shows the details of these test specimens.

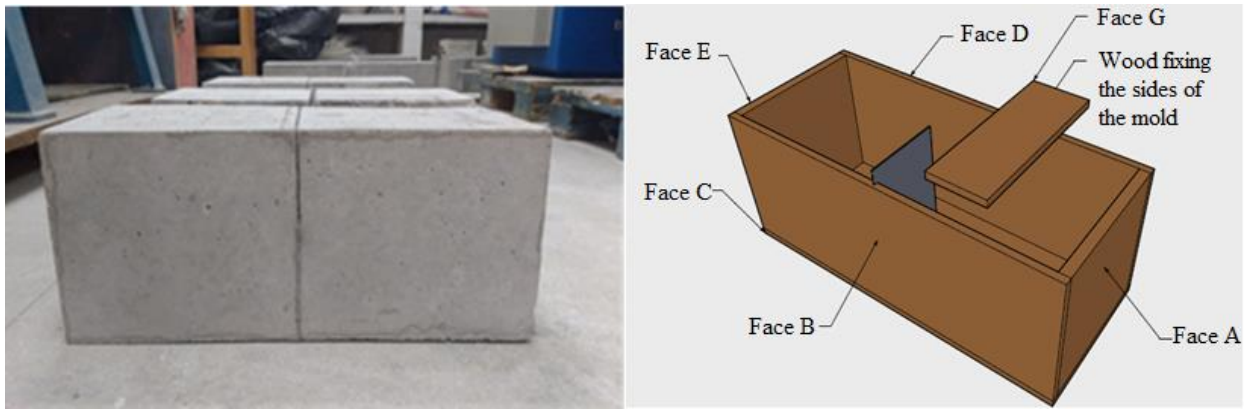


Figure 2. Concrete block details

The water/cement ratio used was 0.5 and the mixture (cement:gravel:sand) was 1:1.46:2.51. The cement used was CII Z-32. The gravel and sand were tested according to standard NBR 7211 (ABNT, 2009), where the granulometric distribution met the recommended limits and the maximum diameter of the gravel was 19 mm.

In order for the number of blocks used in the study to be statistically representative for the analysis of results, it is important that the observations of the independent variables are in a proportion greater than 5 to 1, that is, more than 5 observations for each independent variable. The recommended level is between 15 and 20 observations per variable, so that the sample can be considered representative (Hair et al., 2009). This study analyzed two independent variables, crack depth and test execution distance. When multiplied by 20, this gives an ideal quantity of 40 observations. In total, 96 observations were performed (4 blocks x 3 depths x 4 distances x 2 repetitions), a value well above the recommended amount.

3.2 Mathematical model for estimating crack depth proposed by Bungey, Millard, and Grantham (2006)

The model allows for the estimation of crack depth perpendicular to the concrete surface when the mode of transmission is indirect. Therefore, the transducers should be placed equidistant from the crack, as shown in Figure 3 (a) and (b).

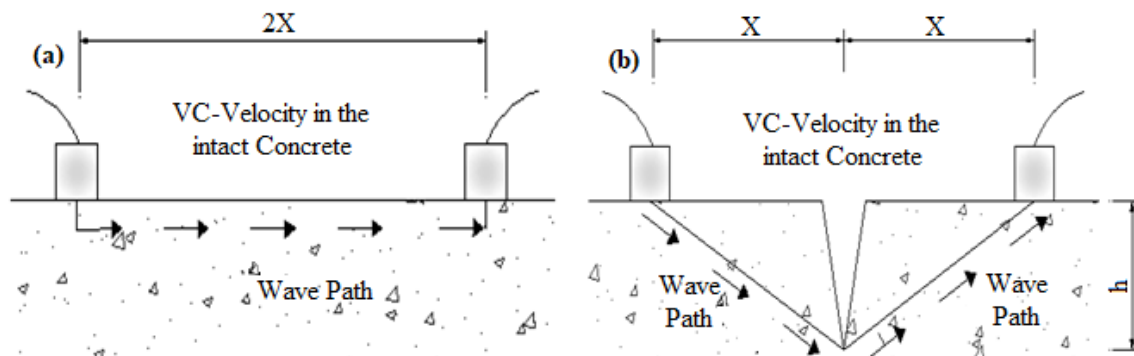


Figure 3. (a) Wave path in unbroken concrete, (b) Wave path around the crack

In order to apply this model, the velocity of the ultrasonic wave through the integral concrete obtained using the indirect mode should be adopted as "Vc". That is, a speed "Vc" is found in a region of the concrete without cracks, having a distance of $Y = 2X$ between the transducers. Considering that the wave will deviate around the crack and that the velocity should remain the same because it is propagating through similar material, it is possible to estimate the depth of a

crack that has its axis located at distance "X" from the transducers, as shown in Figure 3. The difference between these two paths will cause a slower wave propagation time, because the speed "Vc" should be the same.

The model assumes that the velocity will be equal for the two paths and that the wave will deviate because it is a mechanical wave, which requires a medium through which to propagate. Equation (1) represents the proposed mathematical model, a result of the equality of velocities along the two wave paths.

$$h = x \sqrt{\left(\frac{Tf}{Tc}\right)^2 - 1} \text{ (cm)} \tag{1}$$

Where:

h = crack depth estimated by the model (cm);

x = distance from the transducer to the axis of the crack (cm);

Tc = wave propagation time through unbroken whole concrete, defined as a (2).

$$Tc = \frac{2x}{Vc} (\mu s) \tag{2}$$

Tf = wave propagation time around the crack, defined as as (3).

$$Tf = \frac{2\sqrt{x^2+h^2}}{Vc} (\mu s) \tag{3}$$

3.3 Test execution

The ultrasound test was performed using the indirect mode, avoiding roughness on the tested surface as indicated by NM-58 (ABNT, 1996). The calibration of the equipment was performed before beginning the measurements, according to the procedure described in the manual (CONTROLS GROUP, 2017).

An observations grid was marked on the surface used for the test, composed of an upper and lower line, the detail of which is shown in Figure 4. At all points where measurements were to be taken, Vaseline was applied to connect the transducer to the surface.

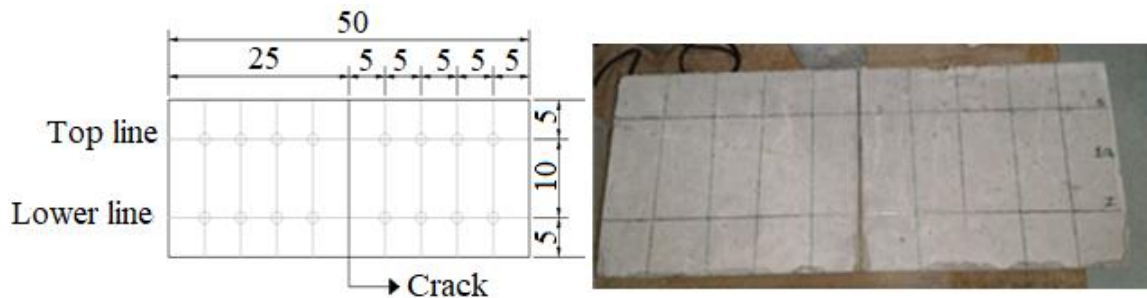


Figure 4. Test marking scheme

At each grid point, two readings were performed using the ultrasound and their average was used for the calculations of the model.

Standard NBR 8802 (ABNT, 2013) provides guidelines for obtaining the velocity of wave using the indirect mode, where the emitting transducer is at a fixed point and the receiving transducer is shifted at predetermined distances. With the data obtained, a time versus distance graph can be plotted to draw the line that best fits the points, with the tangent of the line being the wave velocity.

In order to apply the Bungey, Millard, and Grantham (2006) model, it is necessary to obtain the propagation time of the wave using the indirect mode in intact concrete - T_c , which must be obtained for the same distances that are to be measured in the cracked region - T_f .

To obtain T_c , the emitting transducer was fixed at the first point of the mesh and the receiving transducer was moved in 5-cm steps, obtaining times for the distances $Y = 5\text{cm}$, 10cm , and 15cm , according to Figure 5 (a), (b), and (c), where E is the transmitter, R is receiver, and Y is the distance between transducers (cm).

The results of the three readings of distance (cm) versus time (μs) were plotted to obtain the best fit line (Figure 6) and to find the propagation times through intact concrete, adjusted by the line T_c' for all distances required to apply the model: $Y = 10\text{cm}$, 20cm , 30cm , and 40cm , as shown in Table 1, which presents the results of the first repetition for the first test specimen of Series II. The measurements are identified first by the number of the block in the series (1, 2, 3, or 4), then by the depth ($P5 = 5\text{cm}$, $P10 = 10\text{cm}$, $P15 = 15\text{cm}$), followed by the test execution distance $D10 = 10\text{cm}$, $D20 = 20\text{cm}$, $D30 = 30\text{cm}$, $D40 = 40\text{cm}$) and finally by a unique number for each repetition of the test (1 for the first and 2 for the second).

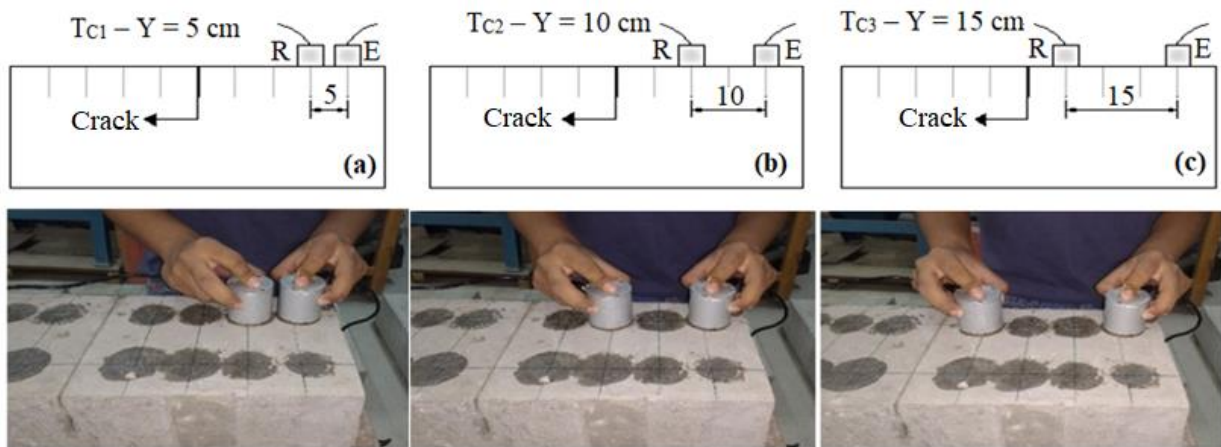


Figure 5. Time readings in the intact concrete - T_c with transducers at distances of: (a) 5 cm; (b) 10 cm; (c) 15 cm

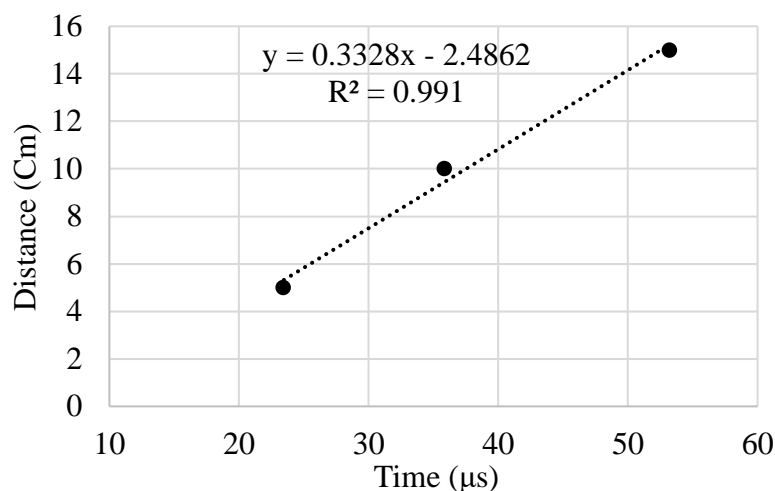


Figure 6. Distance v. time graph (Series II - Block 1 - First repetition)

Table 1. T_c' (Series II - Block 1 – First repetition)

Adjusted time - T_c' (μs) - Series II - block I			
Identification	T_c (μs)	Y (cm)	T_c' (μs)
1P10D5-1	23.45	5.00	22.49
1P10D10-1	35.88	10.00	37.52
1P10D15-1	53.23	15.00	52.54
1P10D20-1	-	20.00	67.56
1P10D30-1	-	30.00	97.61
1P10D40-1	-	40.00	127.66
Linear Equation			$Y = 0.3328X - 2.4862$
Y-intercept			-2.4862
"Vc"(cm/ μs) - Angular coef.			0.3328

The adjusted times (T_c') were found for the distances $Y = 10\text{cm}$, 20cm , 30cm , and 40cm , where $Y = 2X$, with X being the distance between the axis of the crack and the transducer.

In order to measure the propagation time of the wave around the crack (T_f), the readings were taken with distances between the transducers of $Y = 10\text{ cm}$, 20 cm , 30 cm , and 40 cm , as shown in Figure 7 (a) (b) (c) (d).

Once the values for T_c' and T_f have been obtained for the same distances, it is possible to estimate the depth of the crack using the model proposed by Bungey, Millard, and Grantham (2006), following the procedure presented in the previous section.

The procedure shown for obtaining the T_c' and T_f values was repeated two times for each of the four concrete blocks per series, for all three series.

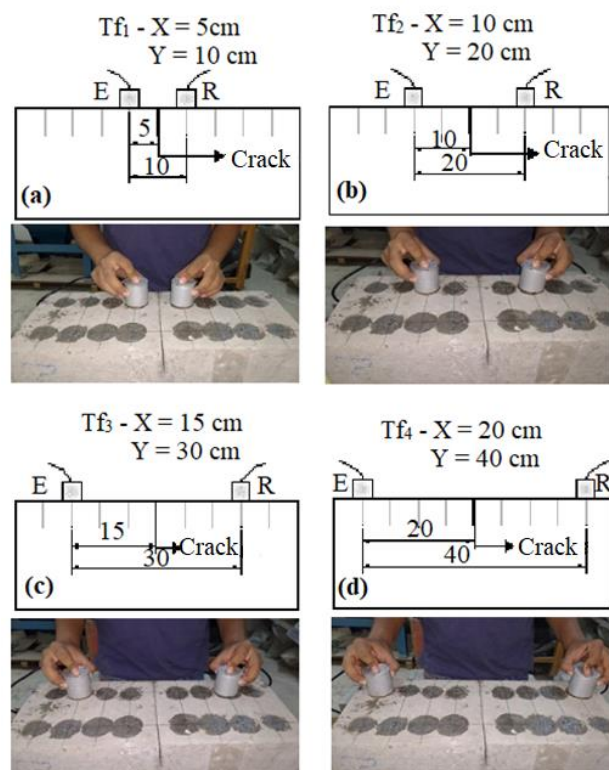


Figure 7. Readings taken around the crack with transducers at distances of: (a) 10 cm; (b) 20 cm; (c) 30 cm; (d) 40 cm

4. ANALYSIS AND DISCUSSION OF RESULTS

A statistical analysis was performed with the results for the crack depths (h') for Series I, II, and III found by the application of the mathematical model proposed by Bungey, Millard, and Grantham (2006), in order to verify which series presented the most significant results.

Table 2. summarizes the results for Series I, II, and III.

CRACK DEPTH h'					
Series I		Series II		Series III	
Identification	h' (cm)	Identification	h' (cm)	Identification	h' (cm)
1P5D10-1	5.68	1P10D10-1	6.71	1P15D10-1	10.43
1P5D20-1	6.34	1P10D20-1	9.82	1P15D20-1	12.27
1P5D30-1	11.20	1P10D30-1	11.22	1P15D30-1	10.51
1P5D40-1	11.15	1P10D40-1	9.78	1P15D40-1	7.23
2P5D10-1	3.82	2P10D10-1	6.05	2P15D10-1	24.40
2P5D20-1	4.00	2P10D20-1	7.15	2P15D20-1	19.57
2P5D30-1	7.35	2P10D30-1	*	2P15D30-1	24.56
2P5D40-1	3.12	2P10D40-1	*	2P15D40-1	21.86
3P5D10-1	4.43	3P10D10-1	5.63	3P15D10-1	11.10
3P5D20-1	3.08	3P10D20-1	7.74	3P15D20-1	15.79
3P5D30-1	9.13	3P10D30-1	6.64	3P15D30-1	14.64
3P5D40-1	14.97	3P10D40-1	11.60	3P15D40-1	11.08
4P5D10-1	3.32	4P10D10-1	6.22	4P15D10-1	9.56
4P5D20-1	4.05	4P10D20-1	8.70	4P15D20-1	9.19
4P5D30-1	3.20	4P10D30-1	5.11	4P15D30-1	5.92
4P5D40-1	10.62	4P10D40-1	7.35	4P15D40-1	*
1P5D10-2	4.82	1P10D10-2	6.38	1P15D10-2	12.21
1P5D20-2	3.74	1P10D20-2	4.96	1P15D20-2	14.95
1P5D30-2	15.17	1P10D30-2	*	1P15D30-2	10.25
1P5D40-2	15.21	1P10D40-2	*	1P15D40-2	7.94
2Z5D10-2	3.08	2P10D10-2	7.01	2P15D10-2	25.73
2P5D20-2	*	2P10D20-2	5.98	2P15D20-2	22.01
2P5D30-2	5.88	2P10D30-2	*	2P15D30-2	27.28
2P5D40-2	9.00	2P10D40-2	*	2P15D40-2	26.97
3P5D10-2	4.70	3P10D10-2	6.58	3P15D10-2	13.64
3P5D20-2	3.93	3P10D20-2	5.27	3P15D20-2	14.70
3P5D30-2	9.04	3P10D30-2	*	3P15D30-2	15.80
3P5D40-2	10.59	3P10D40-2	*	3P15D40-2	11.59
4P5D10-2	2.67	4P10D10-2	8.19	4P15D10-2	14.19
4P5D20-2	*	4P10D20-2	9.54	4P15D20-2	16.19
4P5D30-2	6.48	4P10D30-2	7.61	4P15D30-2	17.45
4P5D40-2	8.94	4P10D40-2	4.17	4P15D40-2	16.87

* Results that could not be calculated by the model, because $T_c > T_f$.

Table 2 shows that the mathematical model of Bungey, Millard, and Grantham (2006) could be applied to calculate the depth of cracks in 88.5% of observations. For the remaining percentage,

11.5%, it was not possible to determine the depth because the wave propagation time in the cracked region was less than the time in the uncracked region, making the model impossible to apply. Analysis of the results from the series using the descriptive statistics are presented in Table 3.

Table 3. Descriptive statistics of the depth variable

Statistics of the results	Actual depth (h)		
	Series I (5 cm)	Series II (10 cm)	Series III (15 cm)
Minimum value	2.67	4.17	5.92
Maximum value	15.21	11.60	27.28
Mean	6.96	7.31	15.35
Median	5.78	6.86	14.64
Variance	15.03	3.83	36.47
Standard Deviation	3.88	1.96	6.04
Coefficient of variation	55.72%	26.78%	39.34%
Number of observations	30	24	31

It can be seen from the results that the model presented significant variation for all three series. Series III (15 cm) presented the highest variance and standard deviation in comparison to the other series, showing a high level of dispersion in the data set. Series II (10 cm) had the best indices in the analysis of the dispersion of the data, presenting smaller variance, standard deviation, and coefficient of variation. Series I (5 cm) had an intermediate level of dispersion, but the coefficient of variation was higher, as the standard deviation represented about 55% of the mean.

Pinto et al. (2010) also studied the estimated depth of cracks in concrete blocks, analyzing four different depths (50 mm, 75 mm, 100 mm and 150 mm), with test execution distances of 100 mm and 150 mm, applying the same mathematical model and arrived at the estimates presented in Figure 8, where the tests were identified by the series, then the depth, and then by the test specimen analyzed. For example, S1-75-B indicated Series 1, depth 75 mm, block B.

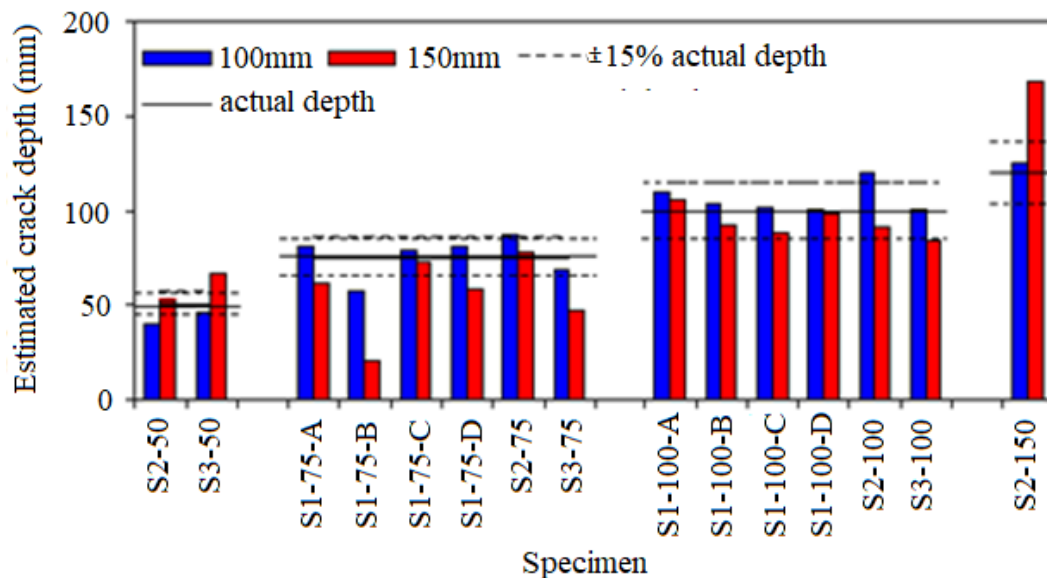


Figure 8. Crack depths (Pinto et al, 2010)

The authors concluded that the results were mostly within the margin of error of 15% of the actual crack depth. A similar result occurred in this study, where the best results were found for crack depths of 10 cm.

To facilitate the understanding of the behavior of the results found, the boxplot of the three series was used in Figure 9, a graphical statistical tool that represents the variation of the data of a numerical variable through quartiles.

A boxplot is formed by drawing a box parallel to the axis of the variable. The lower edge represents the 1st quartile, the thick line the median (2nd quartile), and the upper edge the 3rd quartile. The line that extends vertically indicates the upper and lower limit of the data. This box represents 50% of the central values of the distribution. The flatter the box, the less scattered the data is.

It can be seen that the data from Series II (10 cm) were those with least variability, as data from Series III (15 cm) had greater dispersion. It can be said that the data from Series II (10 cm) behaved better in comparison to the other series in the analysis of descriptive statistics.

To complement the analysis, inferential statistics were used, with the application of a confidence interval (CI) of 95%. This refers to a numeric interval around the mean that will contain 95% of the values, on average. The CI value represents, more or less, a margin of error in relation to the mean.

For this study, a 20% margin of error was considered acceptable. Using the actual crack depth measurement as a reference, this implies margins of error of 1 cm for Series I, 2 cm for Series II, and 3 cm for Series III.

Table 4 shows the confidence intervals of the depth variable for the 3 series analyzed. Figure 10 shows the graphs of the confidence intervals for each series with regard to depth.

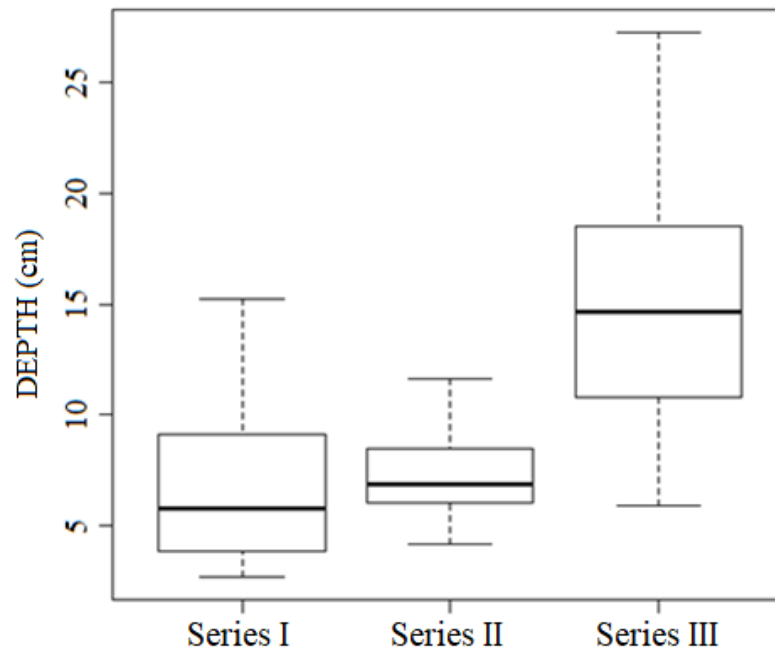


Figure 9. Boxplot for variable: DEPTH

Table 4. Confidence interval for the depth variable

Series	C.I. (error)		Lower limit	Mean	Upper limit
Series I	1.45	29%	5.51	6.96	8.40
Series II	0.83	8%	6.48	7.31	8.14
Series III	2.22	15%	13.14	15.35	17.57

Corroborating what was determined in the descriptive analysis, the data from Series III (15 cm) had a higher value for the C.I. than the other series, while Series II (10 cm) had the smallest C.I. A greater C.I. means that the margin of error that ensures 95% confidence increases, making the interval larger, which can be seen in Table 4.

With too large a range, meaning a high margin of error, the application of this procedure on real structures becomes impractical, as it will lead to a great variation in the estimate of the depth of the cracks.

For Series III, the depth variation calculated by the model falls within the range of 13.14 cm to 17.57 cm, with the actual depth being 15 cm.

In Series II, which had the smallest C.I., the depth calculated by the model varies from 6.48 cm to 8.14 cm. Although this is a small interval, the actual depth measurement of 10 cm does not fall within it, a fact that compromises the application of the model.

For Series I, which had an intermediate C.I., with crack depths calculated by the model ranging from 5.51 cm to 8.40 cm, the actual depth of 5 cm also lies outside the range.

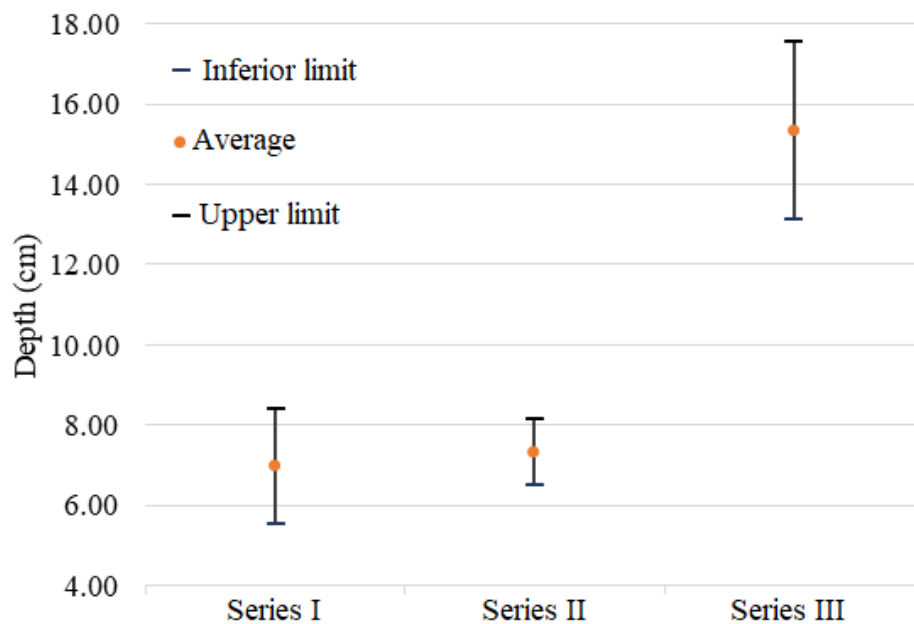


Figure 10. Confidence interval graph (depth variable)

It is also possible to see from the results that, for larger distances between the transducers (30 and 40 cm), there is a greater variation of the data, whereas the smaller test execution distances (10 and 20 cm) had less dispersion and a smaller margin of error.

It is possible to apply the proposed model and determine the depths of cracks, but with a high degree of dispersion in the results. This high variability is mainly due to concrete that is not homogeneous, where the wave propagation velocity can vary. It is also possible that the propagation path of the wave may differ from the ideal path considered by the model.

5. FINAL CONSIDERATIONS

In the current study, an experiment was carried out to statistically evaluate the efficiency of the ultrasound method for the estimation of crack depth.

The test provides clear information on crack detection in concrete, since the wave propagation time is considerably longer than that in areas of intact concrete.

The estimation of crack depth using the model proposed in the literature made it possible to find values for a large percentage of the observations made. However, the values are widely dispersed, and have a high margin of error, compromising the results and the ability to apply the model in the field.

Combining this test with other nondestructive tests may provide better characterization of these defects and more information, in this way eliminating some of the uncertainties presented by the ultrasound method alone.

6. ACKNOWLEDGMENTS

The authors would like to thank CAPES (Coordination for the Improvement of Higher Education Personnel) for their financial support.

7. REFERENCES

- ABNT - Associação Brasileira de Normas Técnicas (2009), “*NBR 7211: Agregados para concreto - especificação*” (Rio de Janeiro, Brasil: ABNT).
- ABNT - Associação Brasileira de Normas Técnicas (1996), “*NM 58: Concreto endurecido - Determinação da velocidade de propagação de onda ultrassônica*” (Rio de Janeiro, Brasil: ABNT).
- ABNT - Associação Brasileira de Normas Técnicas (2013), “*NBR 8802: Concreto endurecido – Determinação da velocidade de propagação de onda ultrassônica*” (Rio de Janeiro, Brasil: ABNT).
- Aggelis, D. G., Kordatos, E. Z., Soulioti, D. V., Matikas, T. E. (2010), “*Combined use of thermography and ultrasound for the characterization of subsurface cracks in concrete*”, Construction and Building Materials, V. 24, No. 10, pp. 1888-1897. DOI: <https://doi.org/10.1016/j.conbuildmat.2010.04.014>
- Bagavathiappan, S., Lahiri, B., Saravanan, T., Philip, J. (2013). “*Infrared thermography for condition monitoring – A review*”, Infrared Physics & Technology, V.60, No. 1, pp. 35-55. DOI: <https://doi.org/10.1016/j.infrared.2013.03.006>
- Bungey, J. H., Millard, S. G., Grantham, M. G. (2006), “*Testing of concrete in structures*” (Oxon, United Kingdom: Taylor & Francis), p. 353.
- Controls Group (2017), “*Catálogo técnico do medidor de pulso ultrassônico*”. Disponível em: < <http://www.controls-group.com/eng/concrete-testing-equipment/ultrasonic-pulse-velocity-tester.php> >. Acesso em 06 de janeiro 2018.
- Dabous, S., Yaghi, S., Alkass, S., Moselhi, O. (2017), “*Concrete bridge deck condition assessment using IR Thermography and Ground Penetrating Radar technologies*”, Automation in Construction, V.74, pp. 340-354. DOI: <https://doi.org/10.1016/j.autcon.2017.04.006>
- Hair, J. F., Black, W. C., Babin, B. J., Anderson, R. E., Tatham, R. L. (2009) “*Análise Multivariada de Dados*”. BOOKMAN, 6 ed. Porto Alegre, Brasil, p. 688.
- In, C. W., Arne, K., Kim, J. Y., Kurtis, K. E., Jacobs, L. J. (2017), “*Estimation of Crack Depth in Concrete Using Diffuse Ultrasound: Validation in Cracked Concrete Beams*”, Journal of Nondestructive Evaluation, V.36, No.4. DOI: <https://doi.org/10.1007/s10921-016-0382-4>
- Lee, F. W., Chai, H. K., Lim, K. S. (2016). “*Assessment of Reinforced Concrete Surface Breaking Crack Using Rayleigh Wave Measurement*”, SENSORS, V.3, No. 3, 337. DOI: <https://dx.doi.org/10.3390/s16030337>
- Lorenzi, A., Reginato, L. A., Lorenzi, L. S., Silva Filho, L. C. P. (2016), “*Emprego de ensaios não destrutivos para inspeção de estruturas de concreto*”, Revista IMED, V.3, No. 3, pp. 3-13. DOI: <https://doi.org/10.18256/2358-6508/rec-imed.v3n1p3-133>

- Lorenzi, A., Reginato, L. A., Favero, R. B., Chies, J. A., Caetano, L. F., Silva Filho, L. C. P. (2013), “*Tomografia Ultrassônica 3D para Avaliação de Estruturas de Concreto*” *Techne: Revista de Tecnologia da Construção* (São Paulo), v. 198, p. 36-44, 2013. Disponível em: < <http://techne17.pini.com.br/engenharia-civil/198/artigo296324-1.aspx> >. Acesso em 18 de setembro 2018.
- Maran, A. P., Menna Barreto, M. F. F., Rohden, A. B., Dal Molin, D. C. C., Masuero, J. R. (2015), “*Análise da espessura do cobrimento de armadura em lajes com diferentes distanciamentos entre espaçadores e pontos de amarração*”, *Revista IBRACON de Estruturas e Materiais*, V.8, No. 5, pp. 625-643. DOI: <http://dx.doi.org/10.1590/S1983-41952015000500005>
- Menezes, V. S., Ferronato, D. N. L., Santos, E. M., Feiteira, J. F. S. (2016), “*Estudo do comportamento da porosidade de pasta de cimento por ultrassom*” in: Congresso Brasileiro de Cerâmica, 60. Águas de Lindóia: IBRACON (Brasil), Disponível em:< <http://www.metallum.com.br/60cbc/anais/PDF/06-048TT.pdf> >. Acesso em 06 de janeiro 2018.
- Mohamad, G., Carmo, P. I. O., Oliveira, M. J. D., Temp, A. L. (2015), “*Métodos combinados para avaliação da resistência de concretos*”, *Revista Matéria*, V.20, No. 1, pp. 83-99. DOI: <http://dx.doi.org/10.1590/S1517-707620150001.0011>
- Pacheco, J., Bilesky, P., Morais, T. R., Grando, F., Helene, P. (2014), “*Considerações sobre o Módulo de Elasticidade do concreto*” in: Congresso Brasileiro do Concreto, 56, Natal: IBRACON (Brasil), (2014). Disponível em:< <http://www.phd.eng.br/wp-content/uploads/2014/06/269.pdf> > . Acesso em 06 de janeiro 2018.
- Pinto, R. C. A., Medeiros, A., Padaratz, I. J., Andrade, P. B. (2010) “*Use of Ultrasound to Estimate Depth of Surface Opening Cracks in Concrete Structures*”, *E-Journal of Nondestructive Testing and Ultrasonics*, V.8, p. 1-11.
- Possani, D., Rodrigues, D., Correia, F., Morais, D. (2017), “*Ondas ultrassônicas: teoria e aplicações industriais em ensaios não-destrutivos*”, *Revista brasileira de física tecnológica aplicada*, V.4, No. 1, p.16-33. DOI: <http://dx.doi.org/10.3895/rbfta.v4n1.5073>
- Rehman, S., Ibrahim, Z., Memon, S., Jameel, M. (2016), “*Nondestructive test methods for concrete bridges: A review*”, *Construction and Building Materials*, V.107, No. 15, pp. 58-86. <http://dx.doi.org/10.1016/j.conbuildmat.2015.12.0111>
- Rocha, J. H. A., Póvoas, Y. V. (2017), “*A termografia infravermelha como um ensaio não destrutivo para a inspeção de pontes de concreto armado: Revisão do estado da arte*”, *Revista ALCONPAT*, V.7, No. 3, p.200-2014. DOI: <http://dx.doi.org/10.21041/ra.v7i3.223>
- Seher, M., In, C. W., Kim, J. Y., Kurtis, K. E., Jacobs, L. J. (2013), “*Numerical and experimental study of crack depth measurement in concrete using diffuse ultrasound*”, *Journal of Nondestructive Evaluation*, V.32, No. 1, p.81-92. DOI: <http://dx.doi.org/10.1007/s10921-012-0161-9>
- Silva Filho, L. C. P., Helene, P. R. L. (2011), “*Análise de estruturas de concreto com problemas de resistência e fissuração*” in.: ISAIÁ, Geraldo C. *Concreto: Ciência e Tecnologia*, 1Edição, São Paulo: Editora IBRACON (Brasil), pp. 1124-1174.
- Souza, G. B. (2016), “*Avaliação do método de propagação de onda ultrassônica na determinação da profundidade de fissura em concreto*”, *Dissertação de mestrado em engenharia civil*, Universidade Católica de Pernambuco, p. 155.
- Tomazeli, A., Helene, P. R. L. (2017), “*Diretrizes para a inspeção em estruturas de obras paralisadas*”, *Revista Estrutura*, 4 ed, p. 30-37. Disponível em: < http://abece.com.br/Revista_estrutura/Edicao4/files/assets/basic-html/page30.html >. Acesso em 20 de setembro 2018.
- Wolf, J., Pirskawetz, S., Zang, A. (2015) “*Detection of crack propagation in concrete with embedded ultrasonic sensors*”. *Engineering Fracture Mechanics*, V.146, p. 161-171. DOI: <https://doi.org/10.1016/j.engfracmech.2015.07.058>

Assess of residual mechanical resistance of reinforced concrete beams after fireR. G. Pereira^{1*}, T. A. C. Pires¹, D. Duarte¹, J. J. Rêgo Silva¹*Contact author: tacpires@yahoo.com.brDOI: <http://dx.doi.org/10.21041/ra.v9i1.299>

Reception: 21/02/2018 | Acceptance: 17/08/2018 | Publication: 30/12/2018

ABSTRACT

This paper presents an experimental program to determine the residual strength of simple supported reinforced concrete beams subject to bending after fire. Also presented is a three-dimensional, nonlinear finite element model capable of predicting the thermal and mechanical (residual) behavior of this type of structural element. The experimental results obtained with beams under up to 120 min. of fire exposure show that it did not have significant reduction in their residual resistance. The numerical model was accurate in predicting temperatures and residual strength when compared to the experimental results.

Keywords: beam; reinforced concrete; residual strength; after fire; experimental and numerical analysis.

Cite as: R. G. Pereira, T. A. Carvalho Pires, D. Duarte, J. J. Rêgo Silva (2019), "Assess of residual mechanical resistance of reinforced concrete beams after fire", Revista ALCONPAT, 9 (1), pp. 93 – 105, DOI: <http://dx.doi.org/10.21041/ra.v9i1.299>

¹ Universidade Federal de Pernambuco, Brasil.

Legal Information

Revista ALCONPAT is a quarterly publication by the Asociación Latinoamericana de Control de Calidad, Patología y Recuperación de la Construcción, Internacional, A.C., Km. 6 antigua carretera a Progreso, Mérida, Yucatán, 97310, Tel.5219997385893, alconpat.int@gmail.com, Website: www.alconpat.org

Responsible editor: Pedro Castro Borges, Ph.D. Reservation of rights for exclusive use No.04-2013-011717330300-203, and ISSN 2007-6835, both granted by the Instituto Nacional de Derecho de Autor. Responsible for the last update of this issue, Informatics Unit ALCONPAT, Elizabeth Sabido Maldonado, Km. 6, antigua carretera a Progreso, Mérida, Yucatán, C.P. 97310.

The views of the authors do not necessarily reflect the position of the editor.

The total or partial reproduction of the contents and images of the publication is strictly prohibited without the previous authorization of ALCONPAT Internacional A.C.

Any dispute, including the replies of the authors, will be published in the third issue of 2019 provided that the information is received before the closing of the second issue of 2019.

Avaliação da resistência mecânica de vigas em concreto armado após o incêndio

RESUMO

Este artigo apresenta um programa experimental para determinar a resistência residual de vigas em concreto armado bi-apoiadas sujeitas à flexão pura após incêndios. Também é apresentado um modelo numérico tridimensional, não linear, em elementos finitos, capaz de prever o comportamento térmico e mecânico (residual) deste tipo de elemento estrutural. As vigas não apresentaram redução significativa na sua resistência residual até 120 min. de exposição ao fogo, caracterizando um bom desempenho após incêndio. O modelo numérico mostrou-se preciso na previsão das temperaturas e da carga de ruptura residual quando comparado aos resultados experimentais.

Palavras-chave: viga; concreto armado; resistência residual; após incêndio; análise experimental e numérica.

Evaluación de la resistencia mecánica de vigas en hormigón armado después del incendio

RESUMEN

Este artículo presenta un programa experimental para determinar la resistencia residual de vigas en hormigón armado bi-apoyadas sujetas a la flexión pura después de los incendios. También se presenta un modelo tridimensional, no lineal, en elementos finitos capaces de predecir el comportamiento térmico y mecánico (residual) de este tipo de elemento estructural. Las vigas presentaron hasta 120 minutos de exposición al fuego, un buen desempeño después de incendio, no presentando una reducción significativa en su resistencia residual, y el modelo numérico se mostró preciso en la previsión de las temperaturas y de la carga de ruptura residual cuando es comparado con los resultados experimentales.

Palabras clave: viga; hormigón armado; resistencia al fuego; análisis experimental y numérico.

1. INTRODUCTION

Due to the Brazilian urbanization, the concern with fire safety in buildings in Brazil has increased. More than this, it becomes increasingly common for engineers and architects to have their services required to assess and recover structures in buildings after fires.

In order to get an idea of this market, the Metropolitan Region of Recife, capital of the state of Pernambuco, Brazil, with 4,046,845 inhabitants, registered an average of 1,634 fires per year in buildings (most of them being residential buildings), according to Corrêa et. al. (2015). This number draws attention from the local technical community to the need to deepen the understanding of the structural behavior of buildings in a fire situation, during its cooling and after the fire.

Advantages of reinforced concrete in fire situation are already mentioned in the literature, for example: being non-combustible, not exhaling toxic gases, not having (usually) thin sections and having low thermal conductivity, delaying the increase of temperature into the interior of the piece and, consequently, minimizing the damage caused by the fire with respect to reduction of the mechanical properties of constituent materials.

Neville (1997) confirms this good performance of the concrete regarding fire resistance, i.e., the time of fire exposure with satisfactory performance is relatively large and there is no release of

toxic gases. Satisfactory performance is understood as the ability to withstand loads, flame penetration resistance and heat transfer resistance.

However, it is also known that the high temperatures reached in the fire cause physical and chemical phenomena that result in the reduction of mechanical properties, that is, in the compressive strength, tensile and modulus of elasticity, of the constituent materials (steel and concrete), besides (spalling) phenomenon that can compromise the structural element's resilient capacity (PIRES, 2007).

Among the causes that can lead to a structure subject to high temperatures to collapse, Morales (2011) highlights the maximum temperature reached, the exposure time, the concrete trace, the type of structure, the structural element and the cooling velocity.

After the fire and the cooling of the structure to reach room temperature, the residual strength of the concrete structure is the main parameter to assess the level of damage and the safety of the structure, having a considerable influence on the structural recovery work (GUO AND SHI, 2011). Silva (2012), also emphasizes that the value of resistance after cooling depends on the temperature reached during the fire and the cooling rate, the faster the cooling, the more damaging it will be for the concrete's resistance.

Experimental research, such as those conducted by Guo and Shi (2011) and Maraveas et. al. (2017), respectively, determined the reduction of residual mechanical properties of concrete and steel after heating to temperature levels. Figure 1 summarizes these results.

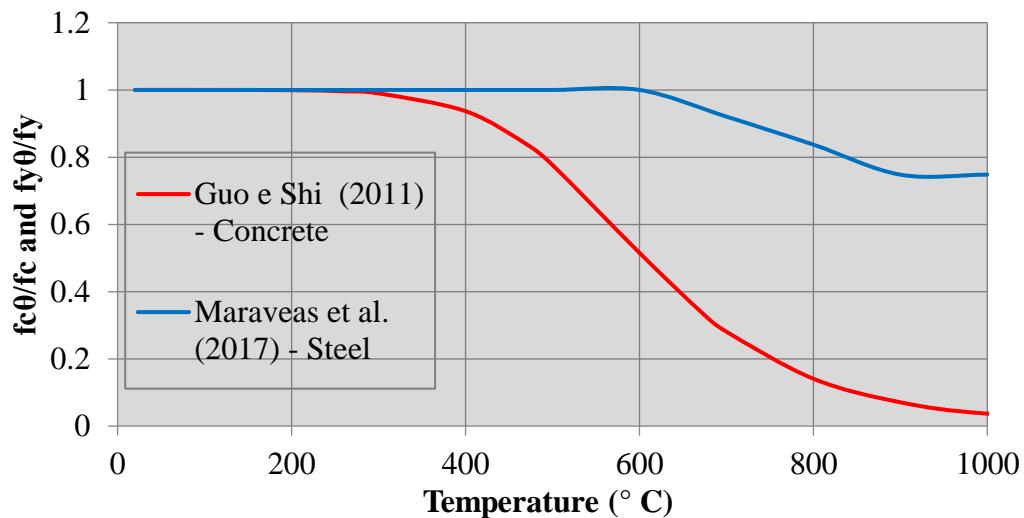


Figure 1. Reduction factors for the residual compressive strength of concrete and for the flow of steel after cooling.

The elevation of the temperature in the steel causes reduction in its resistance. After cooling, steel may, under certain circumstances, recover its initial strength. Transformations in its crystallography, obtained at temperatures above the eutectic point (approximately 720 ° C), partially impede the recovery of the resistance, thus, there is a residual loss of resistance (Smith et al., 1981, apud SILVA et al., 2006). This reduction factor is presented in Figure 1. However, it is worth noting that the international literature presents several values for the reduction of the mechanical properties of the materials after fire and often with very divergent values. This demonstrates the need for more research to reach consensus.

This work aims to simulate experimentally the impact caused by a fire in reinforced concrete beams. Then, a numerical model developed in the ABAQUS finite element program will be presented in order to evaluate the residual mechanical strength of these beams. In this sense, it is expected to contribute to the procedure for evaluating reinforced concrete structures after fires, presenting a valid strategy for this purpose.

2. EXPERIMENTAL MODEL

The experimental program developed in this research was carried out at the Structural and Materials Laboratory of the Civil Engineering Department of the Federal University of Pernambuco and the Francisco Adrissi Ximenes Aguiar Technical School (SENAI - FAXA), in the municipality of Cabo de Santo Agostinho - PE.

In the experimental program, 12 reinforced concrete beams with a length of 1.20 m and cross section of 0.12 mx0.20m, representing the base and the height respectively, were tested. The compressive strength of the concrete after 60 days is $f_c = 47.6$ MPa and was determined, by arithmetic mean, through 4 cylindrical specimens measuring 0.10 m x 0.20 m.

The concrete was dosed and had the characteristics shown in Table 1.

Table 1. Concrete characteristics

Description	Value
Cement CP II F32	837 kg
White Sand - Throw	1809 kg
Average sand	603kg
Brita 25mm	3741 kg
Water	456 l
MBT 61R Handlebar Retractor	2.637 l
Mass Trace (cement : sand : gravel)	1: 2.88: 4.47
Water / cement factor	0.54
Compressive strength at 28 days of design (f_{ck})	30 MPa
Slump	60 ± 10mm
Mean compressive strength at test time (60 days)	47.6 MPa
Mass Humidity	4.4%
Dry Density	2400 kg / m ³

For positive longitudinal reinforcement, two bars $\phi = 10$ mm, CA-50 steel, were employed and for transverse reinforcement, bars of $\phi_t = 6.3$ mm, CA-60 steel were used, with spacing close to the supports of 60 mm and 80mm in the central region of the beam. In the upper part of the beam, 2 bars $\phi_m = 6.3$ mm, Steel CA-60, were used as mounting reinforcement, only with the stirrup holder function. The concrete cover c_1 (distance between the face and the longitudinal reinforcement axis), according to NBR 15200:2012, was 30 mm.

The assay was performed after 60 days of sample curing and consists of two steps. First, the heating of the beams, according to the curve of Figure 2. In this step, there is no application of mechanical load. Then, after 24 hours, time for the cooling, the mechanical load was applied until the rupture, according to the model of Figure 4 (c).

Three beams were tested at room temperature, that is, without heating to determine the reduction of residual resistance.

The heating of the beams, without application of mechanical load, took place in three batteries of fire tests with durations of 60 min., 120 min. and 210 min., corresponding to the programmable limits of the furnace used, with three samples (beams) for each battery. The heating curve is shown in Figure 2.

Due to the limitation of the furnace employed, the standard fire curve (NBR 15200:2012) could not be adopted. For comparison purposes, this curve is also represented in Figure 2.

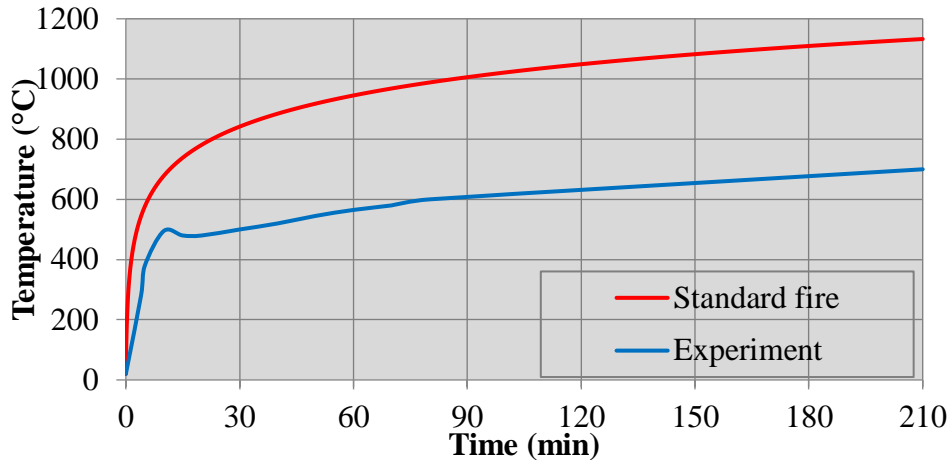


Figure 2. Temperature of the gases inside the furnace during heating for all experiments

In table 2 the characteristics of the furnace used for fire exposition of the beams at elevated temperatures are presented. Figure 3 shows the photo of this furnace.

Table 2. Furnace characteristics used in the exposures

Furnace characteristics	
External dimensions	2.6x2.35 x 1.6 m
Internal dimensions	2.1x1.00 x 1.00 m
Burner power used	402,000 kcal / h
Fuel	Natural gas



Figure 3. Furnace used in the tests

The beams were exposed to fire in 3 faces, considering the worst situation in a fire situation. The compressed face of the beam was insulated with the ceramic fiber blanket (insulation material)

inside the furnace, as shown in Figure 4 (b), to ensure that the top of the beam was not heated by conduction. The temperatures inside the structural part and the gases inside the furnace were monitored by 20 K-type thermocouples: 16 of them were placed along the beam, as shown in Figure 5, and 4 thermocouples located on the top of the furnace.

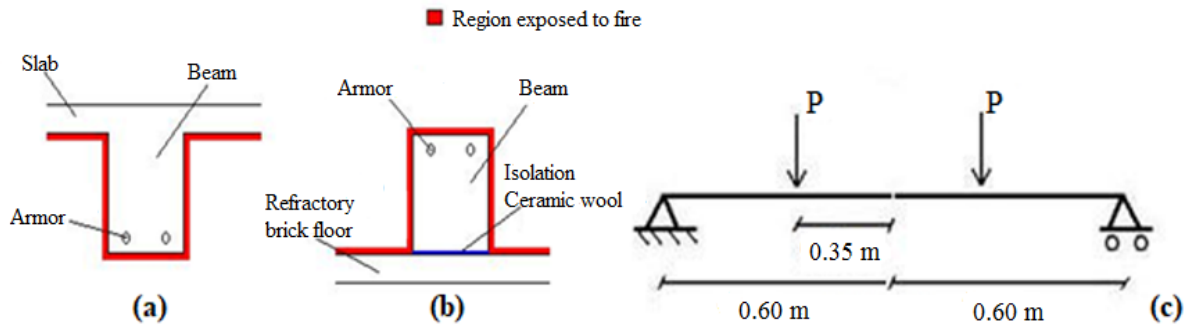


Figure 4. Scheme of the beams: in the actual situation (a), during heating (b) and in the mechanical tests (c)

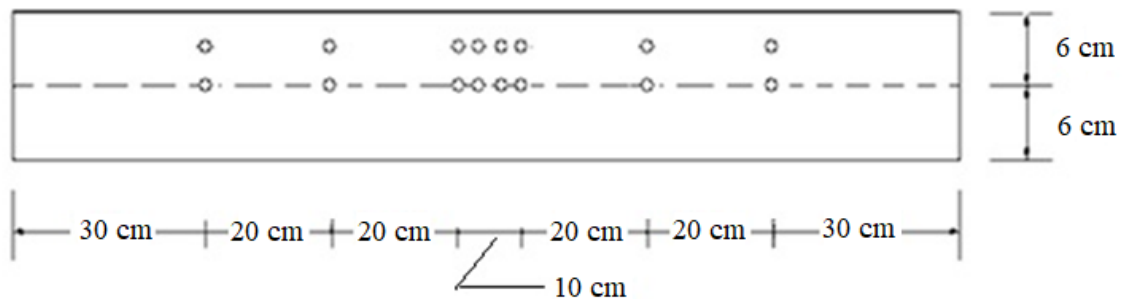


Figure 5. Location of the thermocouples along the beam (top view)

The mechanical test of the beams occurred after cooling to room temperature. The load was applied by a hydraulic press whose maximum load capacity was 3000 kN, according to Figure 6. Throughout the mechanical test the mechanical load applied to the beam was recorded by 300 kN load cells. The test scheme is shown in Figure 4 (c) where the beams were loaded until rupture. The load application rate was 1 kN /s.



Figure 6. Press used for beam bending tests

3. NUMERICAL MODEL

3.1 Geometric Properties of Beams

In this work, the three-dimensional, non-linear numerical model for finite element analysis of reinforced concrete beams was developed in the ABAQUS / Standard program (2013).

The geometric properties of the model follow strictly what is described in the experimental program.

3.2 Type of Finite Element

The ABAQUS library has a variety of finite elements of different types such as Solids, Shell, Membrane, Frame, among others.

In this study, in the thermal analysis, two types of finite elements were used for discretization of the respective beams, being:

- DC3D8, being the same 3D, of linear formation and composed of 8 nodes, for concrete and longitudinal reinforcement;
- DC1D2, element 1D, that is, link, with linear formation and composed of 2 nodes, used in the transverse reinforcement.

For mechanical analysis, the following elements were adopted:

- C3D20R, solid type element, used in the discretization of the concrete. It is a continuous element (C), three-dimensional (3D), with twenty nodes (20), reduced integration and has the option *hourglass control*, which allows to improve the resolution of problems related to obtaining oscillatory solutions, exhibiting spurious modes, that is, when the matrix becomes singular or almost singular (when the matrix does not admit inverse). It presents quadratic formation and three degrees of freedom of translation at each node;
- C3D6, a solid type element used in the discretization of the longitudinal reinforcement. It is a continuous element (C), three-dimensional (3D) and with six nodes (6).
- T3D2, lattice element that has two nodes, presenting three degrees of freedom per node, referring to the translations in the x, y and z directions. This element was used in the discretization of the transverse reinforcement.

Figure 7 illustrates the types of elements used in the numerical model.

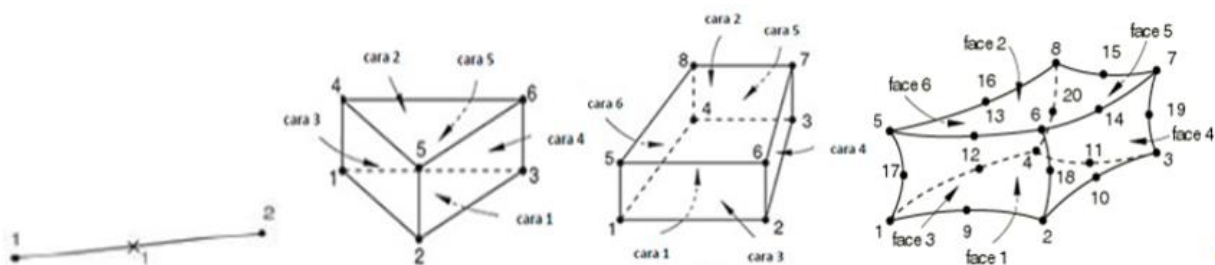


Figure 7. Two-node finite element, six-node prismatic triangular finite element, eight-node hexahedron finite element, twenty-node hexahedron finite element, respectively. (RODRIGUES et al. (2016))

3.3 Finite Element Mesh

The reinforced concrete beams were discretized in the thermal analysis in elements of 10 mm x 10 mm x 10 mm for concrete, 20 mm x 20 mm x 20 mm for longitudinal reinforcement and 20 mm for transverse reinforcement. For mechanical analysis, meshes of 50 mm x 50 mm x 50 mm for the

concrete, 40 mm x 40 mm x 40 mm for the longitudinal reinforcement and 20 mm for the transverse reinforcement were discretized.

For each analysis, thermal and mechanical, approximately 49066 and 2514 elements were generated, connected by 56808 and 9907 nodes, respectively. It was verified that there would be no significant improvement in the results with more refined meshes.

3.4 Properties of Materials

For the numerical analysis, thermal and mechanical properties for the materials of reinforced concrete beams were adopted according to national standards NBR 6118 (2014), NBR15200 (2012) and NBR14323 (2013).

For thermal analysis it is necessary to define the specific mass, coefficient of thermal expansion, thermal conductivity and specific heat for concrete and steel as a function of temperature. The specific mass was considered constant, with values equal to 7850 kg/m³ and 2400 kg/m³ for steel and concrete, respectively.

For mechanical analysis it is necessary to define the modulus of elasticity, Poisson coefficient and the plastic properties of the materials as a function of temperature.

When it is considered that the structure will undergo finite deformations, the tensions (σ) and deformations (ε) must be considered based on the actual geometry of the deformed structure. The true values are given by equations (1) and (2).

$$\varepsilon = \ln(\varepsilon_{nom} + 1) \quad (1)$$

$$\sigma = \sigma_{nom}(\varepsilon_{nom} + 1) \quad (2)$$

In ABAQUS the plastic behavior of the material defined by these measurements is considered, with the true tension related to the plastic part of the true deformation (SILVA, 2006).

The mechanical properties of the materials at room temperature were obtained through experimental tests: compressive strength of 47.6 MPa for the concrete; and flow stresses of 500 MPa and 600 MPa for the steel used in longitudinal bars and transverse bars reinforcements, respectively. The modulus of elasticity adopted for the steel was 210 GPa.

In order to determine the residual value of the mechanical properties, the coefficients proposed by Guo and Shi (2011) and Maraveas et al. (2017), respectively, for concrete and steel, since these values are commonly employed in similar studies.

The Poisson coefficient can also be considered constant, and so the values adopted were 0.3 and 0.2, respectively, for steel and concrete.

3.5 Contour Conditions, Loading and Contact.

To simulate the thermal action in the numerical model, two types of surfaces, around the beam subjected to high temperatures, were used, namely, *film condition* and *radiation*, which represent, respectively, the phenomena of heat transfer by convection and radiation. It should also be noted that the value of 0.95 for the emissivity of the concrete was considered. The value of 25 W/m² was adopted for the heat transfer coefficient by convection.

For the thermal analysis, the contact between concrete and longitudinal and transverse reinforcements were modeled with *Tie* behavior, simulating the perfect contact, so that there was no loss of heat.

In the mechanical model, the contact between the concrete and the reinforcements was made by the *Embedded region* function, in order to guarantee a perfect solidarity between the materials, according to the fundamental hypothesis of the reinforced concrete theory.

The numerical model represented bi-supported condition for the beams used in experiments, with span of 1.20m (Figure 8).

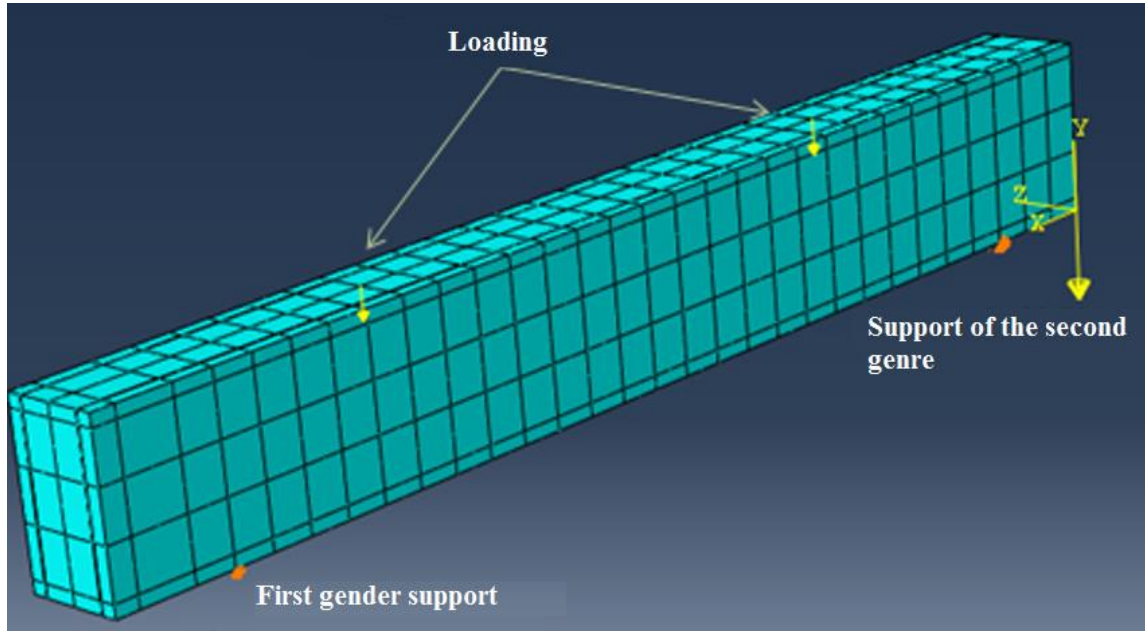


Figure 8. Numerical model used in finite element analysis.

Following the experiment, two equal concentrated loads were applied to the upper face of the beam, equidistant from the middle of the span, that is, 0.35 m, with a velocity of 1 kN /s, according to Figure 4 (c). The auxiliary command *constraint coupling*, located in the *interaction* menu in ABAQUS, which has the function of avoiding the concentration of efforts at the point of application of the concentrated load, was also used. In addition to these loads the weight of the beam was also considered.

Finally, it is emphasized that the geometric nonlinearity parameter was activated (* NLGEOM = ON), so that the effect of large displacements was considered.

4. NUMERICAL AND EXPERIMENTAL RESULTS

4.1 Temperature analysis

In this section, the temperatures results of the concrete beam recorded during the experiments and those obtained from the numerical model are compared.

Figures 9, 10 and 11 (a) shows these results at the beam cross section. The point chosen for comparison is shown in Figures 9, 10 and 11 (b), in red. At this point thermocouples were positioned in the experiment, facilitating this comparison. The temperature gradient in the concrete section is obtained through the numerical results and is represented in the same Figures 9, 10 e 11 (b).

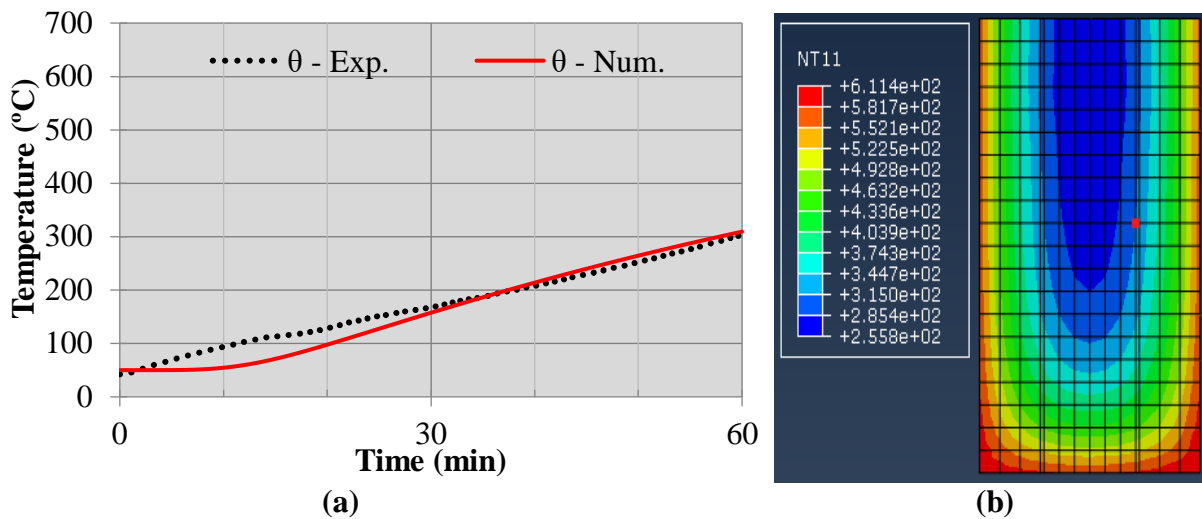


Figure 9. Evolution of temperatures in concrete, num. x exp., in the test of 60min (a) and temperature gradient in the cross section, in the middle of the span, at time $t = 60\text{min}$ (b).

In the three test batteries, i.e. 60 min., 120 min. and 210 min, the experimental and numerical temperatures for the concrete presented very close values, evidencing a strong correlation between these results (Figures 9, 10 and 11). Some divergence is observed for temperatures around 100°C. This difference can be attributed to the movement of water vapor inside the concrete and not faithfully represented in this numerical model. For this, it is necessary to develop a thermo - hydraulic - mechanical model for this analysis.

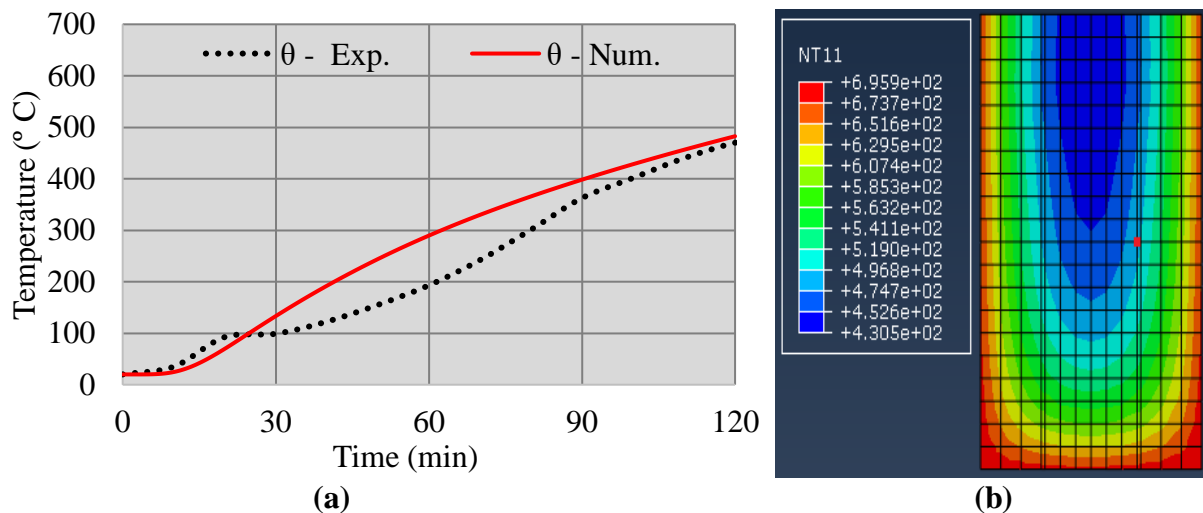


Figure 10. Evolution of temperatures in the concrete, num. x exp., in the test of 120min (a) and temperature gradient in the cross section, in the middle of the span, at time $t = 120\text{min}$ (b).

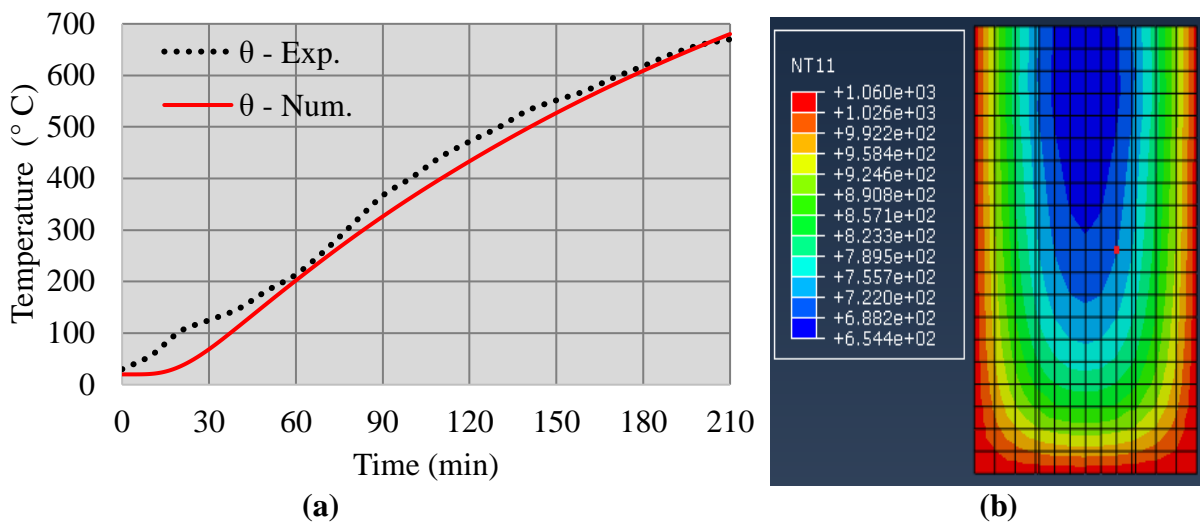


Figure 11. Evolution of temperatures in concrete, num. x exp., in the test of 210min (a) and temperature gradient in the cross section, in the middle of the span, at time $t = 210\text{min}$ (b).

It is evident the low conductivity of the concrete generating high temperature gradients (Figures 9, 10 and 11). This gradient may contribute to the occurrence of spalling, specially at the corners of the cross section. However, in the experimental test there was no spalling, probably because it was a concrete not dense enough ($f_c = 47.6\text{ MPa}$) and low humidity (4.4%).

On the other hand, the low conductivity of the concrete slows down the temperature increase in the region of the steel bars and the inner core of the concrete, allowing it to retain its resistance, and consequently, to perform better in the fire.

It is noteworthy that near $100\text{ }^\circ\text{C}$, temperature growth curves presented a short period of time (around 10 minutes) without significant increase. This is a result of the change of state of free water existing in the parts. This phenomenon was also observed in specimens from previous experiments, as reported by Kalifa et al. (2000). As previously mentioned, in this section the numerical model does not faithfully follow this behavior, but nevertheless, it presents an acceptable approximation of the results, i.e., maximum difference lower than $50\text{ }^\circ\text{C}$.

Thus, it can be concluded that the numerical model was able to represent the temperature distribution in the reinforced concrete beams with results very close to those recorded experimentally.

4.2 Mechanical analysis

This section presents the value of residual strength after cooling of the concrete beams tested, as well as this value obtained by the numerical analysis.

In order to allow the comparison between the loads obtained numerically and experimentally, the value of the vertical displacement in the middle of the span (arrow) for the maximum load supported by the beam was adopted as failure criterion. This value was defined according to the expression recommended by NBR 6118 (2014) for cracked concrete structures as a function of the load of rupture applied to the beam.

Table 3 presents the comparison of the load of rupture of the reinforced concrete beams obtained in the experimental program and through the numerical model.

Table 3. Experimental and numerical load limits

Experiment	Arrow on half goes (mm)	Experimental Breakdown Load (kN)	Numerical Breakdown Load (kN)	Error (%)
Environment	5.3	78.6	74.5	5.2
60 min.	5.2	77.2	73.5	4.9
120 min.	5.2	75.6	70.8	6.4
210 min.	3.7	47.6	44.9	5.7

The times of 60 min and 120 min of fire exposure were not sufficient to significantly reduce the residual strength of the reinforced concrete beam. It is observed that the temperatures developed in the section were not high enough to cause a degradation of the constituent materials up to 120 min. of fire exposure. This shows the good performance of the reinforced concrete structures when subjected to fires. However, the heating of 210min caused a considerable reduction in the residual resistance; the load of rupture in this situation was of 47.6 kN, that means, 60% of the maximum load capacity at ambient temperature (Table 3).

Finally, it was observed that all numerical results had a very similar tendency to those obtained experimentally, with errors less than 7% in determining the load of rupture of the beams of reinforced concrete. In this way the model is valid and accurate enough to predict the residual structural behavior of reinforced concrete beams submitted to pure bending after fire.

5. CONCLUSIONS

This work presented an experimental program to determine the residual strength of reinforced concrete beams after a fire. In addition, a numerical, non-linear numerical model developed in finite elements capable of simulating the thermal and mechanical behavior of this type of structural element was presented. Based on these results the following can be highlighted:

- The reinforced concrete beams presented a good residual performance after fire, resisting to 120 min without loss of resistance;
- The numerical approach developed for thermal analysis produced quite satisfactory results when compared with those obtained experimentally;
- The numerical approach developed for residual mechanical analysis produced accurate results with errors lower than 7% when compared to the experiment;
- The numerical model presented can be used to predict the thermal and mechanical (residual) behavior of reinforced concrete beams bi-supported after the fire;

6. REFERENCES

- ABAQUS/CAE (2013), “*Standard User’s Manual, version 6.13*”, Simulia Corp., USA,
- Associação Brasileira de Normas Técnicas (2014), “*NBR-6118: Projeto de Estruturas de Concreto*”. Rio de Janeiro.
- Associação Brasileira de Normas Técnicas (2013), “*NBR-14323: Projeto de estruturas de aço e de estruturas mistas de aço e concreto de edifícios em situação de incêndio - procedimento*”. Rio de Janeiro.
- Associação Brasileira de Normas Técnicas (2012), “*NBR-15200: Projeto de estruturas de concreto em situação de incêndio*”. Rio de Janeiro.

- Corrêa, C., Rêgo Silva, J. J., Pires, T. A., Braga, G. C. (2015), “*Mapeamento de Incêndios em Edificações: Um estudo de caso na cidade do Recife*”. Revista de Engenharia Civil IMED, V. 2, Nº. 3, 2015. <https://doi.org/10.18256/2358-6508/rec-imed.v2n3p15-34>
- International Organization for Standardization (1999), “*ISO 834 Fire-resistance tests – Elements of building construction – Part 1: General requirements*”.
- Guo, Z., Shi, X. (2011), “*Experiment and calculation of reinforced concrete at elevated temperatures*”. Elsevier, eBook ISBN: 9780123869630, 336p.
- Kalifa, P. et al. “*Spalling and pore pressure in HPC at high temperatures*” (2000). Cemente and concrete Research nº 30. 1915-1927. [https://doi.org/10.1016/S0008-8846\(00\)00384-7](https://doi.org/10.1016/S0008-8846(00)00384-7)
- Maraveas, C., Fasoulakis, Z., Tsavdaridis, K. D. (2017), “*Post-fire assessment and reinstatement of steel structures*”. Journal of structural fire engineering, v. 8, n. 2, p. 181-201. <https://doi.org/10.1108/JSFE-03-2017-0028>
- Morales, G., Campos, A., Fagarello, A. M. P. (2011), “*The action of the fire on the components of the concrete*”. Semina: Ciências Exatas e Tecnológicas, Londrina, v. 32, n. 1, p. 47-55, jan. /mar. DOI: [10.5433/1679-0375.2011v32n1p47](https://doi.org/10.5433/1679-0375.2011v32n1p47)
- Neville, A. M. (1997), “*Propriedades do concreto*”. 2ª ed, Pini.
- Pires, T. A. (2007), “*Gerenciamento de riscos de incêndio: Avaliação do impacto em estruturas de concreto armado através de uma análise experimental de vigas isostáticas*”. Dissertação de mestrado. Universidade Federal de Pernambuco
- Pires, T. A., Rodrigues, J. P. C., e Silva, J. J. R. (2012), “*Fire resistance of concrete filled circular hollow columns with restrained thermal elongation.*”, Journal of Constructional Steel Research, v. 77, pp. 82-94. <https://doi.org/10.1016/j.jcsr.2012.03.028>
- Rodriguez, G., Bonilla, J., Hernandez, J. (2016), “*Modelación numérica de vigas continuas de gran peralte de hormigón armado*”. Revista Ingeniería de Construcción, 2016, vol.31, n.3, p. 163-174. <http://dx.doi.org/10.4067/S0718-50732016000300002>
- Santiago Filho, H. A., Pereira, R. G., Pires, T. A., et. al. (2017), “*Analysis of a reinforced concrete slab in a fire situation*”. Anais 59º IBRACON – Congresso brasileiro do concreto.
- Smith, C. I., Kirby B. R., Lapwood, D. G., Cole, K. J., Cunningham, A. P., Preston, R. R. (1981), “*The Reinstatement of Fire Damaged Steel Framed Structures*” Fire Safety Journal, 4 p. 21-62. [https://doi.org/10.1016/0379-7112\(81\)90004-7](https://doi.org/10.1016/0379-7112(81)90004-7)
- Silva A. L. R. C. (2006), “*Análise numérica não-linear da flambagem local de perfis de aço estrutural submetidos à compressão uniaxial*”, Tese de Doutorado em Engenharia de Estruturas, Escola de Engenharia da Universidade Federal de Minas Gerais, p. 205,
- Silva, V. P., Fakury, R. H., Rodrigues, F. C., Pannoni, F. D. (2006), “*A real fire in small apartment – a case study*”. Anais do 4th structures in fire. Aveiro.
- Silva, V. P. (2012), “*Projeto de estruturas de concreto em situação de incêndio: conforme ABNT NBR 15200:2012*”. São Paulo, Blucher.

Compressive strength and microstructure of concretes manufactured with supersulfated cement based on materials of volcanic origin exposed to a sulfate environment

K. Cabrera Luna¹ , J. I. Escalante García² , D. Nieves Mendoza³ , E. E. Maldonado Bandala^{3*} 

*Contact author: erimaldonado@uv.mx

DOI: <http://dx.doi.org/10.21041/ra.v9i1.374>

Reception: 09/12/2018 | Acceptance: 30/12/2018 | Publication: 30/12/2018

ABSTRACT

This paper presents the results of concretes manufactured with supersulfated cement (SSC) based on volcanic materials. The concretes were cured under two regimes, one for 24 h at 25 °C and another for 22 h at 60 °C and then at 25 °C. The specimens were exposed to two conditions: dry laboratory conditions and immersed in a solution with 3.5% CaSO₄ at 25 °C for up to 180 days. After 180 days, the concrete with a cementitious compound of 5% An-10%PC-10%CaO-75%PM reached a compressive strength of 46 MPa exposed to CaSO₄ solution and of 44 MPa in dry laboratory conditions. The microstructure was analyzed by scanning electron microscopy, energy-dispersive X-ray spectroscopy and X-ray diffraction, which showed that the main hydration products are C-S-H and ettringite.

Keywords: supersulfated concrete; pumice; compressive strength; sulfate environment.

Cite as: K. Cabrera Luna, J. I. Escalante García, D. Nieves Mendoza, E. E. Maldonado Bandala (2019), “Compressive strength and microstructure of concretes manufactured with supersulfated cement based on materials of volcanic origin exposed to a sulfate environment”, Revista ALCONPAT, 9 (1), pp. 106 – 116, DOI: <http://dx.doi.org/10.21041/ra.v9i1.374>

¹ Universidad Autónoma de Baja California, México.

² Centro de Investigación y de Estudios Avanzados del IPN, Unidad Saltillo, México

³ Facultad de Ingeniería Civil, Universidad Veracruzana, Veracruz, México.

Legal Information

Revista ALCONPAT is a quarterly publication by the Asociación Latinoamericana de Control de Calidad, Patología y Recuperación de la Construcción, Internacional, A.C., Km. 6 antigua carretera a Progreso, Mérida, Yucatán, 97310, Tel.5219997385893, alconpat.int@gmail.com, Website: www.alconpat.org

Responsible editor: Pedro Castro Borges, Ph.D. Reservation of rights for exclusive use No.04-2013-011717330300-203, and ISSN 2007-6835, both granted by the Instituto Nacional de Derecho de Autor. Responsible for the last update of this issue, Informatics Unit ALCONPAT, Elizabeth Sabido Maldonado, Km. 6, antigua carretera a Progreso, Mérida, Yucatán, C.P. 97310.

The views of the authors do not necessarily reflect the position of the editor.

The total or partial reproduction of the contents and images of the publication is strictly prohibited without the previous authorization of ALCONPAT Internacional A.C.

Any dispute, including the replies of the authors, will be published in the third issue of 2019 provided that the information is received before the closing of the second issue of 2019.

Resistencia a la compresión y microestructura de concretos fabricados con cementos supersulfatados base materiales de origen volcánico expuestos a un ambiente de sulfato

RESUMEN

Esta investigación presenta los resultados de concretos fabricados con cementos supersulfatados (SSC) bases materiales volcánicos. Los concretos fueron curados bajo dos regímenes uno por 24 h a 25°C y otro por 22 h a 60°C y luego a 25 °C. Los especímenes fueron expuestos a dos condiciones, en seco en condiciones de laboratorio e inmersos en una solución con 3.5% CaSO₄ a 25°C hasta por 180 días. Después de 180 días, el concreto con un cementante compuesto de 5% An-10% PC-10% CaO-75% PM expuesto a la solución de CaSO₄ alcanzó una resistencia a la compresión de 46 MPa y 44 MPa en seco en condiciones de laboratorio. La microestructura fue analizada por microscopia electrónica de barrido, espectroscopia por dispersión de energía y DRX, mostró que los principales productos de hidratación son C-S-H y etringita.

Palabras clave: concreto supersulfatado; pómez; resistencia a la compresión; ambiente de sulfato.

Resistência à compressão e microestrutura de concreto fabricado com materiais à base de cimento supersulfatado de origem vulcânica expostos a um ambiente de sulfato

RESUMO

Esta pesquisa apresenta os resultados de concretos fabricados com cimentos supersulfatados (SSC) com bases de materiais vulcânicos. Os concretos foram curados sob duas condições, uma por 24 h a 25°C e outra por 22 h a 60°C e depois a 25°C. As amostras foram expostas a duas condições, a seco em condições de laboratório e imersos em solução com 3,5% de CaSO₄ a 25°C por até 180 dias. Após 180 dias, o concreto com um cimento composto de 5% An-10% PC-10% CaO-75% PM exposto à solução de CaSO₄ atingiu uma resistência à compressão de 46 MPa e 44 MPa em condições secas de laboratório. A microestrutura foi analisada por microscopia eletrônica de varredura, espectroscopia de dispersão de energia e DRX, mostrando que os principais produtos de hidratação são C-S-H e etringita.

Palavras-chave: concreto supersulfatado; pedra-pomes; resistência à compressão; ambiente de sulfato.

1. INTRODUCTION

Concrete is the most widely used composite material in the world, which implies that Portland cement (PC) is the construction material with the highest consumption and production, with an annual production of almost 2 billion tonnes, emitting approximately 2 billion tonnes of CO₂ (Shi et al., 2011). The effort to reduce air pollution has led to the development and use of new environmentally friendly cementitious materials, such as supersulfated cements (SSC), due to their energy savings, low carbon emissions, and reuse of waste (Ding et al., 2014). These cements can reduce CO₂ emissions up to 90% compared to PC (Woltron, 2009). The SSCs are commonly composed of granulated blast furnace slag, a sulfate source such as hemihydrate (HH) or anhydrite (An), and a small amount of alkaline activator, mainly clinker and PC (Kühl, 1908; Midgley and Pettifer, 1971; Bijen and Niël, 1981; Mehrotra et al., 1982; Dutta and Borthakur, 1990; Grounds et al., 1995; Taylor, 1998; Juenger et al., 2011) or calcium hydroxide and potassium hydroxide (Kamlet, 1960). Few investigations have studied SSCs composed of natural pozzolans (Cabrera-Luna et al., 2018).

The purpose of this research is to present a study of the mechanical properties and microstructure of concretes manufactured with SSC composed of pumice (PM). At 28 days of age, the concretes were exposed to dry laboratory conditions and immersed in a solution of 3.5% CaSO_4 . This study is part of research on volcanic-based SSC (Cabrera-Luna et al., 2018).

2. MATERIALS

Supersulfated cement is based on PM material of volcanic origin, with a surface area of $600 \text{ m}^2/\text{kg}$, two sulfate sources—commercially available HH and industrial byproduct An—and two alkaline sources—Portland-composite cement PCC 30R (PC) (ONNCCE, 2014) and commercially available calcium oxide (CaO). Table 1 shows the chemical composition of the main oxides of the starting materials.

The fine aggregate was of volcanic origin with a fineness modulus of 2.84. The coarse aggregate had a maximum nominal size of 12.5 mm and a volumetric density of $1,388.54 \text{ kg/m}^3$. A polycarboxylate-type superplasticizer was used to maintain the water/cement ratio of 0.30 and slump of 75 to 100 mm.

Table 1. Chemical composition of the starting materials by X-ray fluorescence (% wt)

Oxide %wt	SiO ₂	Al ₂ O ₃	K ₂ O	Na ₂ O	Fe ₂ O ₃	CaO	MgO	SO ₃	Other
PM	68.73	14.01	5.45	3.69	2.50	1.64	0.34		3.64
An					0.11	43.83		55.45	0.61
HH	0.94					39.70	0.58	51.69	7.09
PC	17.74	3.97	1.09		3.65	62.71	1.36	4.45	5.03
CaO						87.68	0.35	0.83	11.14

3. EXPERIMENTAL PROCEDURE

3.1 Design of mixtures and manufacture of specimens

Four concrete mixtures were designed based on the procedure proposed by the absolute volume method, published by ACI 211.1 (ACI Committee 211, 2002), with a water/binder ratio of 0.30, with regard to 720 kg/m^3 of a cementitious material and a slump of 75 to 100 mm. Four different cementitious materials were used, composed of 1) 5%HH-20%PC-75%PM, 2) 15%HH-10%PC-10%CaO-65%PM, 3) 5%An-10%PC-10%CaO-75%PM, and 4) 15%An-20%PC-65%PM. Table 2 shows the quantity of cementitious compounds. A reference concrete was made with 100% PC (C-R).

For the compressive strength test, cubes 100 mm on each side were manufactured according to UNE-EN 12390-1 (AENOR, 2001). The concrete specimens had an initial curing treatment: one at 25 °C (T25) for 24 h and another at 60 °C for 22 h and then at 25 °C (T60) for the remainder of time.

After 28 days, the specimens were exposed to two environments: one in dry laboratory conditions at 25 °C (L) and another consisting of 7-day cycles immersed in a solution of 3.5% CaSO_4 at 25 °C and then 7 days under laboratory conditions at 25 °C (S).

Table 2. Cementitious composition for concretes (kg/m³)

Nomenclature	Pumice (PM)	Hemihydrate (HH)	Anhydrite (An)	Calcium oxide (CaO)	Portland cement (PC)
	kg/m ³				
C-1	540	36	-	-	144
C-2	468	108	-	72	72
C-3	540	-	36	72	72
C-4	468	-	108	-	144
C-R	-	-	-	-	415

3.2 Characterization

The concrete compressive strength was determined up to 180 days by applying a load with a speed of 0.4 MPa/s according to the UNE-EN 12390-3 Standard (AENOR, 2003). Fragments of tested cubes were dried for 72 h in methanol and then in a vacuum chamber at 38 °C for 72 h. Later, fragments of dry cubes were mounted in resin, roughened, polished, and carbon-coated. These specimens were analyzed through a scanning electron microscope (Phillips model XL-30ESEM) operated at 20 kV.

4. RESULTS

4.1 Compressive strength

The reported values represent the average of three cubes. The evolution results of the concrete compressive strength for the curing regime of T25, exposed to dry laboratory conditions at 25 °C (L) and immersed in a solution of 3.5% CaSO₄ at 25 °C (S) up to 180 days of age, are shown in Figure 1. At 28 days, it was observed that the C-2 concrete showed the lowest strength of 22 MPa; however, after 180 days, the strength increased, reaching approximately 41 MPa for both exposure conditions, higher than the value of the reference concrete. In contrast, the C-3 concrete reached the highest strength of approximately 44 MPa when exposed to the 3.5% CaSO₄ solution, 24% higher than the reference concrete (C-R) at 180 days of age. The standard deviation values of the averages were ±0.10–2.30 MPa.

Figure 2 shows the compressive strength results of the specimens for the curing regime of T60, exposed to laboratory conditions at 25 °C and immersed in a solution of 3.5% CaSO₄ at 25 °C. The compressive strength of the C-1 and C-3 concrete at 28 days reached values of approximately 32 MPa, similar to C-R; however, after 180 days of exposure to laboratory conditions, C-1 and C-3 reached approximately 42 and 44 MPa, respectively, higher than the reference concrete with 36 MPa, while C-3 immersed in a solution of 3.5% CaSO₄ reached 46 MPa. The initial curing favored the initial and later strength in agreement with previous results (Cabrera-Luna et al., 2018). The standard deviation values of the averages were ±0.17–1.76 MPa.

In general, it was observed that the chemical composition and initial curing influenced the strength development according to previous results (Cabrera-Luna et al., 2018). These factors favorably influenced the densification of the matrix, providing resistance to the calcium sulfate (Grounds et al, 2003). However, the strength development of SSC is slower than that of the PC (Noor-ul-Amin, 2014) because the hydration process of SSC is slow at early ages, and then, the concrete compressive strength abruptly increases at advanced ages (Ding et al., 2014). The increase of compressive strength beyond 28 days may be related to the speed of the hydration products and the morphology of the formed plaster (Cabrera-Luna et al., 2018).

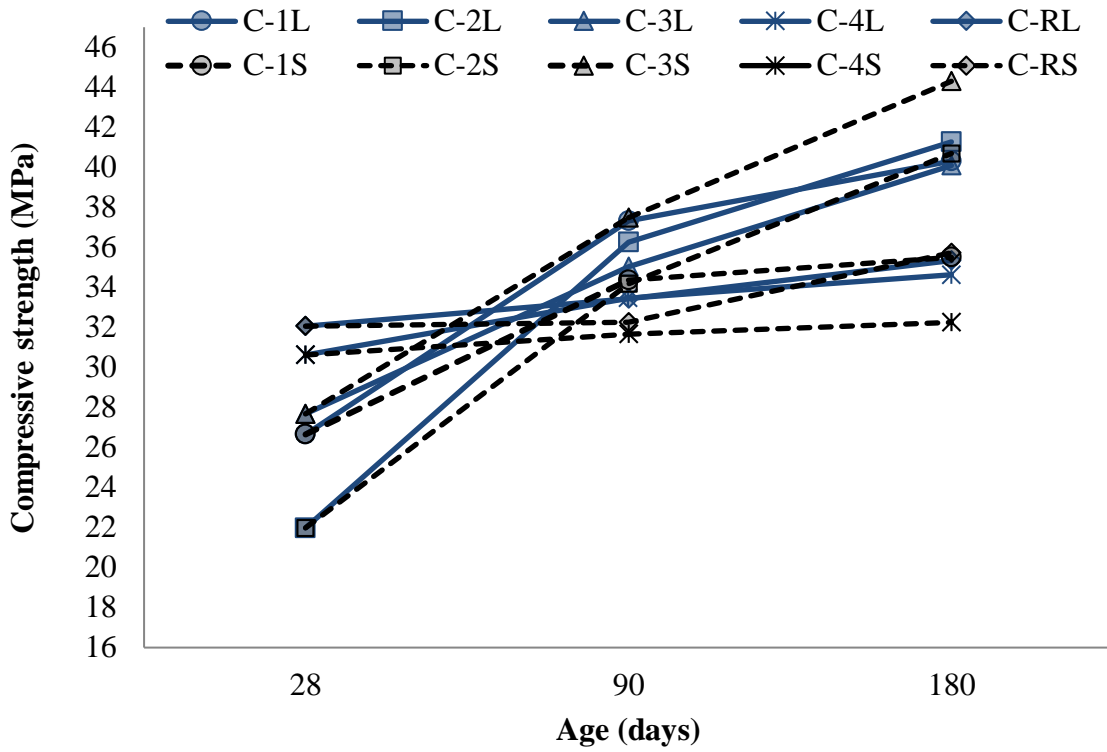


Figure 1. Compressive strength of specimens for the T25 regime exposed to dry laboratory conditions (L) and immersed in a solution of 3.5% CaSO₄ at 25 °C (S).

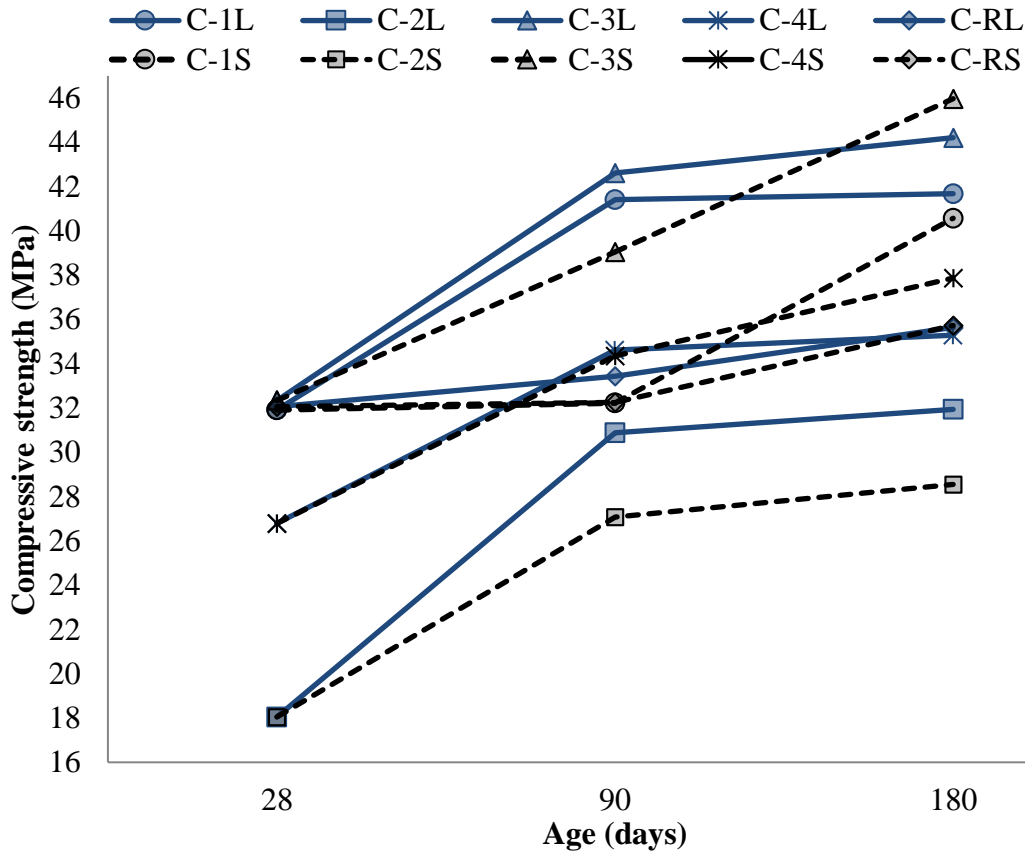


Figure 2. Compressive strength of specimens for the T60 regime exposed to dry laboratory conditions (L) and immersed in a solution of 3.5% CaSO₄ at 25 °C (S).

4.2 X-ray diffraction (XRD)

Figure 3 presents the XRD patterns of the PM and the cementitious compound of 15% An-20% PC -65% PM at 28 days, which was used to make the C-4 concrete. After the chemical activation of the PM at 28 days, the amorphous halo of the PM decreased in intensity and was slightly displaced to the right, suggesting that the PM particles reacted with the activators to form the hydration products, such as ettringite, An, gypsum, and C-S-H, identified as the primary hydrating phases. The An reflection peaks reveal low solubility and reactivity, which influenced a low amount of formed ettringite. This agrees with the presence of weak ettringite reflection peaks, suggesting that late-age strength development is mainly due to the formation of C-S-H according to (Cabrera-Luna *et al.*, 2018).

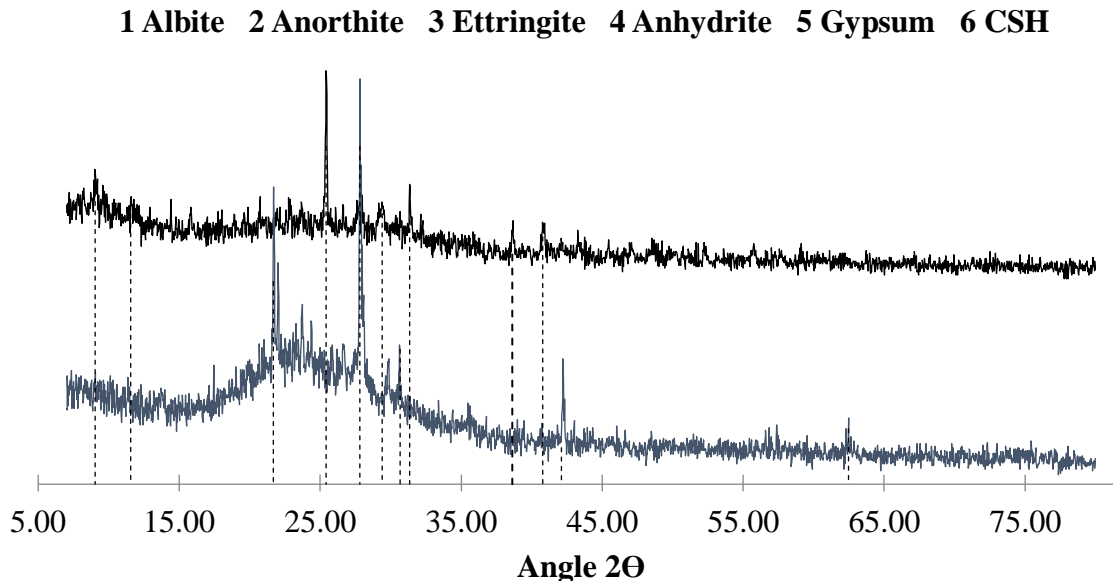


Figure 3. XRD patterns of the composite cement 5% An-20% PC -75% PM (C-4)

4.3 Scanning electron microscopy (SEM)

Figure 4 and Figure 5 show the microstructure of the C-3 concrete (5% An-10% PC-10% CaO-75% PM) for the T60 regime exposed to dry laboratory conditions at 25 °C (L) at 28 days and immersed in a 3.5% CaSO₄ solution at 25 °C (S) at 90 days, respectively. The images were obtained using backscattered electrons. In all micrographs, PM particles identified by an irregular morphology of different sizes were observed, suggesting that not all particles reacted to form hydration products; moreover, due to their size, it is easy to distinguish aggregate particles embedded in the matrix of reaction products. An particles were not observed, suggesting that the Ca²⁺ and SO₄²⁻ ions reacted with the alumina phase of the PM to form ettringite (Juenger *et al.*, 2011; Sadique *et al.*, 2012; Bazaldúa-Medellín *et al.*, 2015; Gracioli *et al.*, 2017; Rubert *et al.*, 2018). In Figure 4, the absence of PC grains suggested that they reacted with water to form more Ca(OH)₂, promoting the dissolution of PM to produce C-S-H and other products (Sadique *et al.*, 2012). The microstructure was dense with cracks caused by the drying of the gel under the high vacuum conditions in the electron column of the microscope (Avila-López *et al.*, 2015). In general, the matrix–aggregate interface is continuous; no cracks were observed in this area, showing good adherence. However, in the polished samples, the ettringite was difficult to detect; moreover, it easily decomposed under the high vacuum drying conditions of the electron column of the microscope (Bazaldúa-Medellín *et al.*, 2015). Although the X-ray microanalysis spectra (EDS) allowed their identification, they showed that the primary hydration products of the SSC concretes

were C-S-H and ettringite, distributed through the finely intermixed matrix. This agrees with (Cabrera-Luna *et al.*, 2018). The presence of ettringite crystals provides strength instead of expansion (Sadique *et al.*, 2012); these crystals were deposited in the air voids (Wolfe *et al.*, 2001) initially occupied by water (Cabrera-Luna *et al.*, 2018), densifying the matrix microstructure together with the C-S-H (Bazaldúa-Medellín *et al.*, 2015) and improving the strength. Therefore, this phase was not accompanied by expansion (Wolfe *et al.*, 2001), and there was no visible expansion in the concrete samples after 180 days. These results coincide with the XRD patterns.

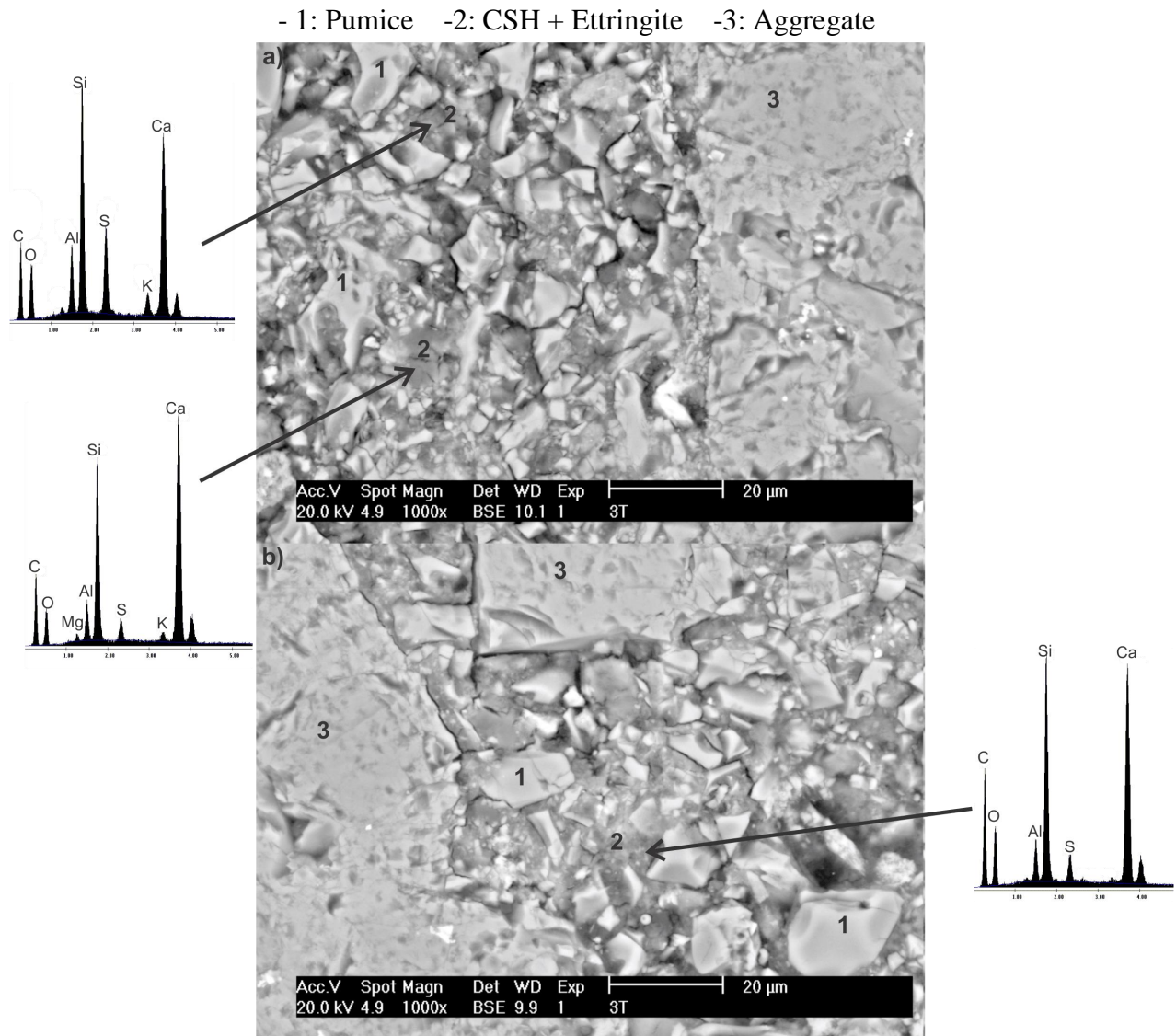


Figure 4. SEM images with backscattered electrons of the C-3 concrete (5% An-10% PC-10% CaO-75% PM) for the T60 regime exposed to dry conditions at 25 °C for 28 days.

-1: Pumice -2: CSH + Ettringite -3: Partially hydrated PC -4: Aggregate

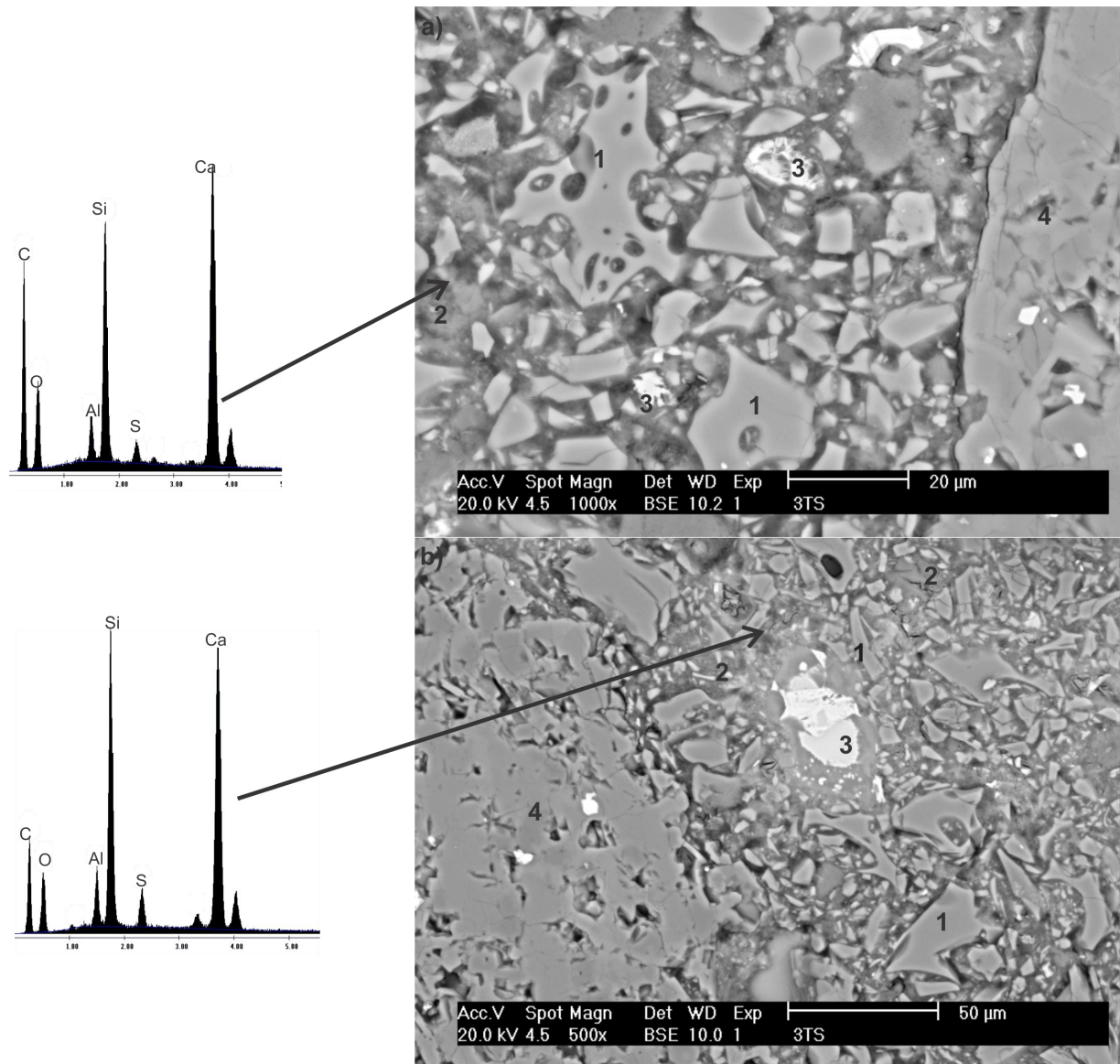


Figure 5. SEM images with backscattered electrons of the C-3 concrete (5% An-10% PC-10% CaO-75% PM) for the T60 regime immersed in a 3.5% CaSO_4 solution at 25 °C for 90 days.

5. DISCUSSION

Concrete degradation by sulfate attack mechanisms depends on several factors, such as cement type, presence of mineral additions, water/cement ratio, cation type associated with sulfate anions, sulfate concentration, time and duration of exposure, environment, hydration degree, and curing conditions (Hossain and Lachemi, 2006; Prasad *et al.*, 2006; Indu Siva Ranjani and Ramamurthy, 2012), in addition to other parameters, such as pore structure, permeability, diffusivity and mechanical properties (Prasad *et al.*, 2006). In concretes made with PC, the degree of sulfate attack depends on the availability of $\text{Ca}(\text{OH})_2$ and C_3A (Hossain and Lachemi, 2006); therefore, the chemical composition of the cement has an important role in its resistance to sulfate (Prasad *et al.*, 2006). The SSCs of this investigation were based on volcanic PM, calcium sulfate and alkaline sources. When the SSCs were exposed to a calcium sulfate solution by means of hydrating and

drying cycles, they increased in stability and strength, with stable microstructures. This suggests that the external sulfate ions did not have suitable conditions to decalcify the $\text{Ca}(\text{OH})_2$ or C-S-H. Moreover, the decrease in PC consumption reduced the amount of calcium aluminates, which had already found an abundant source calcium sulphate from the additives of the SSC, so these formed ettringite that stabilized as such; moreover, the low Al content from the PM and abundance of calcium sulphate also minimized the possibility of deleterious delayed ettringite. Nonetheless, the expansion does not only depend on the amount and time of formation of ettringite; the location of formation is also important (Wojciech, Marczewska and Jaworska, 1985); in this case, the nature of the microstructures, the rate of reaction of the components of the SSC, favored a sequence of reactions and deposition of reaction products that showed in a favorable balance that resulted in strong microstructures forming durable cements. On the other hand, the low water/binder ratio used must have had a positive effect, as it reduced the volume and connectivity of the porous network, which reduced the penetration of external agents (Indu Siva Ranjani and Ramamurthy, 2012). In general, no physical degradation was noted during the period of study, such as cracking, spalling, loss of strength and adhesion. The concretes SSC seem suitable for use in marine conditions and for construction of sewage pipes

6. CONCLUSIONS

The compressive strength of specimens cured at 25 °C showed that the concretes made with cementitious compounds of 15%HH-10%PC-10%CaO-65%PM and 5%An-10%PC-10%CaO-75%PM reached approximately 41 and 44 MPa, respectively, when immersed in a solution of 3.5% CaSO_4 .

Supersulfated concretes with cementitious compounds of 5%HH-20%PC -75%PM, 5%An-10%PC-10%CaO-75%PM and 15%An-20%PC -65%PM cured at 60 °C showed greater strength than the reference concrete by up to 30% when immersed in a solution of 3.5% CaSO_4 .

The main hydration products of the supersulfated concretes detected by XRD, SEM and EDS were C-S-H and ettringite, which provided a favorable compressive strength when exposed to laboratory conditions and calcium sulfate.

Curing at 60 °C for 22 h favors early-age strength and late-age development, mainly in the samples exposed to sulfate in almost all concretes.

The microstructure of the concrete with a cementitious compound of 5%An-10%PC-10%CaO-75%PM showed unreacted PM particles and aggregates embedded in a paste structure of a relatively dense matrix.

In general, supersulfated concretes show favorable compressive strength values when exposed to a 3.5% CaSO_4 solution, presenting adequate properties for use in marine environments.

7. ACKNOWLEDGEMENTS

The authors would like to thank the National Council of Science and Technology for the scholarship to K Luna-Cabrera and the Conacyt FC-2015-2 / 906 project for financial support.

8. REFERENCES

- ACI Committee 211 (2002), *Standard Practice for Selecting Proportions for Normal, Heavyweight, and Mass Concrete (ACI 211.1-91)*.
 AENOR (2001), *UNE-EN 12390-1, Testing hardened concrete. Part 1: Shape, dimensions and other requirements for specimens and moulds*.
 AENOR (2003), *UNE-EN 12390-3, Testing hardened concrete Part 3: Compressive strength of*

test specimens.

Avila-López, U., Almanza-Robles, J. M., Escalante-García, J. I. (2015), "*Investigation of novel waste glass and limestone binders using statistical methods*", *Construction and Building Materials*, 82, pp. 296–303. <https://doi.org/10.1016/j.conbuildmat.2015.02.085>

Bazaldúa-Medellín, M. E., Fuentes, A. F., Gorokhovskiy, A., Escalante-García, J. I. (2015), "*Early and late hydration of supersulphated cements of blast furnace slag with fluorgypsum*", *Materiale de Construcție*, 65(317), p. e043. <https://doi.org/10.3989/mc.2015.06013>.

Bijen, J., Niël, E. (1981), "*Supersulphated cement from blastfurnace slag and chemical gypsum available in the Netherlands and neighbouring countries*", *Cement and Concrete Research*, 11(3), pp. 307–322. [https://doi.org/10.1016/0008-8846\(81\)90104-6](https://doi.org/10.1016/0008-8846(81)90104-6).

Cabrera-Luna, K., Maldonado-Bandala, E. E., Nieves-Mendoza, D., Escalante García, J. I. (2018), "*Supersulfated binders based on volcanic raw material: Optimization, microstructure and reaction products*", *Construction and Building Materials*, 176, pp. 145–155. <https://doi.org/10.1016/j.conbuildmat.2018.05.024>.

Ding, S., Shui, Z., Chen, W., Lu, J., Tian, F. (2014), "*Properties of supersulphated phosphogypsumslag cement (SSC) concrete*", *Journal Wuhan University of Technology, Materials Science Edition*, 29(1), pp. 109–113. <https://doi.org/10.1007/s11595-014-0876-9>.

Dutta, D. K., Borthakur, P. C. (1990), "*Activation of low lime high alumina granulated blast furnace slag by anhydrite*", *Cement and Concrete Research*, 20(5), pp. 711–722, [https://doi.org/10.1016/0008-8846\(90\)90005-I](https://doi.org/10.1016/0008-8846(90)90005-I)

Gracioli, B., Favero Varela, M. V., Beutle, C. S., Frare, A., Angulski da Luz, C., Pereira Filho, J. I. (2017), "*Considerações sobre a resistência mecânica e o processo de hidratação de cimentos supersulfatados (CSS) formulados com fosfogesso*", *Matéria (Rio de Janeiro)*, 22(1). <https://doi.org/10.1590/s1517-707620170001.0107>.

Grounds, T., Nowell, D. V., Wilburn, F. W. (2003), "*Resistance of supersulfated cement to strong sulfate solutions*", *Journal of Thermal Analysis and Calorimetry*, 72(1), pp. 181–190. <https://doi.org/10.1023/A:1023928021602>.

Grounds, T., Nowell, D. V., Wilburn, F. W. (1995), "*The influence of temperature and different storage conditions on the stability of supersulphated cement*", *Thermal Analysis*, 45, pp. 385–394. <https://doi.org/10.1007/BF02549342>.

Hossain, K. M. A., Lachemi, M. (2006), "*Performance of volcanic ash and pumice based blended cement concrete in mixed sulfate environment*", *Cement and Concrete Research*, 36(6), pp. 1123–1133. <https://doi.org/10.1016/j.cemconres.2006.03.010>.

Indu Siva Ranjani, G., Ramamurthy, K. (2012), "*Behaviour of foam concrete under sulphate environments*", *Cement and Concrete Composites*. Elsevier Ltd, 34(7), pp. 825–834. <https://doi.org/10.1016/j.cemconcomp.2012.03.007>.

Juenger, M. C. G., Winnefeld, F., Provis, J. L., Ideker, J. H. (2011), "*Advances in alternative cementitious binders*", *Cement and Concrete Research*. Elsevier Ltd, 41, pp. 1232–1243. <https://doi.org/10.1016/j.cemconres.2010.11.012>.

Kamlet, J. (1960), "*US2947643A Hydraulic Cements*".

Kühl, H. (1908), "*German Patent No. 237777*". German.

Mehrotra, V.P., Sai, A. S. R., Kapur, P. C. (1982), "*Plaster of Paris activated supersulphated slag cement*", *Cement and Concrete Research*, 12(4), pp. 463–473. [https://doi.org/10.1016/0008-8846\(82\)90061-8](https://doi.org/10.1016/0008-8846(82)90061-8).

Midgley, H. G., Pettifer, K. (1971), "*The microstructure of hydrated super sulphated cement*", *Cement and Concrete Research*, 1(1), pp. 101–104. [https://doi.org/10.1016/0008-8846\(71\)90086-X](https://doi.org/10.1016/0008-8846(71)90086-X).

Noor-ul-Amin (2014), "*An overview on comparative study of alternatives for Ordinary Portland cement*", *Journal of Basic and Applied Chemistry*, 4(6), pp. 15–22, ISSN 2090-424X

ONNCCE (2014), *NMX-C-414-ONNCCE, Building industry - hydraulic cement -specifications*

and testing methods.

- Prasad, J. *et al.* (2006), "*Factors Influencing The Sulphate Resistance of Cement Concrete and Mortar*", Asian Journal of Civil Engineering (Building and Housing), 7(3), pp. 259–268.
- Quanlin, N., Rui, Z. (2015), "*Experimental study on some properties of a low-carbon cement*", in International Conference on Advances in Energy and Environmental Science, pp. 1440–1443.
- Rubert, S., Angulski da Lu, C., Varela, M. V. F., Pereira Filho, J. I., Hooton, R. D. (2018), "*Hydration mechanisms of supersulfated cement: The role of alkali activator and calcium sulfate content*", Journal of Thermal Analysis and Calorimetry. Springer Netherlands, 134(2), pp. 971–980. <https://doi.org/10.1007/s10973-018-7243-6>.
- Sadique, M., Nageim, H. A., Atherton, W., Seton, L., Dempster, N. (2012), "*A new composite cementitious material for construction*", Construction and Building Materials. Elsevier Ltd, 35, pp. 846–855. <https://doi.org/10.1016/j.conbuildmat.2012.04.107>.
- Shi, C., Jiménez, A. F., Palomo, A. (2011), "*New cements for the 21st century: The pursuit of an alternative to Portland cement*", Cement and Concrete Research. Elsevier B.V., 41(7), pp. 750–763. <https://doi.org/10.1016/j.cemconres.2011.03.016>.
- Taylor, H. F. W. (1998), *Cement chemistry*. 2nd edn, *Cement and Concrete Composites*. 2nd edn. Thomas Telford Publishing. [https://doi.org/10.1016/S0958-9465\(98\)00023-7](https://doi.org/10.1016/S0958-9465(98)00023-7).
- Wojceich, P., Marczevska, J., Jaworska, M. (1985), "*Some Aspects and Mechanisms of sulphate attack*", Structure, pp. 19–24.
- Wolfe, W. E. *et al.* (2001), "*The Effect of Ettringite Formation on Expansion Properties of Compacted Spray Dryer Ash*", in International Ash Utilization Symposium.
- Woltron, G. (2009), "*The utilisation of GGBFS for advanced supersulfated cements*", World Cement.